4-3 Survey Method

Time domain method was used for the IP electric survey.

When direct current is let to flow in the rock containing electric conductive minerals such as ore deposit and mineralized zone, charge and discharge phenoména are observed at the interface between the rock and the electric conductive minerals.

The discharge voltage, called chargeability, is measured in the time domain method.

The wave forms of the primary current and the measured voltage are shown in Fig. 4-4. Three integrated values, M31, M32 and M33 of transient voltage with a width of 0.52 seconds shown in the figure were measured 0.13 seconds after the primary current had been cut off. These integrated values are called chargeability and expressed in unit of milli-seconds.

Pole-Dipole array shown in Fig. 4-5 was used as configuration of electrodes of measurement of chargeability. In this array, 2 seconds on and 2 seconds off pulse current shown in Fig. 4-4 was supplied repeatedly between current electrode C_2 earthed at an infinite point and another current electrode C_1 to measure electric potential when the current was on and chargeability when the current was off at potential electrodes P_1 and P_2. Measurement was also made at each survey point for three different electrode distance (a) of 100 m, 200 m and 300 m to obtain data at points 100 m, 200 m and 300 m directly below the survey point.

Usually the distance between C_1 and C_2, $\overline{C_1C_2}$, is required to be longer than 5a. Under the present electrode array, therefore $\overline{C_1C_2} \fallingdotseq 2,000$ m was used, because 5a = 1,500 m.

In this survey, chargeability M, electric potential Vp and supplied current I were measured and from the measured values of Vp and I apparent resistivity ρa was calculated by the following formula:

$$\rho a = 4\pi a \frac{Vp}{I}$$

where a represents the distance of electrodes.

Also apparent metal factor (AMF) was defined by the following formula and AMF was calculated from the values of M and ρa:

$$AMF = \frac{M}{\rho a} \times 1000$$

AMF is used when it is desired to emphasize IP effect of electric conductive media.

The term "IP value" or "IP" used hereunder is synonymous with the chargeability mentioned above, and "IP anomaly" means anomaly of chargeability.

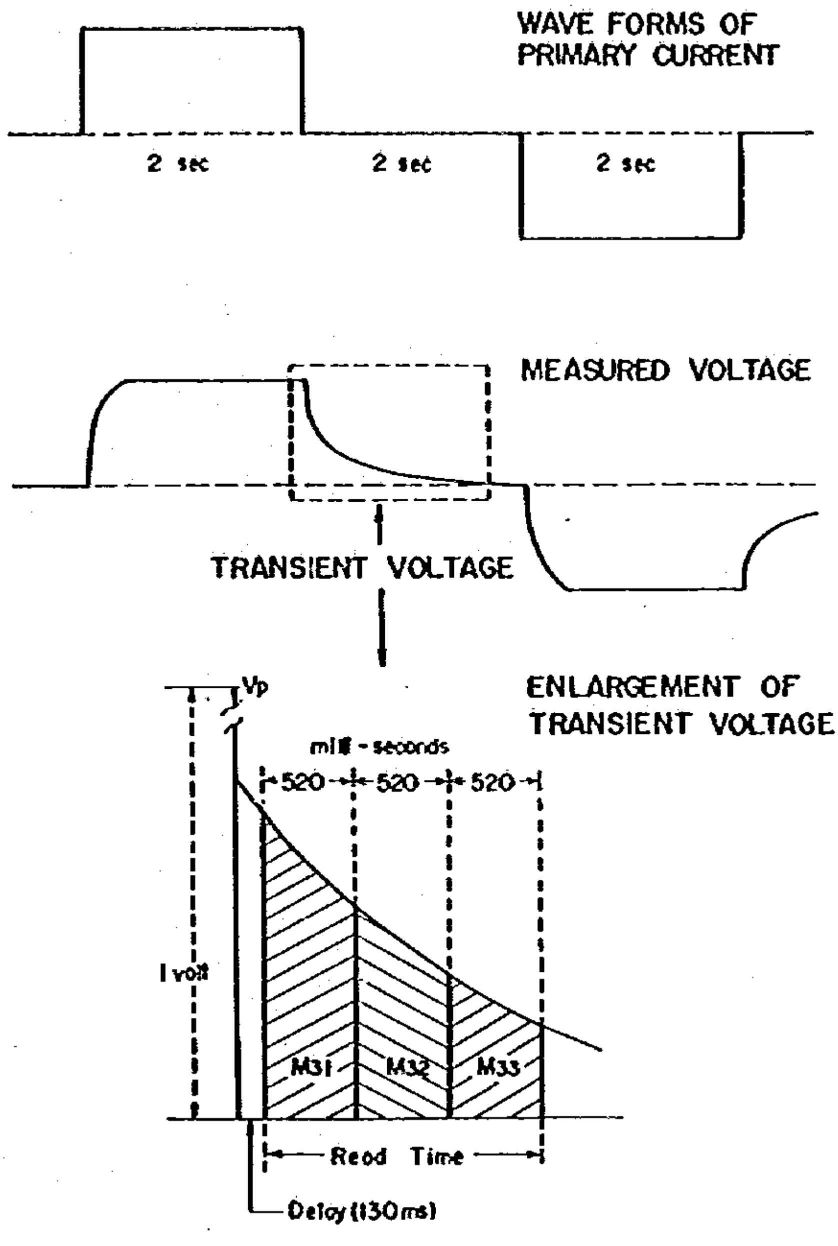

Fig. 4-4 Wave Forms of Primary Current and Measured Voltage

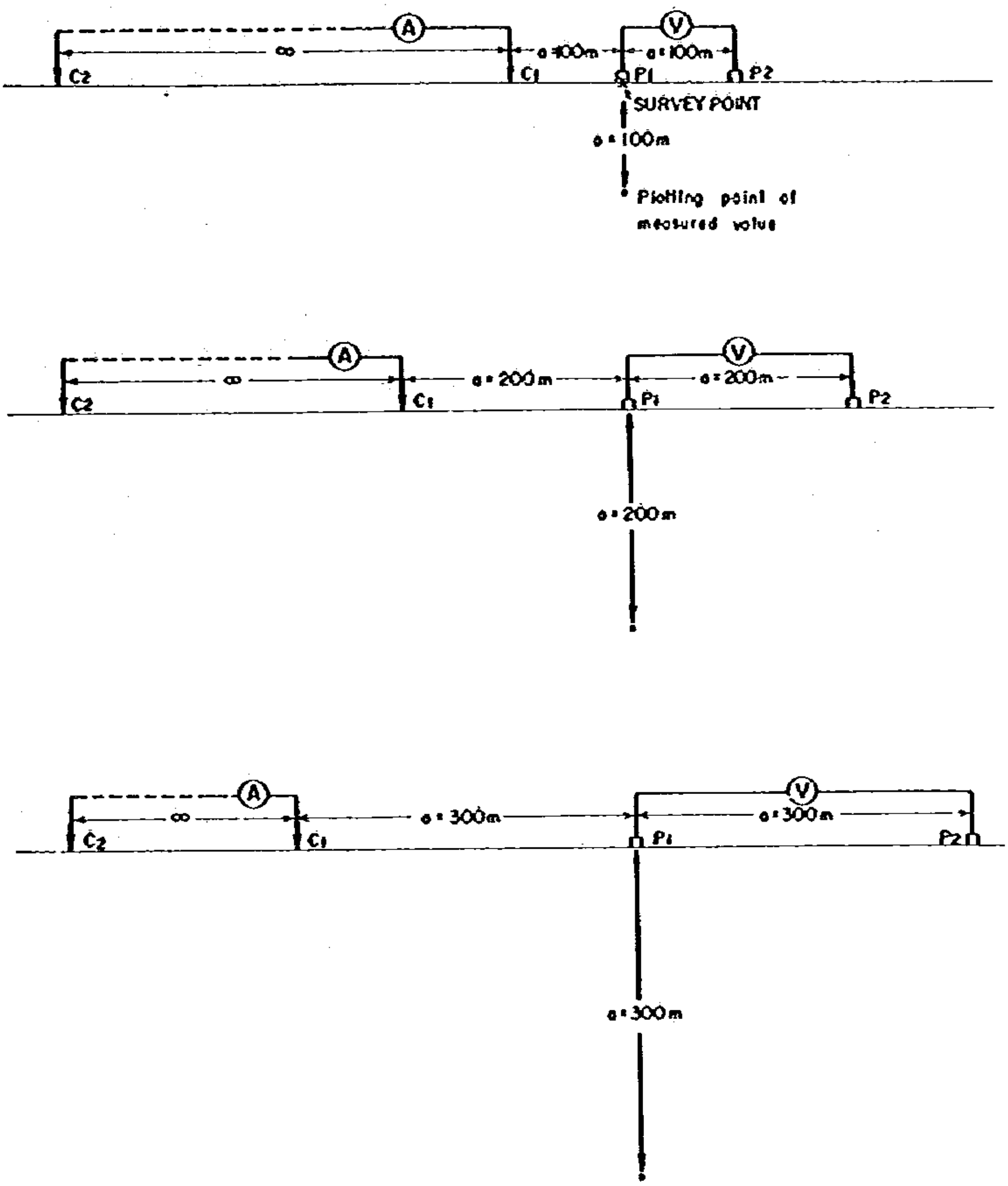

Fig.4-5 Electrode Configuration of Pole - Dipole Array

4-4 Analysis of Survey Results

4-4-1 El TEJOCOTE Area

Survey results and the result of calculation were shown in PL. 4-1 (MAPS OF IP SURVEY, EL TEJOCOTE AREA), Fig. 4-7 ∿ 4-11 (IP profiles), Fig. 4-12 ∿ 4-16 (ρa profiles) and Fig. 4-17 ∿ 4-21 (AMF profiles).

4-4-1-1 Analysis of Chargeability Maps

The chargeability measured in the survey area is very small in values such as 0.67 milli-second in minimum and 4.13 milli-seconds in maximum (milli-second is abbreviated hereafter) as shown in the chargeability maps (PL. 4-1, M-1, M-2 and M-3).

The average, minimum and maximum values of chargeability at each depth (a = 100, 200 and 300 meters) are as follows, and the chargeability increases with the increase of depth:

	a = 100 m.	a = 200 m.	a = 300 m.
Min. ∿ Max.	0.87 ∿ 3.67	0.67 ∿ 3.63	0.78 ∿ 3.83
Average	2.21	2.22	2.29
Anomalous zone	≧2.50	≧2.50	≧2.60

Supposing here that the values above the additional 10 percent of the average are to be anomalous, $M \geq 2.5$ (M is chargeability) at a = 100 m, a = 200 m and $M \geq 2.6$ at a = 300 m are the anomalies of chargeability. The values smaller than these are to be considered the background values in the area. The size of anomalies was classified into three categories of 'small', 'medium' and 'grand' by the number of survey point in an area confined by the contour line when M = 2.5, such as 2 and less, 3 to 5 and 6 and over respectively, provided that the values of $M < 2.6$ are to be considered anomalous even if at a = 300 m, for those having close relation to the anomalies at a = 100 and 200 m.

The marks such as A(a = 100), B(a = 100), ... were put for each anomaly.

(1) Chargeability map at a = 100 m (See M-1 in PL. 4-1)

A(a = 100) : 2.60 ∿ 2.87, medium.

B(a = 100) : 2.53, small, anomaly by one survey point.

C(a = 100) : 2.67, small, anomaly by one survey point.

D-1(a = 100) : 2.50∿ 2.67, medium.

D-2(a = 100) : 2.87, small, anomaly by one survey point.

E-1(a = 100) : 2.70, small, anomaly by one survey point.

E-2(a = 100) : 2.63, small, anomaly by one survey point.

F(a = 100) : 2.57, small, anomaly by one survey point.

G(a = 100) : 2.50 ∿ 3.00, medium.

H(a = 100) : 2.57 ∿ 3.53, medium.

I(a = 100) : 2.50 ∿ 2.67, grand.

J(a = 100) : 2.57 ∿ 3.13, medium.

K(a = 100) : 2.60 ∿ 3.67, grand. Maximum value of anomaly at a = 300 m.

This is a large anomaly further connecting toward the south.

L(a = 100) : 2.50 ∿ 3.07, medium.

M(a = 100) : 2.73, small, anomaly by one survey point.

N(a = 100) : 2.63 ∿ 2.83, medium.

O(a = 100) : 2.67, small.

No anomaly has been detected at a = 200 and 300 m to correspond the anomalies of M, N and O.

(2) Chargeability map at a = 200 m (See M-2 in PL. 4-1)

A(a = 200) : 2.93, small, anomaly by one survey point.

B(a = 200) : 2.50 ∿ 3.10, medium.

C(a = 200) : 2.57, small, anomaly by one survey point.

D(a = 200) : 3.07, small, anomaly by one survey point.

Two anomalies of D-1 and D-2 were detected at a = 100 m, but one isolated anomaly was observed at a = 200 m.

E-1(a = 200) : 2.50∿ 3.63, grand. 3.63 is maximum value of anomaly at a = 200 m.

E-2(a = 200) : 2.73, small, anomaly by one survey point.

F(a = 200) : 2.53 ∿ 3.17, medium.

G(a = 200) : 2.60 ∿ 3.00, grand.

H-1(a = 200) : 3.33, small, anomaly by one survey point.

H-2(a = 200) : 2.69, small, anomaly by one survey point.

H-1 and H-2 become one isolated anomaly H at a = 100 and 300 m.

I(a = 200) : 2.60 ∿ 2.90, medium.

J(a = 200) : 2.50 ∿ 3.00, medium.

K(a = 200) : 2.60 ∿ 2.87, grand, considered further to expand southward.

P(a = 200) : 2.63, small, anomaly by one survey point, and no anomaly has been observed to correspond to it at a = 100 and 300 m.

(3) Chargeability map at a = 300 m (See M-3 in PL. 4-1)

A-1(a = 300) : 2.57, small, anomaly by one survey point.

A-2(a = 300) : 2.90, small, anomaly by one survey point.

These anomalies formed an isolated anomaly A at a = 100 and 200 m, which was observed as two separate anomalies at a = 300 m.

B-1(a = 300) : 2.53, small, anomaly by one survey point.

B-2(a = 300) : 2.60, small, anomaly by one survey point.

These anomalies also formed an isolated anomaly B at a = 100 and 200 m.

C(a = 300) : 2.60 ∿ 3.00, medium. This anomaly is strongly possible to expand further northward.

D(a = 300) : 2.50 ∿ 2.83, medium.

E(a = 300) : 2.50 ∿ 3.00, grand.

F(a = 300) : 2.63 ∿ 3.17, grand. This anomaly is strongly expand further eastward.

G(a = 300) : 2.57 ∿ 3.00, medium.

H(a = 300) : 2.87, small, anomaly by one survey point.

I(a = 300) : 2.70 ∿ 3.83, grand. It has the strongest chargeability among the anomalies at a = 300 m.

J-1(a = 300) : 2.60 ∿ 3.00, medium.

J-2(a = 300) : 2.70 ∿ 3.00, medium. J-1 and J-2 formed an isolated anomaly J at a = 100 and 200 m.

K(a = 300) : 3.00 ∿ 3.23, grand. This anomaly is strongly possible to expand further southward.

L(a = 300) : 2.60 ∿ 2.87, medium.

As described above, the distribution of anomalies takes such complicated forms that an isolated anomaly at a certain depth becomes two separate ones at other depths and that they occur as anomalies to be observed at a definite depth and anomalies which can be observed at all depths. These were summarized to a table shown in the following.

Table 4 − 1 Measured Chargeability Anomaly (EL TEJOCOTE Area)

Name of Anomaly \ a	100m			200m			300m		
	Magnitude	Average	Max.Value	Magnitude	Average	Max.Value	Magnitude	Average	Max.Value
A − 1	} A,○	2.75	2.87	} A,o	2.93*	2.93*	o	2.57*	2.57*
A − 2							o	2.90*	2.90*
B − 1	} B,o	2.53*	2.53*	} B,◎	2.82	3.10	o	2.53*	2.53*
B − 2							o	2.60*	2.60*
C	o	2.67*	2.67*	o	2.57*	2.57*	○	2.74	3.00
D − 1	○	2.61	2.67	} D,o	3.07*	3.07*	} D,○	2.72	2.83
D − 2	o	2.87*	2.87*						
E − 1	o	2.70*	2.70*	◎	2.86	3.63	} E,◎	2.75	3.00
E − 2	o	2.63*	2.63*	o	2.73*	2.73*			
F	o	2.70	2.87	○	2.90	3.17	◎	2.80	3.17
G	○	2.74	3.00	◎	2.72	3.00	○	2.69	3.00
H − 1	} H,○	2.89	3.53	o	3.33*	3.33*	} H,o	2.87*	2.87*
H − 2				o	2.50	2.69			
I	◎	2.62	2.67	○	2.74	2.90	◎	3.12	3.83
J − 1	} J,○	2.76	3.13	} J,○	2.69	3.00	○	2.77	3.00
J − 2							○	2.90	3.00
K	◎	2.88	3.67	◎	2.76	2.87	◎	3.15	3.23
L	○	2.79	3.07	◎	2.73	3.07	○	2.76	2.86
M	o	2.73*	2.73*	−	−	−	−	−	−
N	○	2.71	2.83	−	−	−	−	−	−
O	o	2.67*	2.67*	−	−	−	−	−	−
P	−	−	−	o	2.63*	2.63*	−	−	−
Q	−	−	−	o	3.33*	3.33*	−	−	−
R	−	−	−	o	3.57*	3.57*	−	−	−

Magnitude: ◎ = grand, ○ = medium, o = small. *: Anomaly by one survey point. Average: Average value in anomalous zone. unit: milli-sec.

4-4-1-2 Analysis of Maps of Apparent Resistivity

Maps of apparent resistivity (PL. 4-1, M-4, M-5, and M-6) show that apparent resistivity ρa of the survey area was 174 Ω-m in minimum, 3716 Ω-m in maximum and 653 Ω-m in average of the whole measured values (Ω-m is abbreviated hereafter), which show slightly lower values as that of resistivity in the terrain of limestone. The maximum, minimum and average values at each depth are as follows:

	a = 100 m	a = 200 m	a = 300 m
Min. ∿ Max.	184 ∿ 3716	174 ∿ 3255	176 ∿ 2601
Average	646	658	655

The average values seem to show a uniform geologic structure, broadly speaking, from the surface of the area up to the depth of 300 meters in regard to apparent resistivity. In addition, the zones of low resistivity are well consistent with the distribution of the valleys, which leads to the estimation that these zones of low resistivity are consistent with the distribution of ungerground water.

In order to investigate the relation between apparent resistivity ρa and chargeability M, anomalous zones of chargeability at each depth described in the clause 4-4-1-1 were transcribed to the maps of apparent resistivity, of which average of ρa among these anomalous zones were found and listed in the following table.

Although $\overline{M}'$ and $\overline{\rho a}'$ are the averages of $\overline{M}$ and $\overline{\rho a}$ respectively at three depths of each anomaly, it will be an effective mean to examine the relation between $\overline{M}'$ and $\overline{\rho a}'$ in order to investigate the three dimensional characters of the IP anomalies. Fig. 4-6 shows these relations.

Table 4－2 Average of Chargeability and Apparent Resistivity in Anomalous Zones of Chargeability (EL TEJOCOTE Area)

a / Name of Anomaly	100m			200m			300m			100~300m	
	Magnitude	$\bar{M}$	$\bar{\rho}a$	Magnitude	$\bar{M}$	$\bar{\rho}a$	Magnitude	$\bar{M}$	$\bar{\rho}a$	$\bar{M}$	$\bar{\rho}a'$
A－1	} A, ○	275	710	} A, o	293*	1908*	o	257*	740*	} A, 279	1331
A－2							o	290*	1964*		
B－1	} B, o	253	419	} B, ◎	282	949	o	253*	1377*	} B, 269	843
B－2							o	260*	625*		
C	o	263*	660*	o	257*	318*	○	274	675	266	551
D－1	○	261	796	} D, o	307*	543*	} D, ○	272	713	} D, 282	795
D－2	o	287*	1131*								
E－1	o	270*	1100*	◎	286	576	} E, ◎	275	409	} E, 273	791
E－2	o	263*	1355*	o	273*	514*					
F	o	270	375	○	290	468	◎	280	667	280	503
G	○	274	705	◎	272	741	○	269	633	272	693
H－1	} H, ○	289	1682	o	333*	3255*	} H, o	287*	672*	} H, 295	1526
H－2				o	269	494					
I	◎	262	672	○	272	524	◎	312	546	283	581
J－1	} J, ○	276	911	} J, ○	269	893	○	277	773	} J, 278	916
J－2							○	290	1085		
K	◎	288	1628	◎	276	1559	◎	315	1223	293	1470
L	○	279	576	◎	273	329	○	276	453	276	453
M	o	273	431	－	－	－	－	－	－	－	－
N	○	271	881	－	－	－	－	－	－	－	－
O	o	267	612	－	－	－	－	－	－	－	－
P	－	－	－	o	263*	240*	－	－	－	－	－
Q	－	－	－	o	333*	452*	－	－	－	－	－
R	－	－	－	o	357*	243*	－	－	－	－	－
Average of all anomalous values										278	871
Average of all measured values										224	653

Magnitude: ◎ = grand, ○ = medium, o = small.

*: Anomaly by one survey point. $\bar{M}$: Average of chargeability

$\bar{\rho}a$: Average of apparent resistivity.

The study of the figure leads to describe the following things.

(1) The anomalous zones can be divided into three groups of I, II and III by the difference of ρa.

(2) In terms of $\bar{M}'$, no marked difference was found among the three groups, but a distinct difference is found in the values of ρa'. The average values of ρa in the group, are 1442 Ω-m, 837 Ω-m and 556 Ω-m in the order of I, II and III, among which I is extremly great compared with II and III. The difference of values of ρa seems to show the difference of lithology.

(3) The geological map (PL. 2-2-1) shows the occurrence of plutonic rocks to the north of A and to the south of K, both of which belong to the group I, and it is considered that A and K are the anomalies to be related to these plutonic rocks. H seems also to be similar to K.

(4) In terms of ρa of II and III groups, that of II is about 200 Ω-m greater than the average of the whole measured values, and that of III is about 100 Ω-m smaller than the average. Although these are not considered to be especially significant difference, the anomalies which belong to II and III seem to be caused by the medium in limestone which might have more strong IP effect than the average of the whole point.

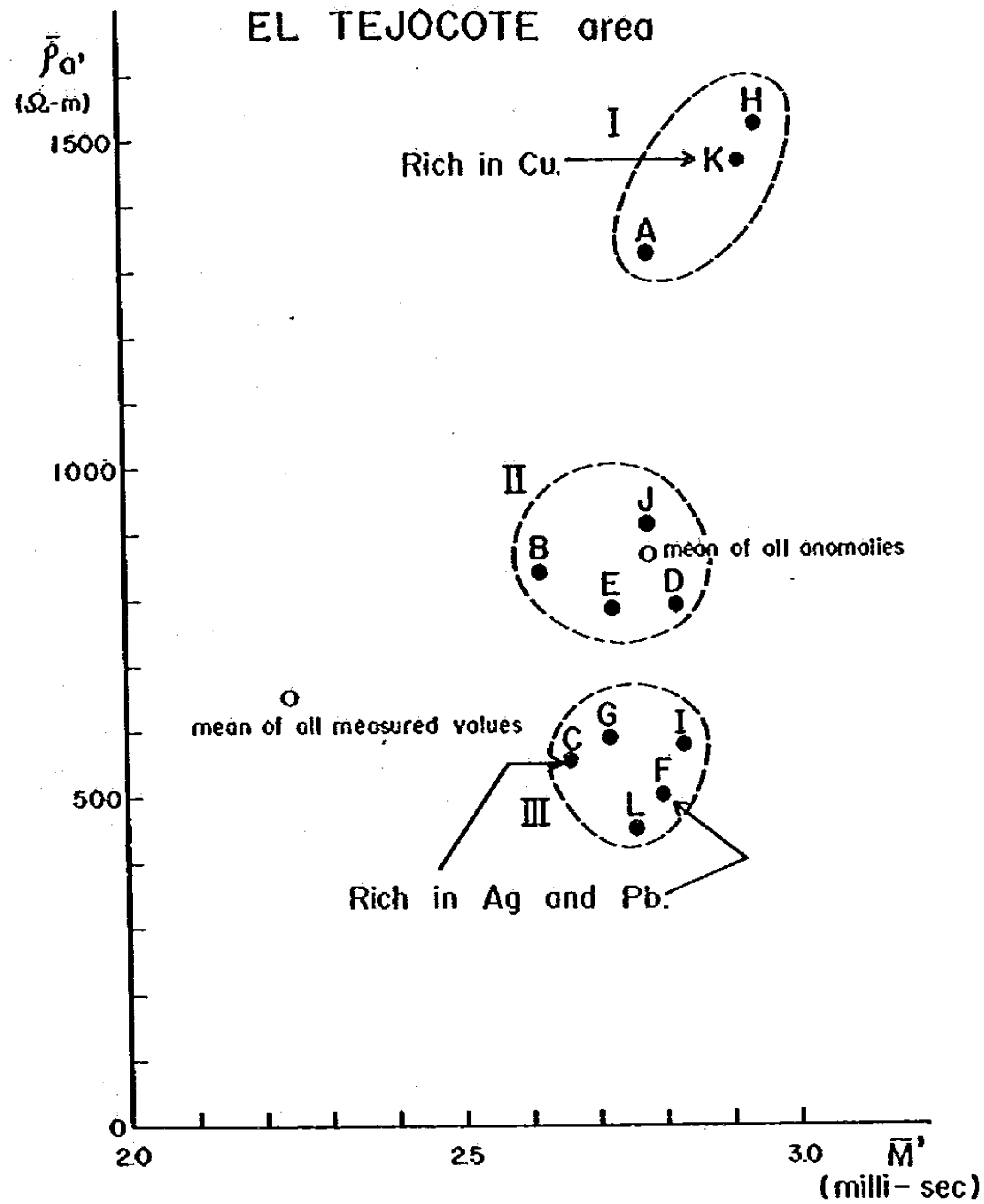

Fig. 4-6 Relation of chargeability and apparent resistivity inside the IP anomalous zone.

4-4-1-3 Analysis of Maps of Apparent Metal Factor

Apparent metal factor is defined by the next formula as mentioned in 4-3.

$$AMF = \frac{M}{\rho a} \times 1000 \text{ (milli-sec/}\Omega\text{-m)}$$

Since the range of variation of M in this area is very small compared with that of ρa, M can be considered constant. Therefore AMF becomes small where ρa is great. On the contrary, at the place where the variation of M is great and that of ρa is small, AMF becomes great, and the AMF map becomes to be similar to the pattern of M map.

As shown in M-7, M-8 and M-9 of PL. 4-1, the values of AMF are small where ρa is great in Figures M-4, 5 and 6, and those of AMF are great where ρa is small.

Although the AMF map is quite similar to the pattern of contours in the ρa maps (M-4, M-5 and M-6) in which H was replaced by L and L by H, no distinct correlation with the pattern of IP maps (M-1, M-2 and M-3) has been observed.

4-4-1-4 Profile Analysis

The result of analysis of profiles of chargeability (Fig. 4-7 ∿ 11), apparent resistivity (Fig. 4-12 ∿ 16) and apparent metal factor (Fig. 4-17 ∿ 21) on each survey line are shown summarized on the table because they overlap in many cases to the results of analysis of each map.

Table 4-3 Result of Profile Analysis (EL TEJOCOTE Area)

sp: survey point

Line	Anomaly name in M map (survey point)	M(milli-sec)	ρa anomaly	AMF anomaly	Remarks
L-10	L(10,11,12) M(19) N(14,15,16)	2.50 ~ 4.10 2.50 ~ 2.73 2.50 ~ 2.83	Low ρa deep below sp 10 and 11. High ρa near surface at sp 14,15,16. Low ρa deep below sp 18 and 19.	AMF anomalous pattern is similar to the ρa anomalous pattern when H(L) of ρa profile is replaced to L(H) of AMF profile.	IP anomelies are distributed at near groundsurface.
L-12	L(10,11,12) P(15)	2.50 ~ 2.69 2.50 ~ 2.63	High ρa near surface at sp 13 and 14. Low ρa below sp 15, 19 and 20.	Same as above.	IP anomaly L is remarkable a little.
L-14	A(25) D(15) L(11)	2.50 ~ 2.77 2.50 ~ 2.70 2.50 ~ 2.80	High ρa below sp16, 17 and 18. Low ρa below sp 21, 22 and 23.	Same as above.	Magnitude of IP anomaly is very small.
L-16	A(24,25) D(15,16) L(11)	2.50 ~ 2.93 2.50 ~ 3.17 2.50 ~ 2.87	High ρa near surface at sp 13,14. High ρa deep below sp 16 and 17. High ρa below sp 24 and 25	Same as above.	Three IP anomalies are distributed from near ground surface to the deep parts.
L-18	A(24) B(18,19,20) D(16,17) O(11)	2.50 ~ 2.90 2.50 ~ 3.10 2.50 ~ 2.67 2.50 ~ 2.67	High ρa with V figured from near surface of sp 12 → deep below sp 14 → near surface of sp 17. High ρa below sp 19 and 20. Low ρa below sp 21 and 22.	Same as above.	Anomalies A and B are from near surface to the deep parts. D and O are near surface anomalies.
L-20	B(18,19) E(15,16) G(10,11) I(7,8,9) R(5)	2.50 ~ 3.07 2.50 ~ 3.63 2.50 ~ 3.00 2.50 ~ 3.83 2.50 ~ 3.57	Low ρa with vertical shape below sp 6 and 12. High ρa from near surface of sp 11 to deep below of sp 9. High ρa near surface of sp 11 to deep below sp 20. Low ρa at deep below sp 16,17 and 18.	Same as above.	Many anomalies are distributed in this line. E,G and I anomalies are from near sarface to the deep parts. B and R are near surface anomalies.
L-22	C(20) E(13,14,15,16) G(11,12,13) I(5,6,7,8,9)	2.50 2.60 ~ 3.00 2.50 ~ 2.93 2.80 ~ 3.67	Low ρa at sp 5 ~ 8. High ρa at sp 9 ~ 12. Low ρa at sp 14 ~ 17. High ρa at sp 19 ~ 20. High and low ρa anomalies are distributed reciprocally.	Same as above.	Background value below sp 5 ~ 12 is relatively high. All anomalies are from near ground surface to the deep parts.
L-24	C(18,19,20) E(15) G(11,12) I(9,10) K(5,6,7)	2.50 ~ 3.33 2.50 ~ 2.73 2.50 ~ 3.00 2.60 ~ 2.73 2.70 ~ 3.23	High and low ρa anomalies are distributed reciprocally with complicated shape.	Same as above.	C,G,I and K anomalies are distributed to the deep part, but E is near surface anomaly.
L-26	C(20) F(17) H(14,15) J(11) K(5,6,7,8)	2.50 ~ 3.00 2.50 ~ 2.63 2.50 ~ 2.87 2.50 ~ 2.70 2.70 ~ 3.17	Remarkably high ρa below sp 5,6 and 10. Anomaly pattern is relatively simple.	Same as above.	All IP anomalies are distributed to the deep parts. Many anomalies are seen in this line.
L-28	F(15,16,17,18,19,20) H(12,13,14) J(9,10,11) K(5,6,7,8)	2.70 ~ 3.17 2.50 ~ 3.53 2.60 ~ 3.13 2.70 ~ 3.00	Low ρa anomalies are distinguished.	Same as above.	Many anomalies are seen in this line. H is small anomaly and all others are to the deep parts.

EL TEJOCOTE

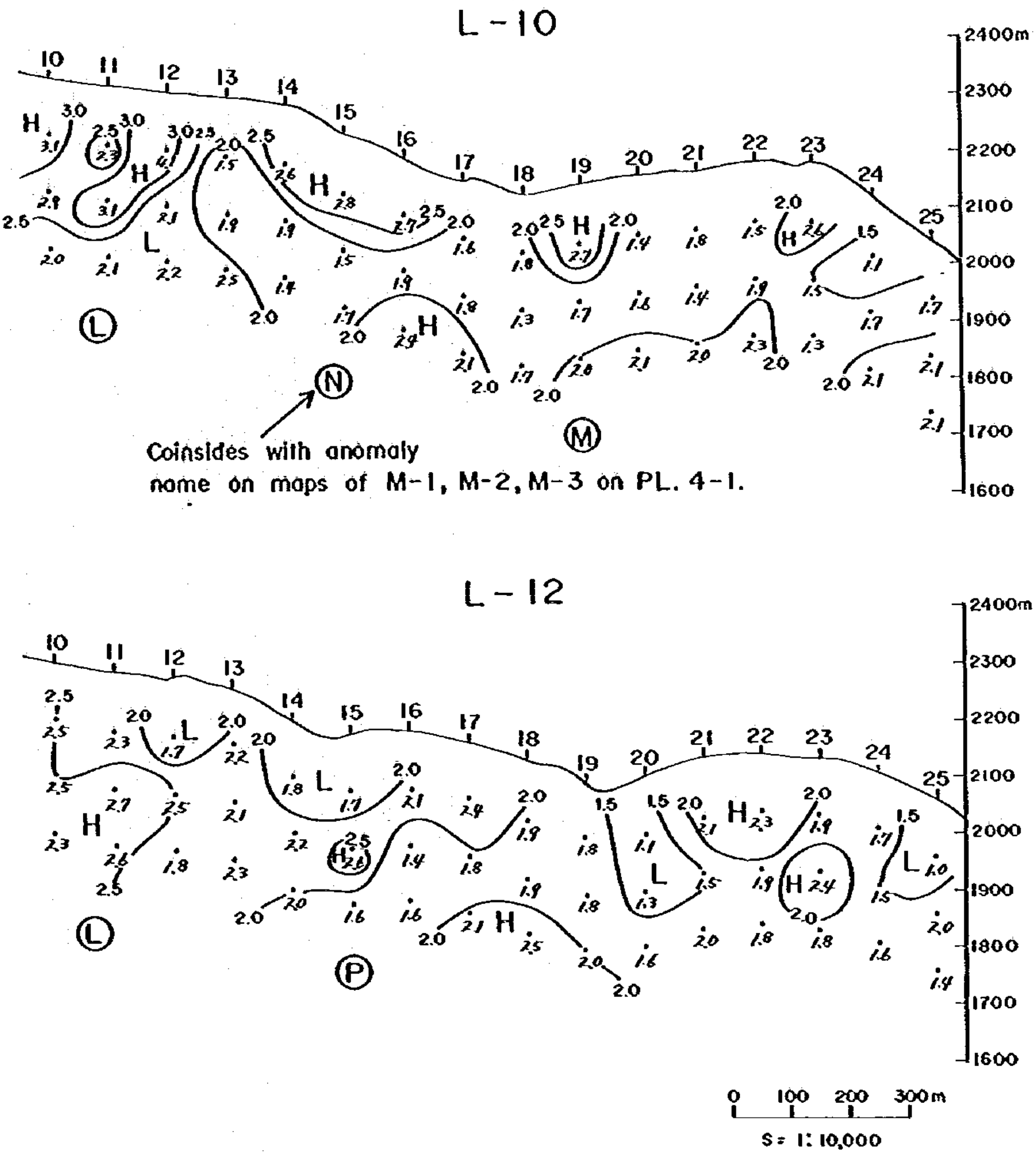

Fig. 4-7 IP profile
(Chargeability)

EL TEJOCOTE

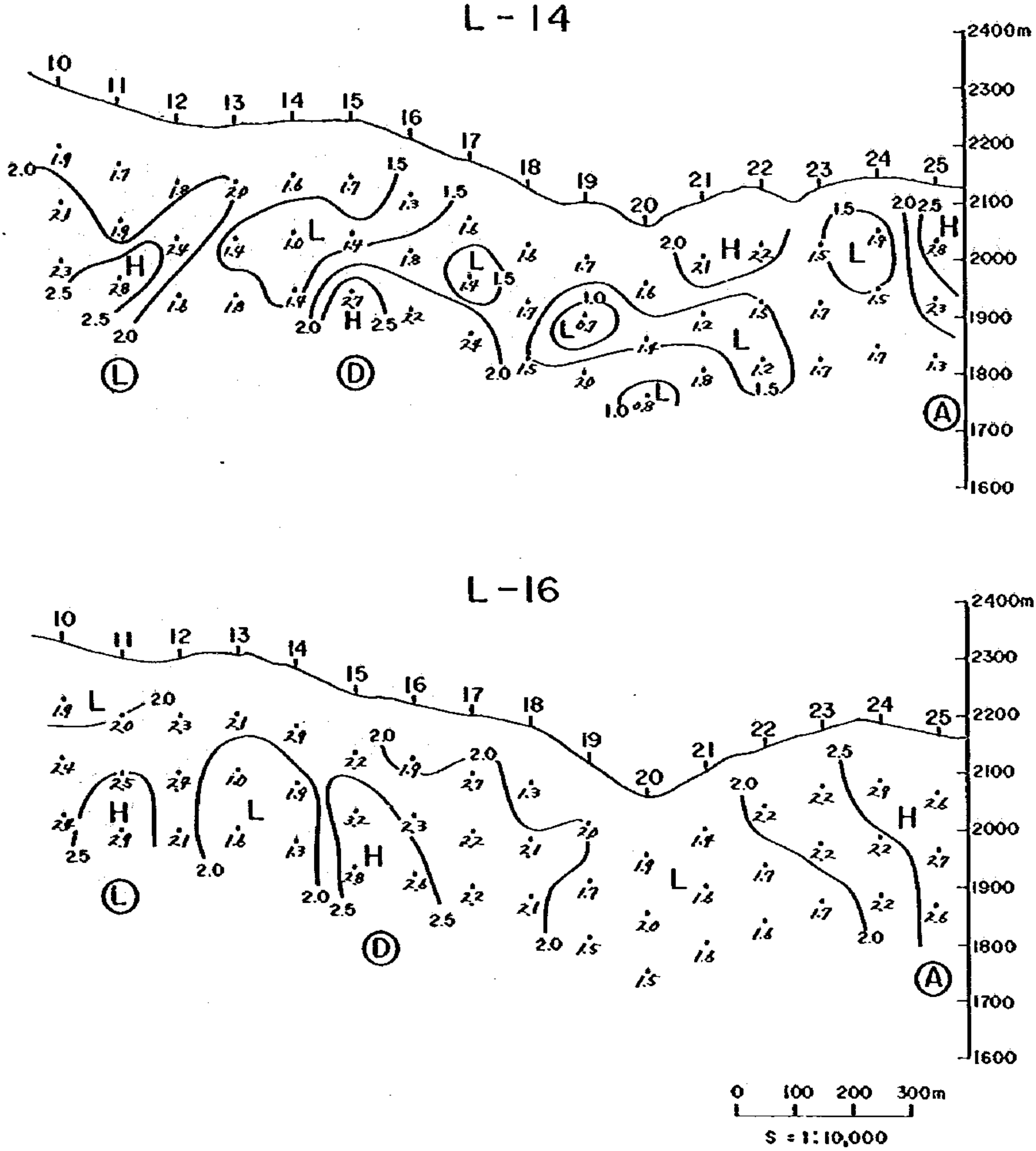

Fig. 4-8 I P profile

EL TEJOCOTE

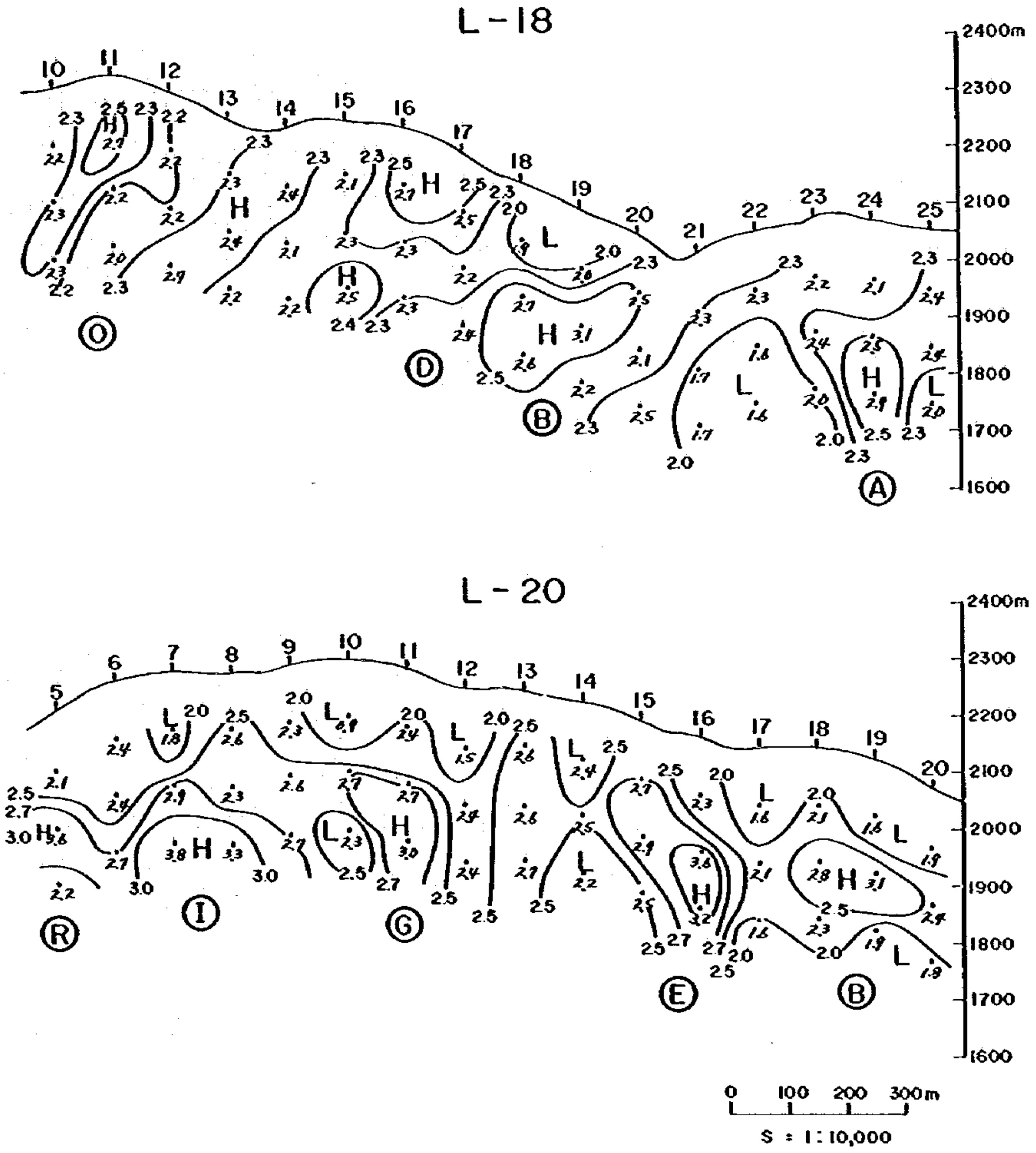

Fig. 4-9 I P profile

EL TEJOCOTE

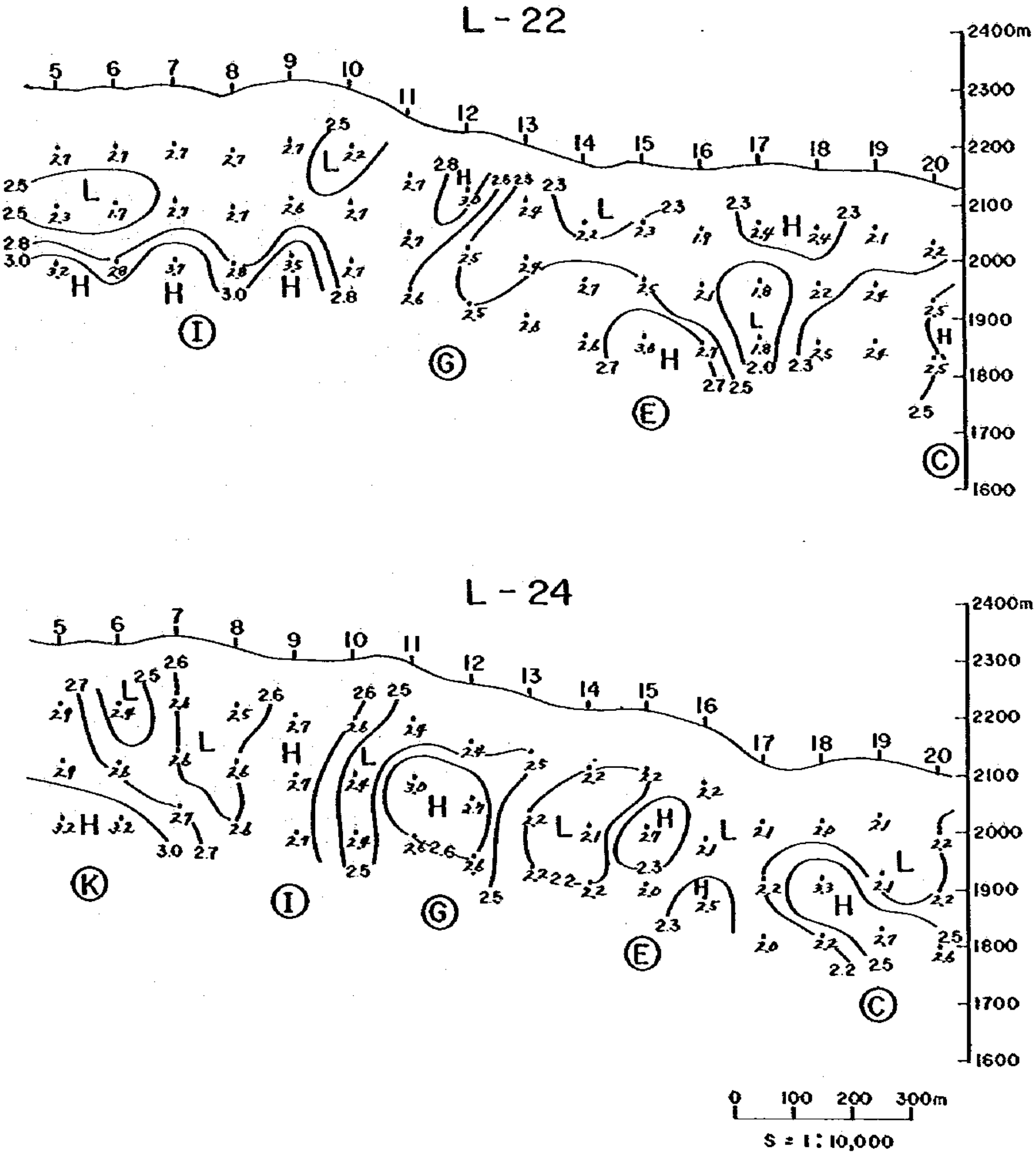

Fig. 4-10 I P profile

EL TEJOCOTE

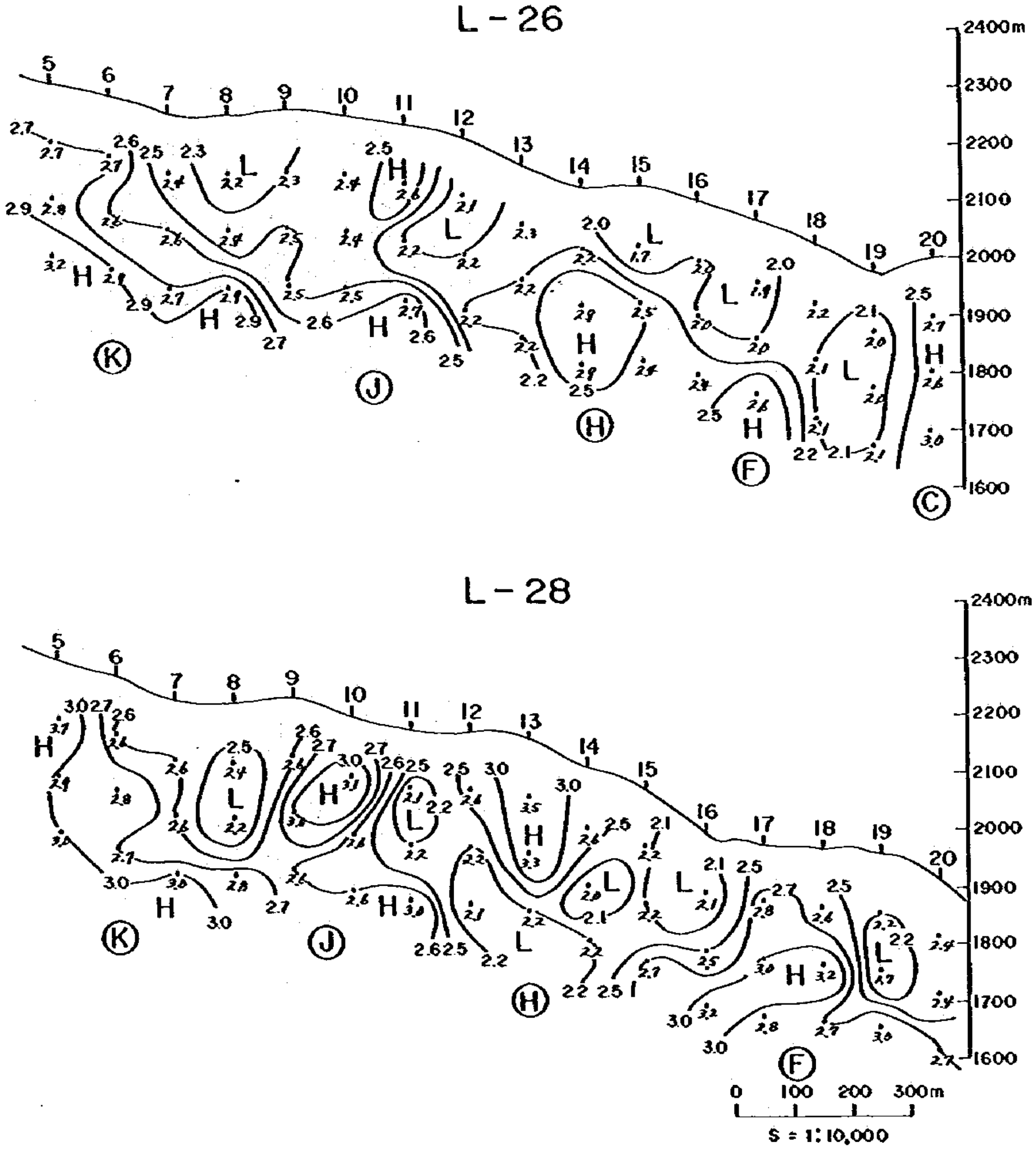

Fig. 4 - 11 IP profile

EL TEJOCOTE

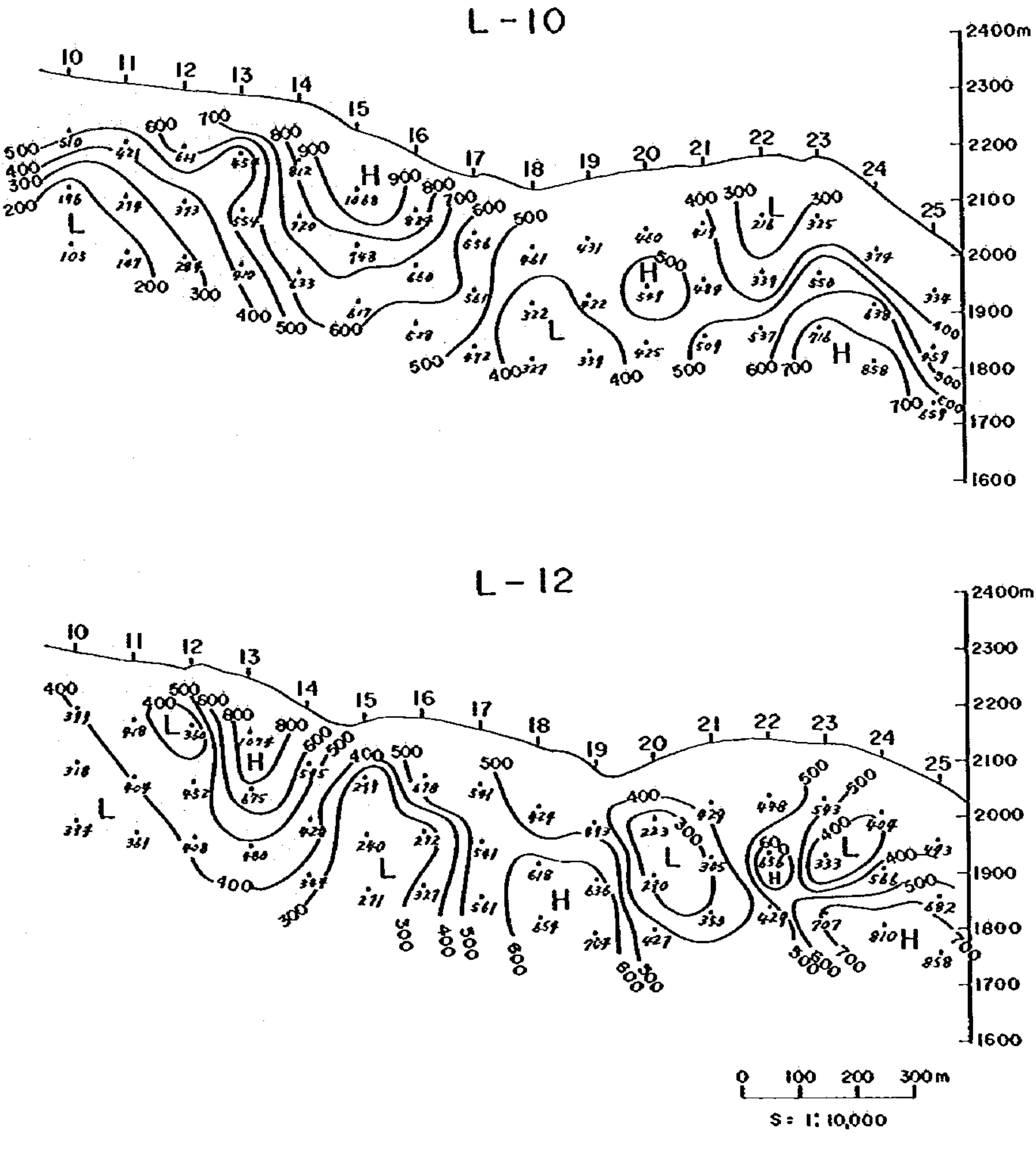

Fig. 4 - 12 ρ_a profile
(Apparent Resistivity)

EL TEJOCOTE

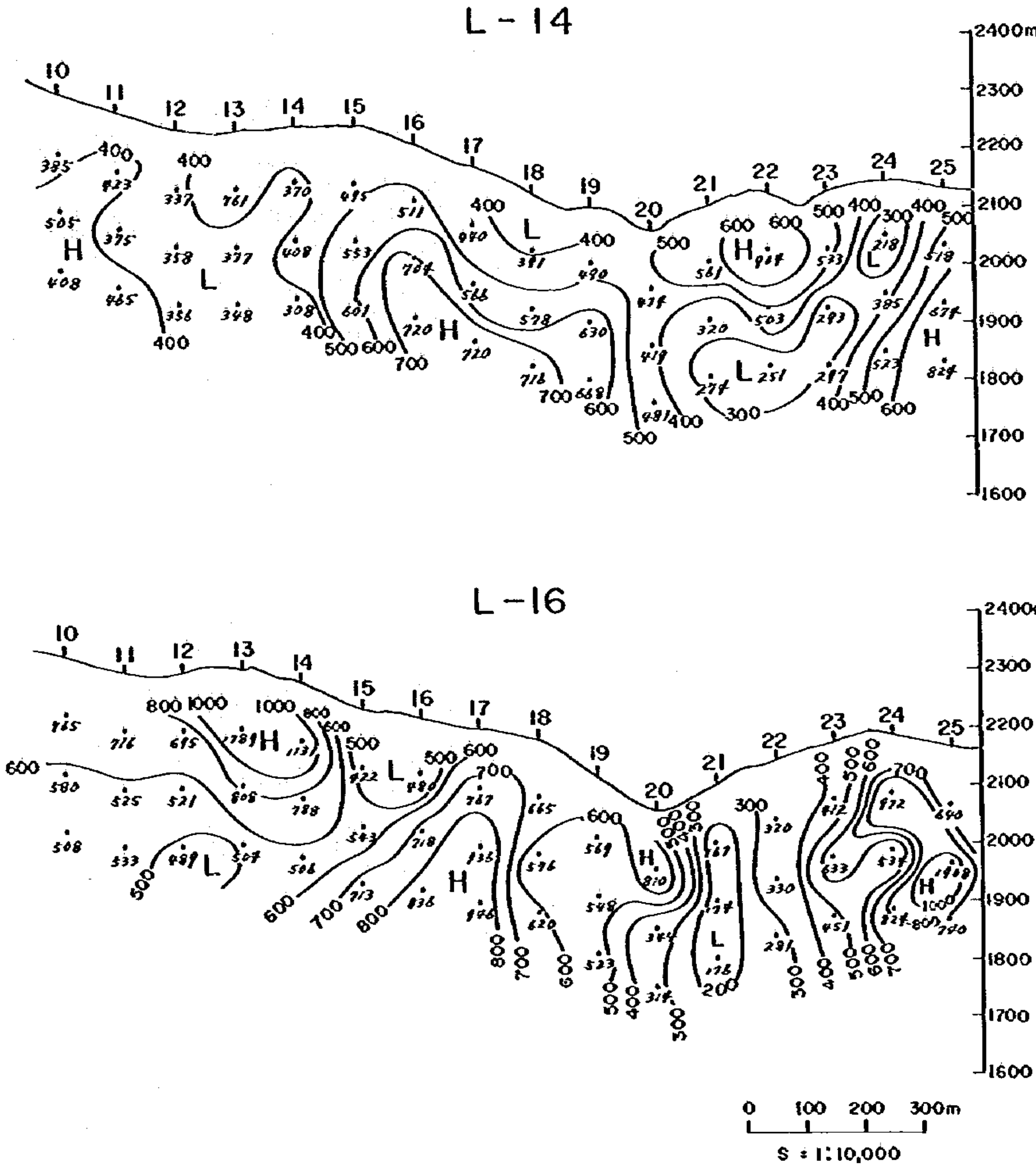

Fig. 4 - 13 ρ_a profile

EL TEJOCOTE

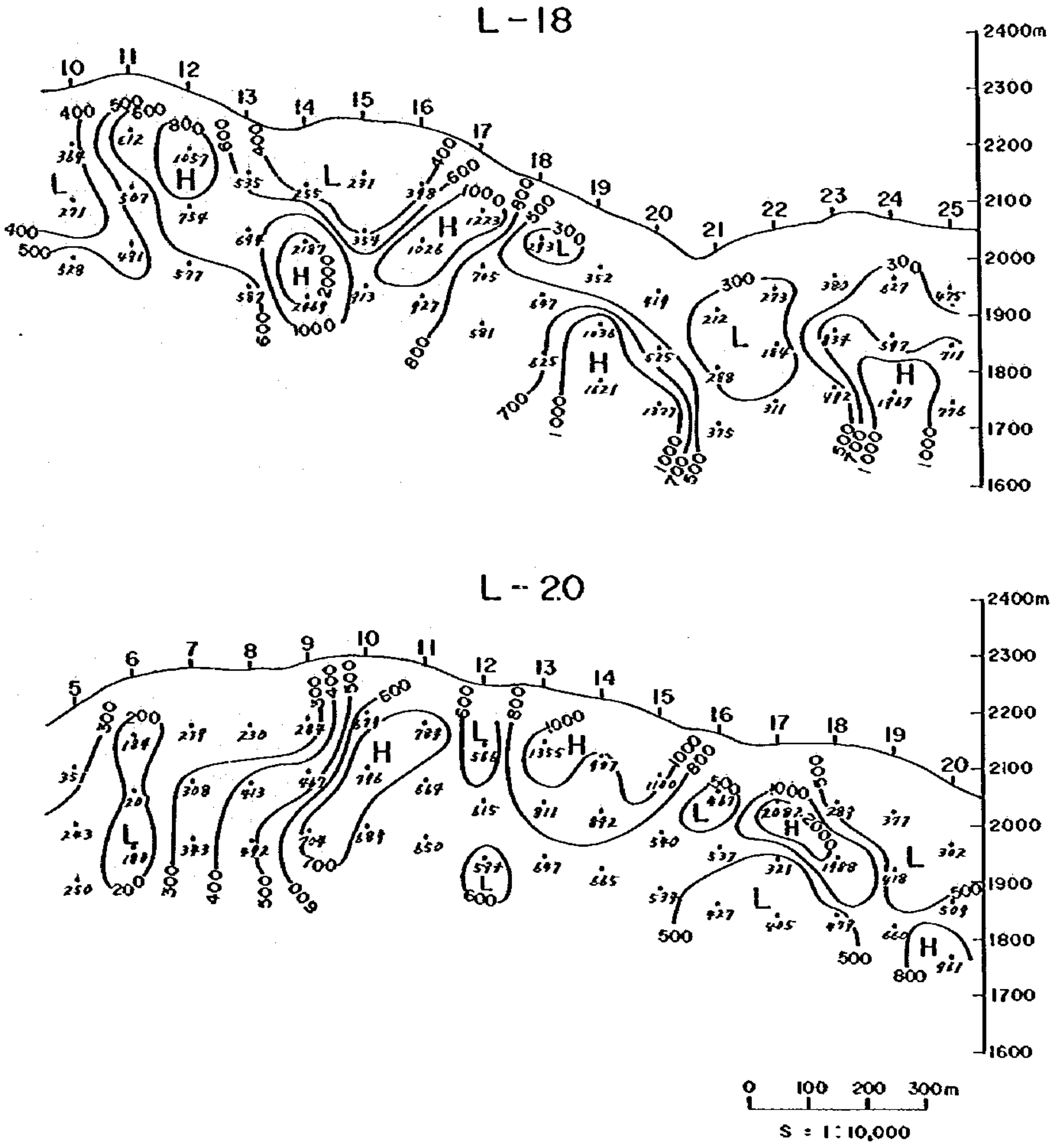

Fig. 4-14 ρ_a profile

EL TEJOCOTE

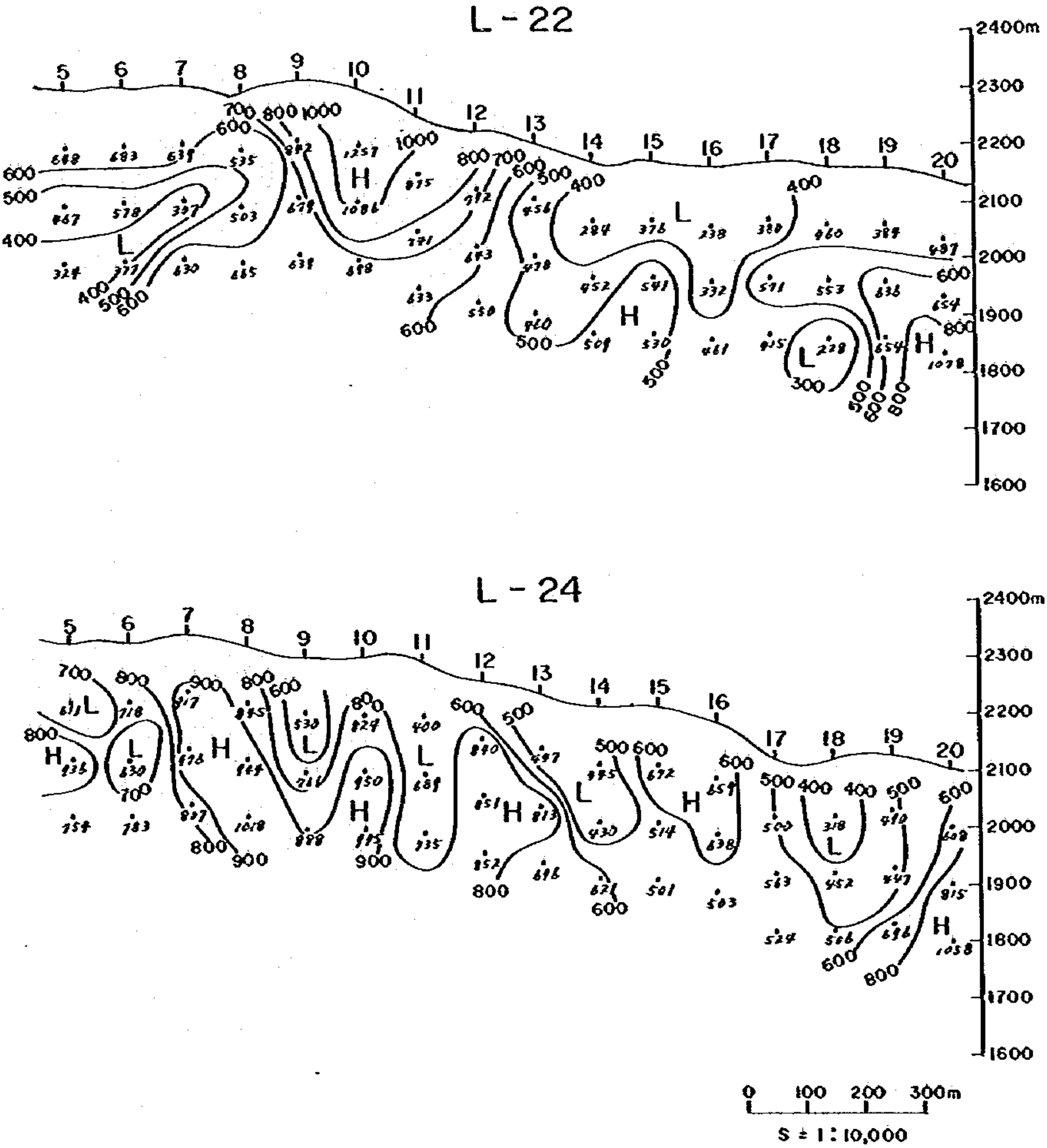

Fig. 4-15 ρ_a profile

EL TEJOCOTE

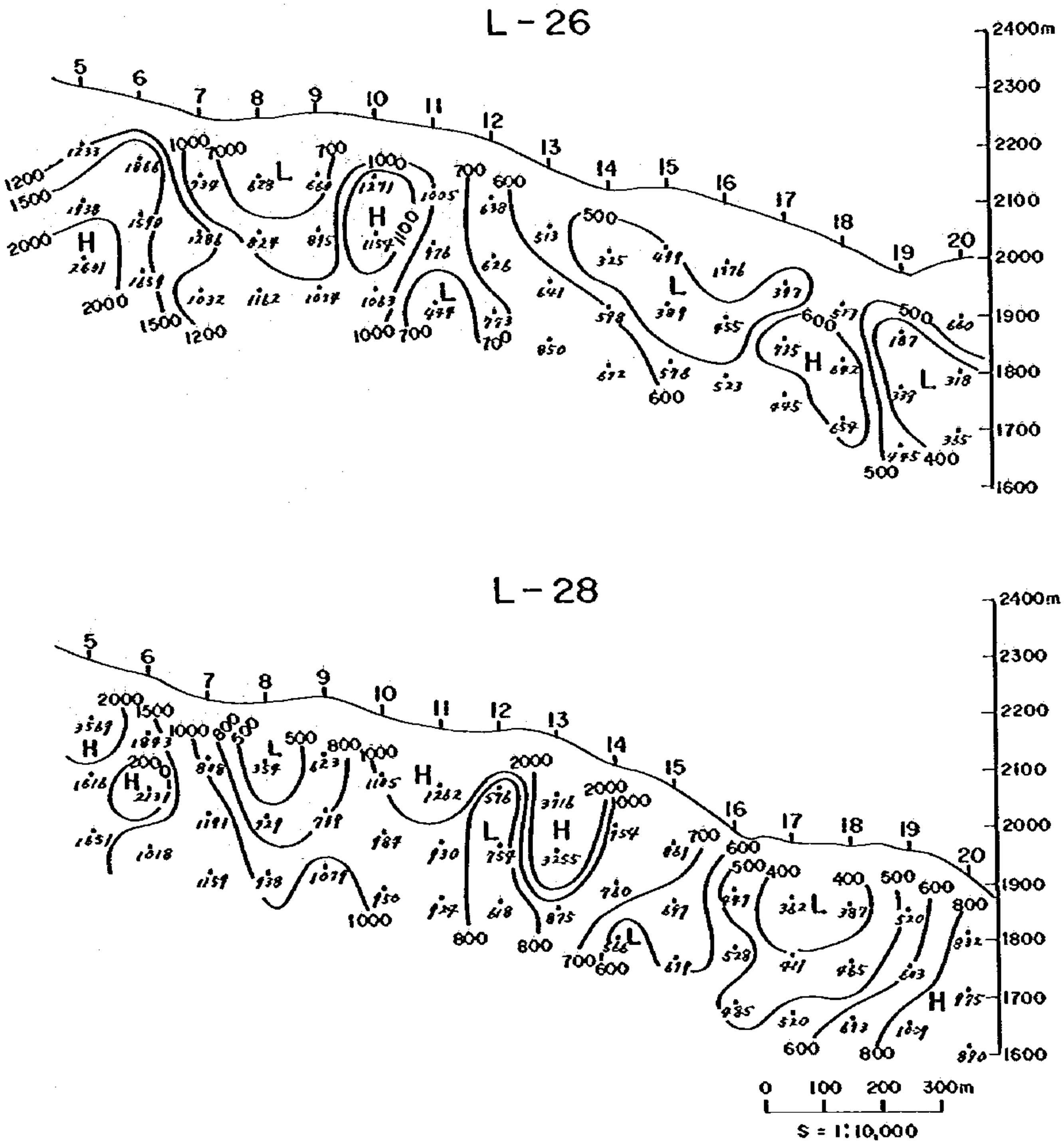

Fig. 4 - 16 ρa profile

EL TEJOCOTE

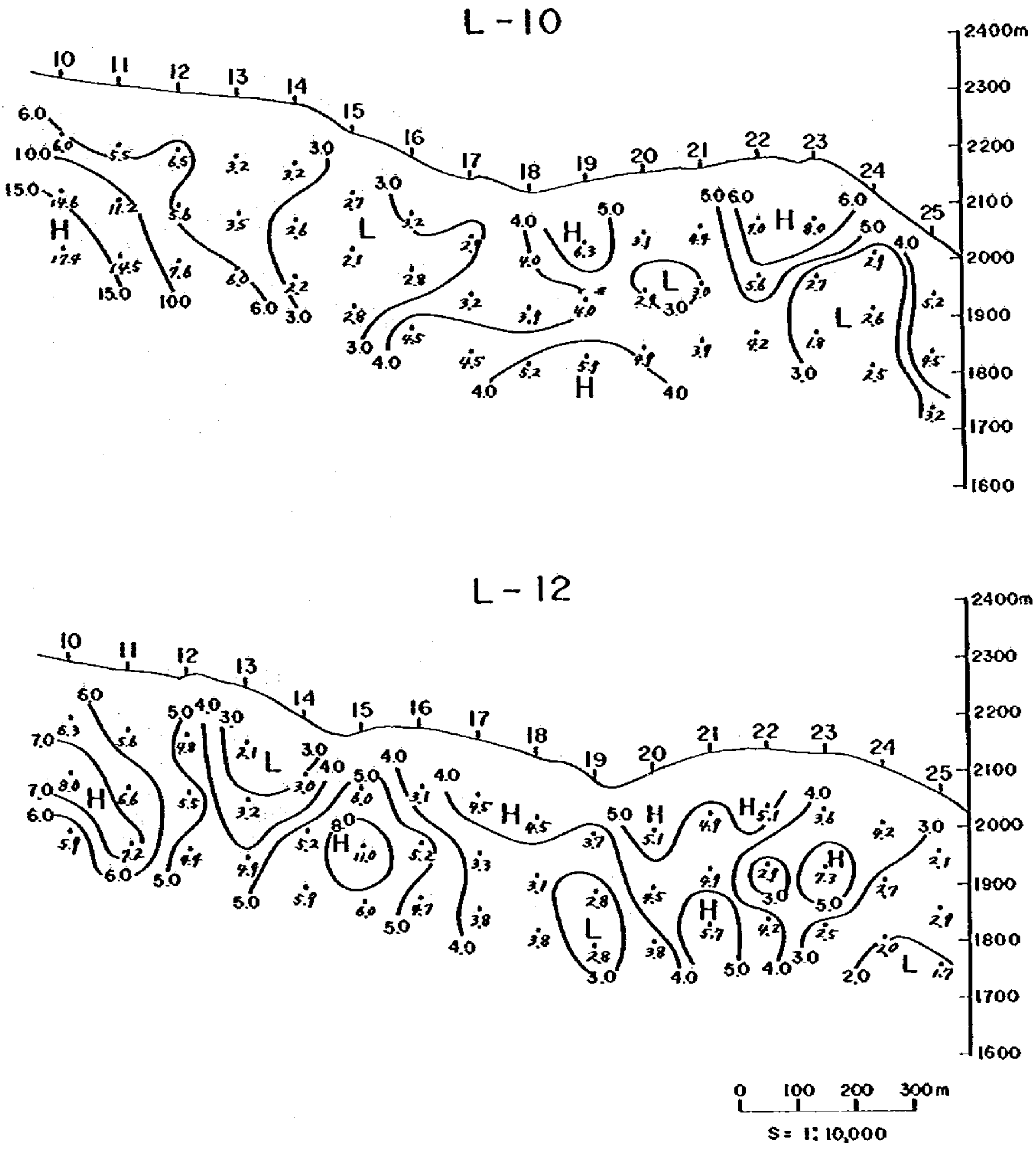

Fig. 4-17 AMF profile
(Apparent Metal Factor)

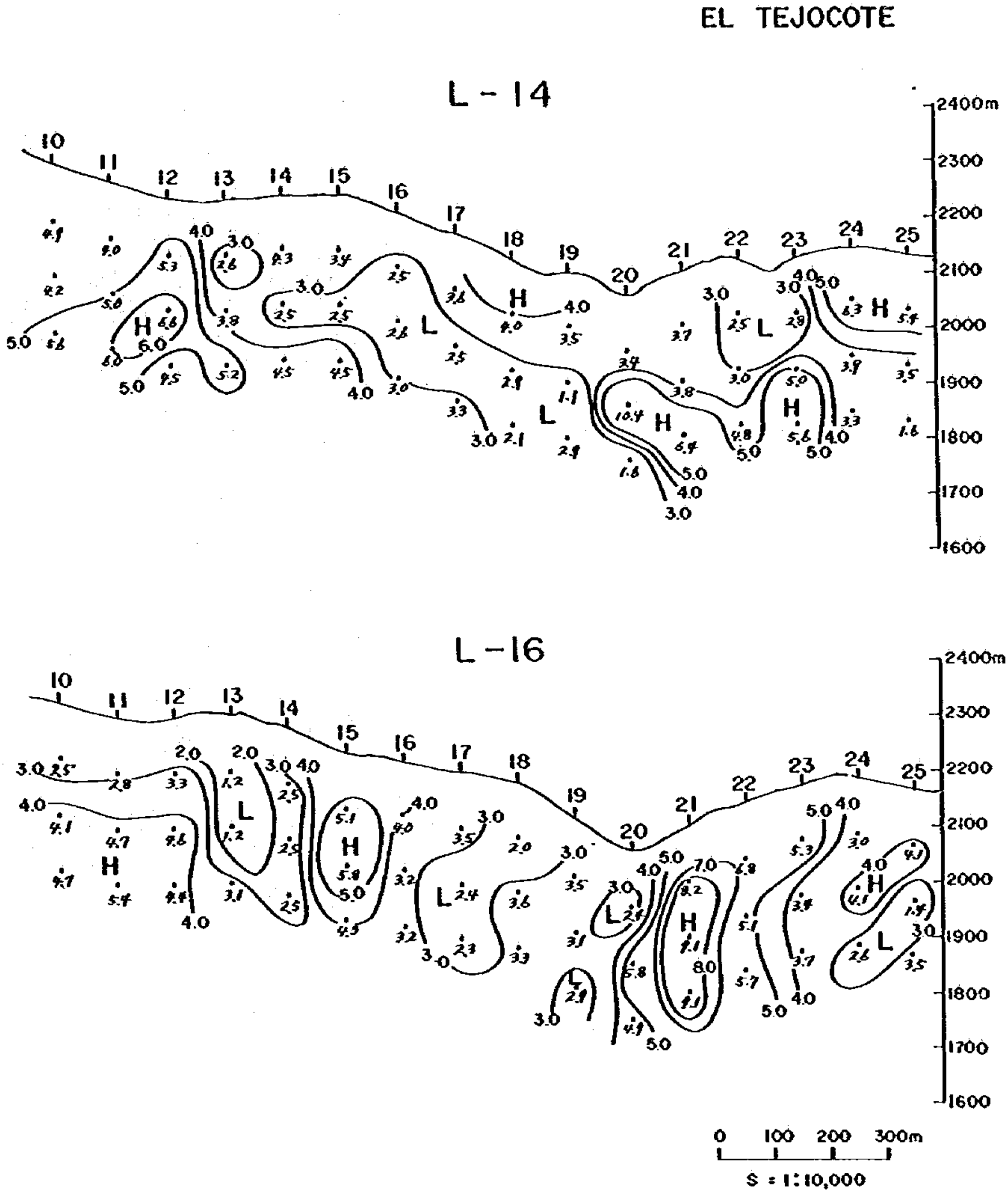

Fig. 4 -18 AMF profile

EL TEJOCOTE

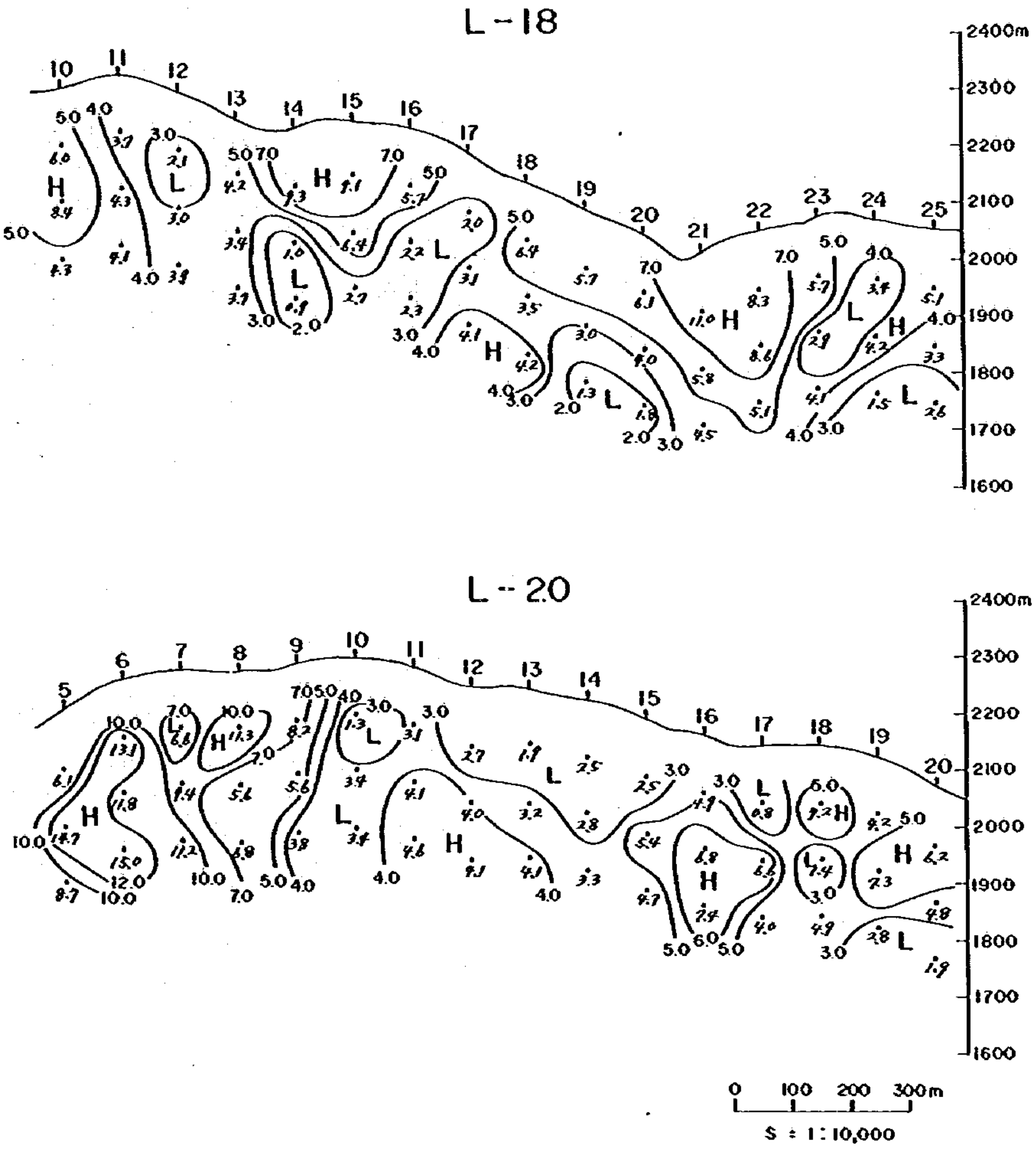

Fig. 4-19 AMF profile

EL TEJOCOTE

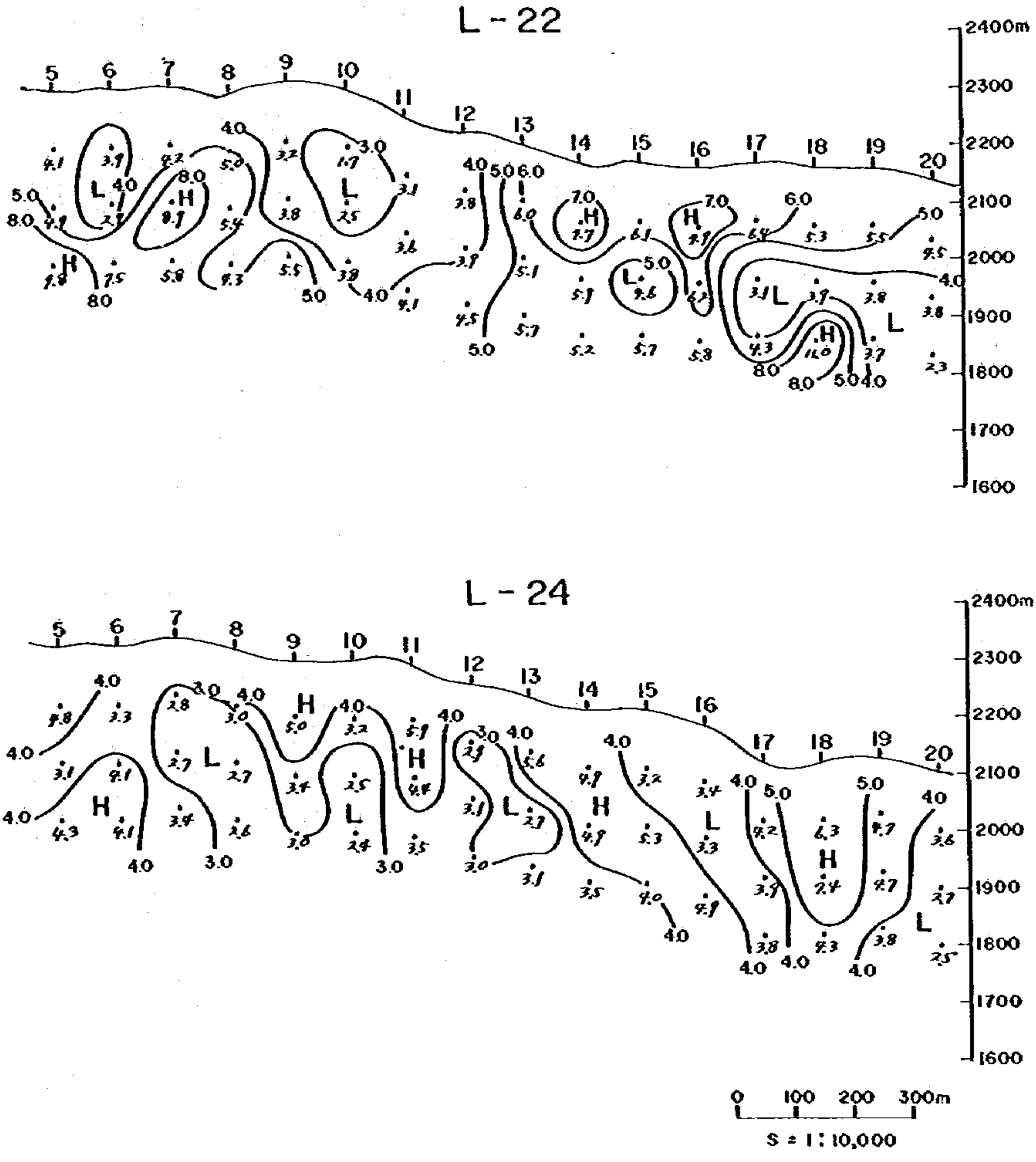

Fig. 4-20 AMF profile

EL TEJOCOTE

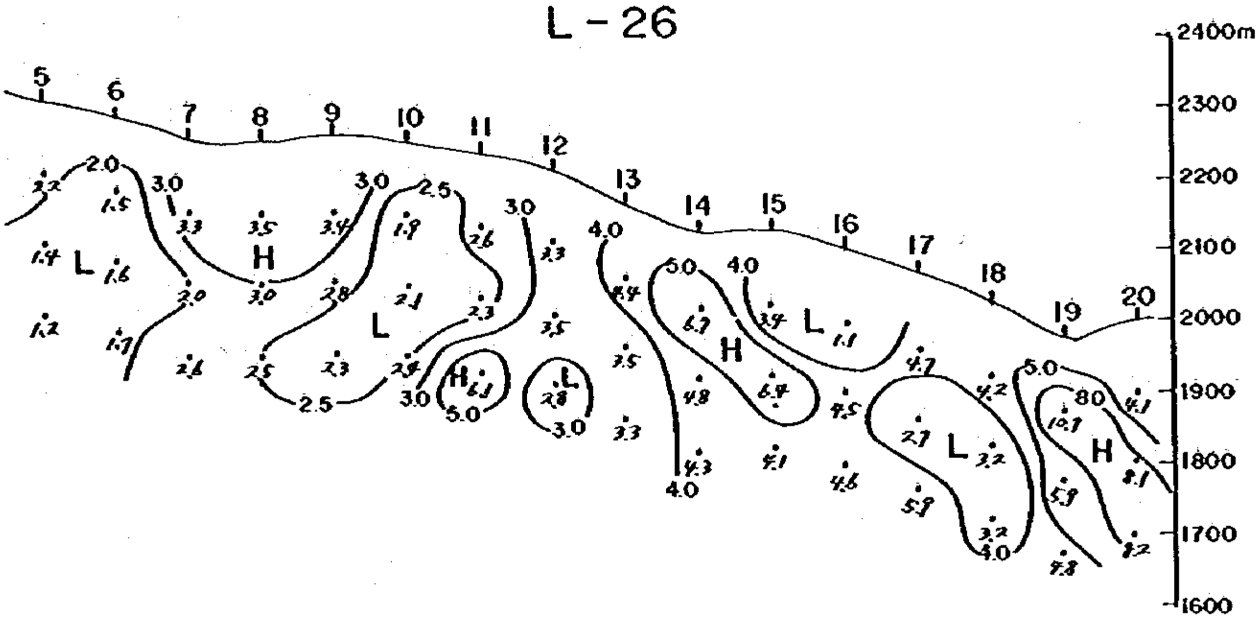

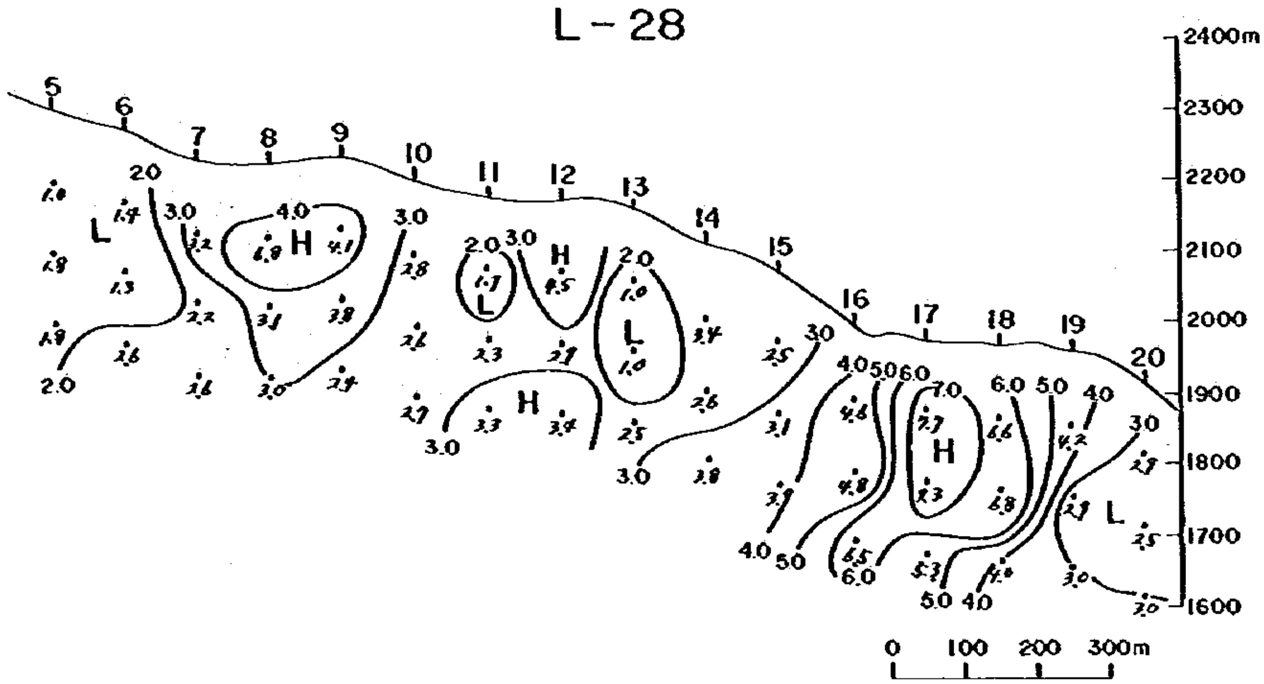

Fig. 4 - 21 AMF profile

4-4-1-5 Comparison to the Geochemical Anomaly

Some of the chargeability-anomalous zones are well consistent with the anomalous zones of copper, silver and lead which were obtained as the result of geochemical prospecting, which are shown in the following.

Copper anomalous zone	- K anomaly. Both chargeability and resistivity are great.
Silver anomalous zone Lead anomalous zone	} - C and F anomalous zones. Chargeability is great and resistivity is small.

K anomaly belongs to the group I shown in Fig. 4-6, and C and F anomalies belong to III. No distinct anomaly of the metals mentioned above has not been observed in the anomalous zones belonging to II. Therefore, it can be said in general that

(1) High IP and high resistivity anomalies among those in the area are related to copper, and

(2) High IP and low resistivity anomalies are related to silver and lead. High resitivity and low resistivity are, however, considered to be attributed to that of the country rock and not to the ore deposit from their values.

4-4-2 PROVIDENCIA Area

The result of survey and the result of calculation are shown in PL. 4-2 (MAPS OF IP SURVEY, PROVIDENCIA AREA), Fig. 4-23 ∿ 4-27 (IP profile), Fig. 4-28 ∿ 4-32 (ρa profile) and Fig. 4-33 ∿ 4-37 (AMF profile).

4-4-2-1 Analysis of Chargeability Maps

The chargeability maps (PL. 4-2, M-1, M-2 and M-3) shows that the minimum chargeability measured in the area was 1.77 and the maximum 9.00, both of which have the values a little more than twice those of the EL TEJOCOTE area. They are, however, small as the values of chargeability. The minimum values, the maximum values and the average values at each depth are as follows:

	a = 100 m	a = 200 m	a = 300 m
Min. ∿ Max.	1.90 ∿ 6.43	2.00 ∿ 7.67	1.77 ∿ 9.00
Average	3.19	3.38	4.42
Anomalous zone	≧3.50	≧3.70	≧4.80

It is shown that chargeability becomes greater with the increase of depth. This shows that the IP effect peculiar to the medium increased with increase of depth. Supposing here that the values above the additional 10 percent of the average are to be anomalous, the values such as M ≧ 3.50 at a = 100 m, M ≧ 3.70 at a = 200 m and M ≧ 4.80 at a = 300 m are the chargeability anomalies. At a = 300 m, however, the zones of M ≧ 4.50 were regarded as anomaly even if the values of M are smaller than those mentioned above in consideration of the values of the surrounding area and that of each depth. The values smaller than those shown in the above were regarded as background. The anomalies were marked with A(a = 100), B(a = 100), ...

Two zonal anomalies extends in the area in the direction of NW-SE in the northeastern part and in the southwestern part of the area, stretching over almost all the survey lines. The direction is consistent with that of the geologic structure of the area.

A conspicuous anomaly occurs in almost the center of the area between the above two zonal anomalies, and the IP structure of the area is characterized by these three anomalies.

(1) Chargeability map at a = 100 m (See PL. 4-2, M-1)

A-1(a = 100) : 3.50 ∿ 5.83, grand, zonal.

A-2(a = 100) : 3.50 ∿ 5.83, small.

B(a = 100) : 3.50 ∿ 4.23, grand.

C(a = 100) : 3.50 ∿ 6.43, zonal. Grand. The strongest anomaly at a = 100 m.

D(a = 100) : 3.50 ∿ 4.00, small, anomaly by one survey point.

E-1(a = 100) : 3.50 ∿ 3.87; medium.

E-2(a = 100) : 3.50 ∿ 4.00, small, anomaly by one survey point.

E-3(a = 100) : 3.50 ∿ 4.23, small, anomaly by one survey point.

F(a = 100) : 3.50 ∿ 3.67, small, anomaly by one survey point.

G(a = 100) : 3.50 ∿ 3.60, small anomaly by one survey point.

(2) Chargeability map at a = 200 m (See PL. 4-2, M-2)

A-1(a = 200) : 3.70 ∿ 7.67, grand, zonal. The strongest anomaly at a = 200 m.

A-2(a = 200) : 3.70 ∿ 4.07, small.

B(a = 200) : 3.70 ∿ 4.67, grand.

C(a = 200) : 3.70 ∿ 6.17, grand, zonal.

D(a = 200) : 3.70 ∿ 3.90, small, anomaly by one survey point.

E(a = 200) : 3.50 ∿ 3.57, small, anomaly by one survey point. E-1, E-2 and E-3 at a = 100 are considered to have been derived from this anomaly.

(3) Chargeability map at a = 300 m (See PL. 4-2, M-3)

A-1(a = 300) : 4.50 ∿ 9.00, grand, zonal. The strongest anomaly at a = 300 m.

A-2(a = 300) : 4.50 ∿ 6.33, grand.

B(a = 300) : 4.30 ∿ 4.73, medium.

C(a = 300) : 4.50 ∿ 7.37, grand, zonal.

E(a = 300) : 4.50 ∿ 4.67, small.

H(a = 300) : 4.50 ∿ 5.23, small.

Anomalies corresponding to D, F and G at a = 100 and a = 200 m have not been observed at this depth.

These are summarized in the Table 4-4.

Among these anomalies, A(A-1, A-2) anomalous zone is consistent with the zones of distribution of siltstone, sandstone and shale interbedded with marl, and C anomaly is consistent with the zone of distribution of massive limestone. B anomaly, among these, seems to be related to some ore deposits having the remains of old mine workings on the surface.

Table 4-4 Measured Chargeability Anomaly (PROVIDENCIA Area)

a / Name of Area	100m			200m			300m		
	Magnitude	Average	Max.Value	Magnitude	Average	Max.Value	Magnitude	Average	Max.Value
A-1	◎	469	583	◎	568	767	◎	686	900
A-2	∘	583*	583*	∘	400	407	◎	540	633
B	◎	386	423	◎	413	467	○	457	473
C	◎	435	643	◎	480	617	◎	565	737
D	∘	400*	400*	∘	390*	390*	–	–	–
E-1	○	377	617						
E-2	∘	400*	400*	E, ∘	357*	357*	E, ∘	459	467
E-3	∘	423*	423*						
F	∘	367*	367*	–	–	–	–	–	–
G	∘	360*	360*	–	–	–	–	–	–
H	–	–	–	–	–	–	∘	523*	523*

Magnitude: ◎ = grand, ○ = medium, ∘ = small. *: Anomaly by one survey point. Average: Average value in anomalous zone. unit: milli - sec.

4-4-2-2 Analysis of Maps of Apparent Resistivity

Maps of apparent resistivity (PL. 4-2, M-4, M-5 and M-6) show that apparent resistivity ρa of the survey area was 171 Ω-m in minimum, 3392 Ω-m in maximum and 950 Ω-m in average of the whole measured values. The minimum, maximum and average values at each depth are as follows:

	a = 100 m	a = 200 m	a = 300 m
Min. ∿ Max.	171 ∿ 2941	205 ∿ 2807	307 ∿ 3392
Average	850	950	1050

This table shows that the average resistivity increased 100 Ω-m to every 100 meters of increase of depth. Although this increase is not so great, it is likely to show that the rock facies varies with the increase of depth.

In order to investigate the relation between apparent resistivity ρa and chargeability M, anomalous zones of chargeability at each depth described in the clause 4-4-2-1 were transcribed to the map of apparent resistivity, of which average of ρa among these anomalous zones were found and listed in the following table.

$\overline{M}'$ and $\overline{\rho a}'$ are the average of $\overline{M}$ and $\overline{\rho a}$ respectively at three depths of each anomaly, which are considered to be effective of studying the three dimensional characters of the IP anomalous zones. These relations are shown in Fig. 4-22.

Geological map shows that anomalies of B and E are in massive limestone, and A and C in shale, siltstone, sandstone and marl. Massive limestone is generally high in ρa and the other rocks including shale to marl are low in ρa. In addition, shale and marl have far greater IP effect than limestone. Fig. 4-22 obviously shows these matters.

The comparison of the chargeability map with the map of apparent resistivity shows that A-1 and A-2 are consistent with the low zones of ρa and B with high zones, and that C is generally low in ρa, whereas no distinct similarity in the pattern of ρa to that of M can not be observed.

Table 4 - 5 Average of Chargeability and Apparent Resistivity in Anomalous Zones of Chargeability (PROVIDENCIA Area)

a / Name of Area	100m			200m			300m			100~300m	
	Magnitude	$\bar{M}$	$\bar{\rho a}$	Magnitude	$\bar{M}$	$\bar{\rho a}$	Magnitude	$\bar{M}$	$\bar{\rho a}$	$\bar{M}$	$\bar{\rho a}$
A-1	◎	469	360	◎	568	568	◎	686	743	A, 541	535
A-2	o	583*	483*	o	400	357	◎	540	701		
B	◎	356	1427	◎	413	1340	○	457	1618	419	1462
C	◎	435	732	◎	480	866	◎	565	768	493	789
D	o	400*	623*	o	390*	1157*	–	–	–	–	–
E-1	○	377	809								
E-2	o	400*	1709	E,o	357*	2801	E,o	459	2333	E, 405	2277
E-3	o	423*	2576*								
F	o	367*	841*	–	–	–	–	–	–	–	–
G	o	360*	539	–	–	–	–	–	–	–	–
H	–	–	–	–	–	–	o	523*	300*	–	–
Average of all anomalous values										465	1266
Average of all measured values										366	951

Magnitude: ◎ = grand, ○ = medium, o = small. *: Anomaly by one survey point. $\bar{M}$: Average of chargeability, $\bar{\rho a}$: Average of apparent resistivity.

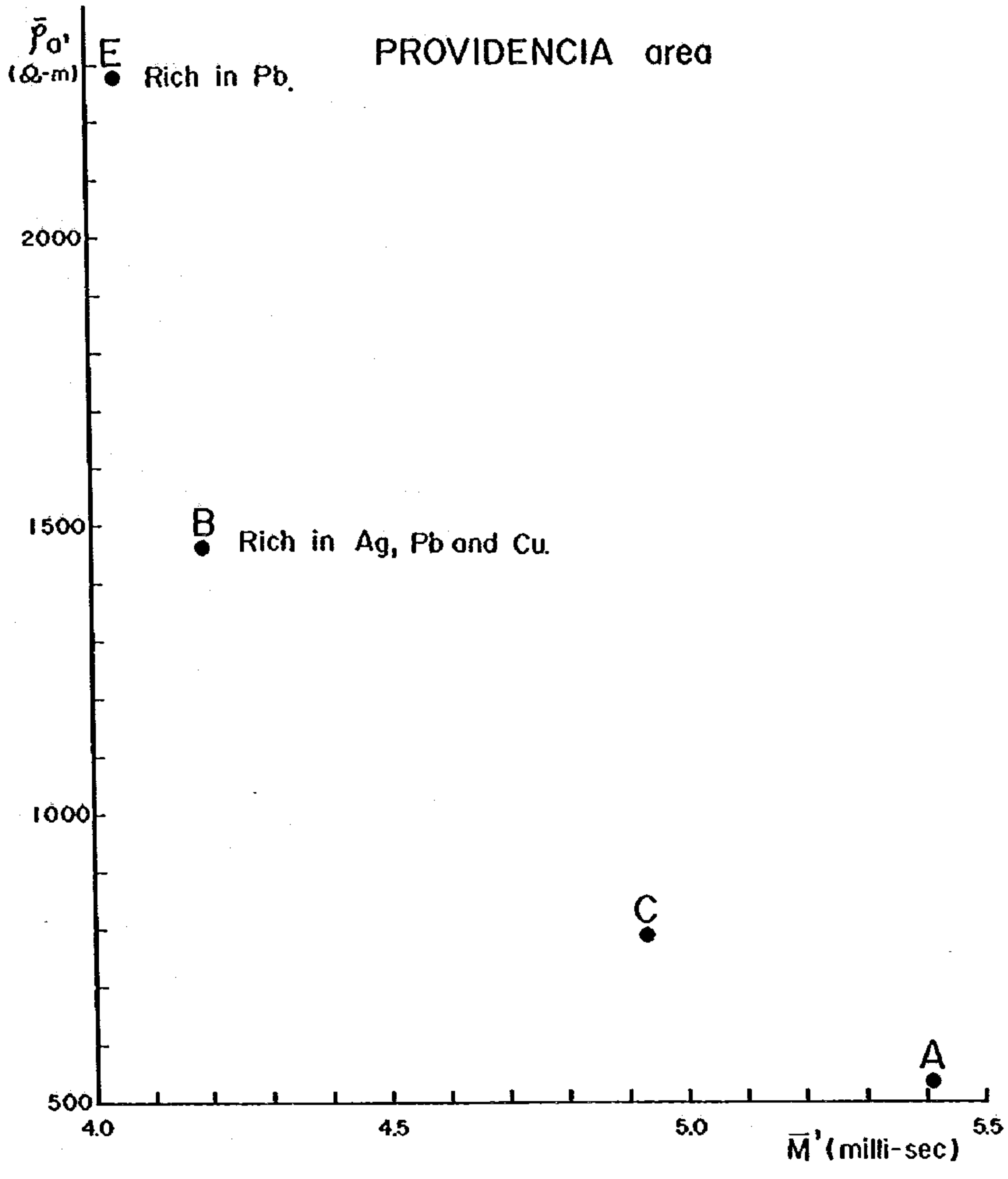

Fig. 4 - 22 Relation of chargeability and apparent resistivity inside the IP anomalous zone.

4-4-2-3 Analysis of Maps of Apparent Metal Factor

Since the range of variation of M is very small in this area, similar to that in the EL TEJOCOTE area, compared with that of ρa, M can be considered to be constant. Therefore, at the place where ρa is great (small), M becomes small (great).

The comparison of M-7, M-8 and M-9 on the maps of apprent metal facter (PL. 4-2) with M-4, M-5 and M-6 on the ρa maps shows that at the place where ρa is great (small), AMF becomes small (great). Accordingly, although the AMF map is quite similar to the pattern of contour in the ρa maps in which H was replaced by L and L by H, no distinct correlation with the pattern of IP maps has been observed.

4-4-2-4 Profile Analysis

The result of analysis of profiles of chargeability (Fig. 4-23 ∿ 27), apparent resistivity (Fig. 4-28 ∿ 32) and apparent metal factor (Fig. 4-33 ∿ 37) on each survey line are shown in the following table.

4-4-2-5 Comparison to the Geochemical Anomaly

The zones of distribution of high anomalies of silver, copper and lead detected as the result of geochemical prospecting are well consistent with some of the high anomalies of chargeability as shown in the following.

B anomaly - high anomalies of silver, copper and lead

E anomaly - high anomalies of lead

Chargeability anomalies of A and C are low in resistivity. These anomalies are consistent with the zone of distribution of shale and marl as described in 4-4-2-2.

Table 4-6 Result of Profile Analysis (PROVIDENCIA Area)

Line	Anomaly name in M map (survey point)	M(milli-sec)	ρa anomaly	AMF anomaly	Remarks
L-12	A-2(15~20) C (5~10)	3.50 ~ 6.33 3.50 ~ 6.13	Remarkable high ρa below sp 13 and 14.	High AMF from deep below sp 5 to 7 and from sp 17 to 20.	High IP anomalies are distributed at both ends of this line.
L-14	A-2(15~20) C (5~ 8)	3.50 ~ 6.00 3.50 ~ 6.10	Remarkable high ρa below sp 9 and 12~14.	High AMF deep below sp 5~9 and below sp 20. AMF pattern below sp 12~14 and 9 is similar to that of ρa.	Same as above.
L-16	A-2(13~20) C (5~10)	3.50 ~ 5.00 3.50 ~ 6.83	High ρa from near surface of sp 12,13 and 15 to the deep of sp 17.	High AMF deep below sp 5~9 and below sp 20.	High IP anomalies are seen in the deep part of this line.
L-18	A-1(20) B (13~18) C (5~10)	4.00 ~ 4.80 4.00 ~ 4.73 4.00 ~ 7.17	Remarkable high ρa directly below sp 14.	High AMF deep below sp 7~9.	High IP anomalies at both ends and central part of this line are very remarkable.
L-20	A-1(17~20) B (12~15) C (5~ 9)	4.50 ~ 8.00 4.00 ~ 4.50 3.50 ~ 7.37	Specially high ρa below sp 13~15.	High AMF deep below sp 5~8 and below sp 19 and 20.	Same as above.
L-22	A-1(16~20) B (13~14) C (5~ 8)	4.00 ~ 8.17 3.50 ~ 4.00 3.50 ~ 6.67	High ρa from near surface of sp 7 to deep part of sp 9, deep below sp 11~14 and directly below sp 19.	High AMF deep below sp 5~7, near surface of sp 14~16 and directly below sp 20.	Same as above.
L-24	A-1(17~20) E, E-2(15) F (12~13) C (5~ 8)	4.00 ~ 9.00 3.50 ~ 4.50 3.50 ~ 3.67 3.50 ~ 7.17	Extremely high ρa deep below sp 14~16.	High AMF deep below sp 5~9 and directly below sp 19 and 20.	Three IP anomalies are seen in the central part of this line.
L-26	A-1(18~20) C (5~ 9) E (15~16)	4.00 ~ 8.17 3.50 ~ 7.17 4.00 ~ 4.67	Extremely high ρa in the near surface of sp 12 and directly below sp 15.	High AMF below sp 5~10 and sp 20.	High IP anomalies are distributed at both ends and central part in this line.
L-28	A-1(17~20) E-1(17) E-3(14~15) C (5~ 8)	4.00 ~ 7.93 3.50 ~ 3.80 3.50 ~ 4.23 3.50 ~ 6.43	Very high ρa deep below sp 11~13 and directly below sp 15.	High AMF directly below sp 19 and 20.	IP anomalies at both ends of this line are remarkable.
L-30	A-1(16~20) C (5~ 9)	3.50 ~ 8.17 3.50 ~ 6.00	Remarkable ρa deep below sp 11,12 and sp 14~16.	High AMF deep below sp 6,7 and below sp 18~20.	Same as above.

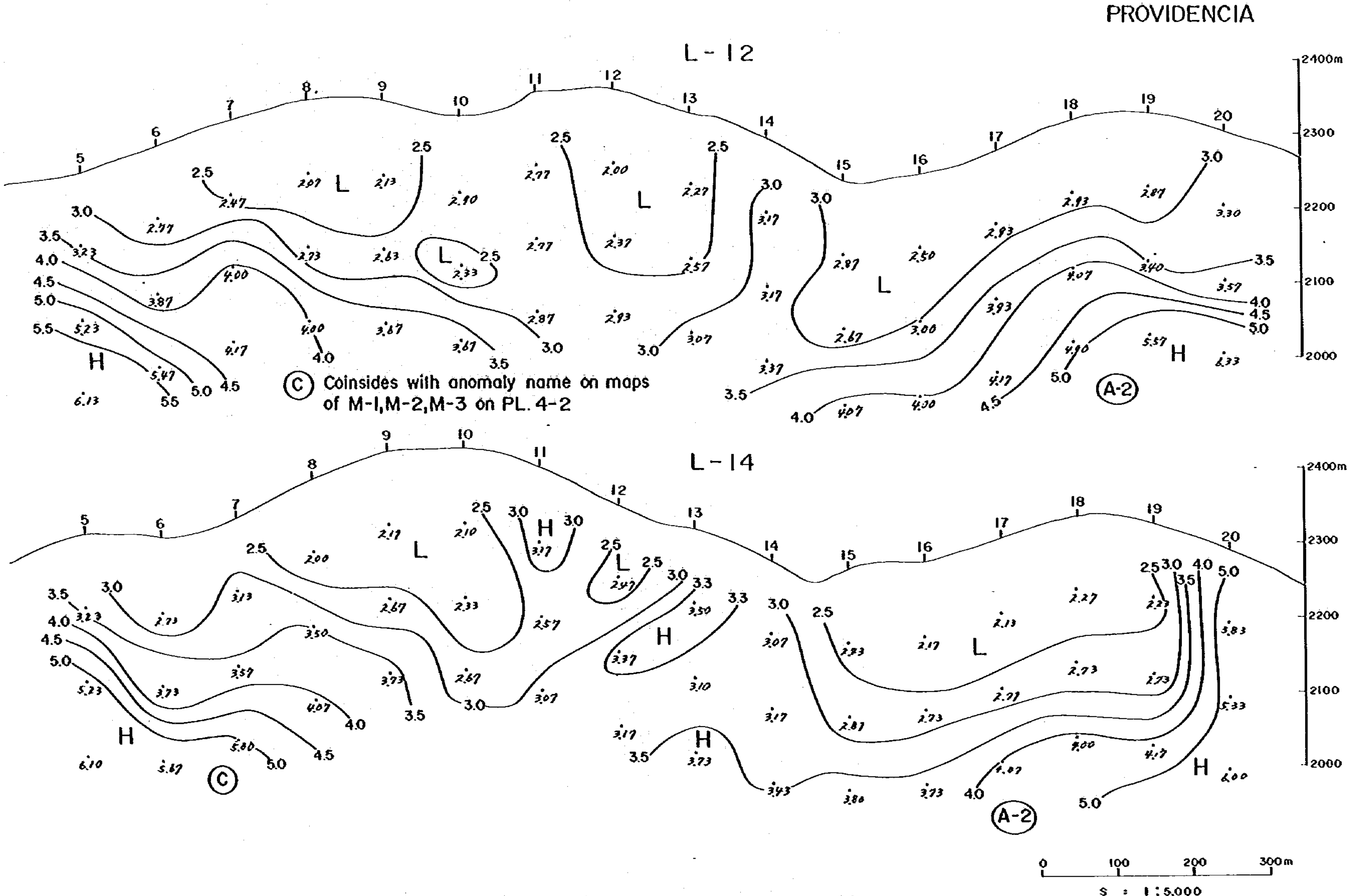

Fig. 4-23 IP profile (chargeability)

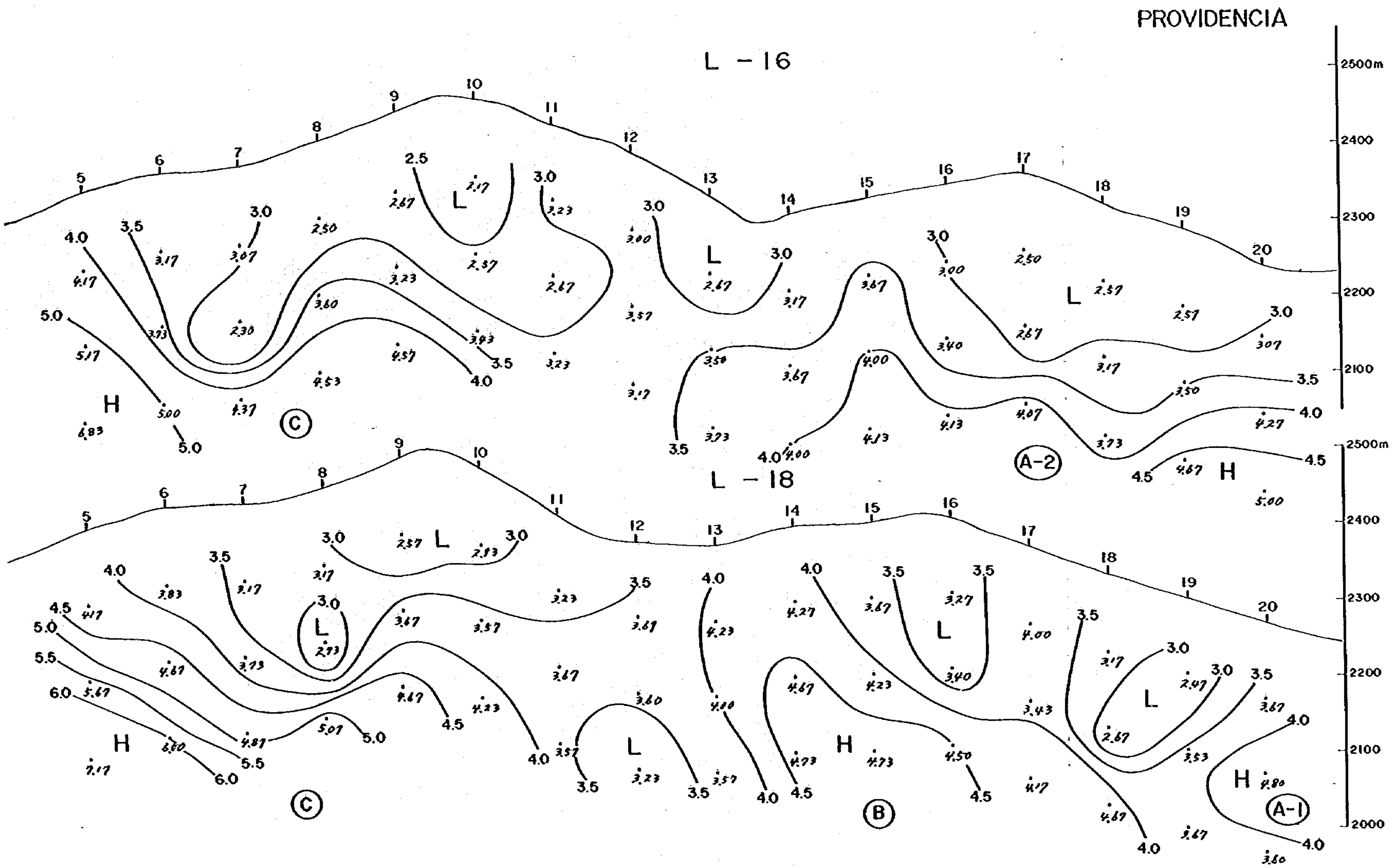

Fig. 4-24 IP profile

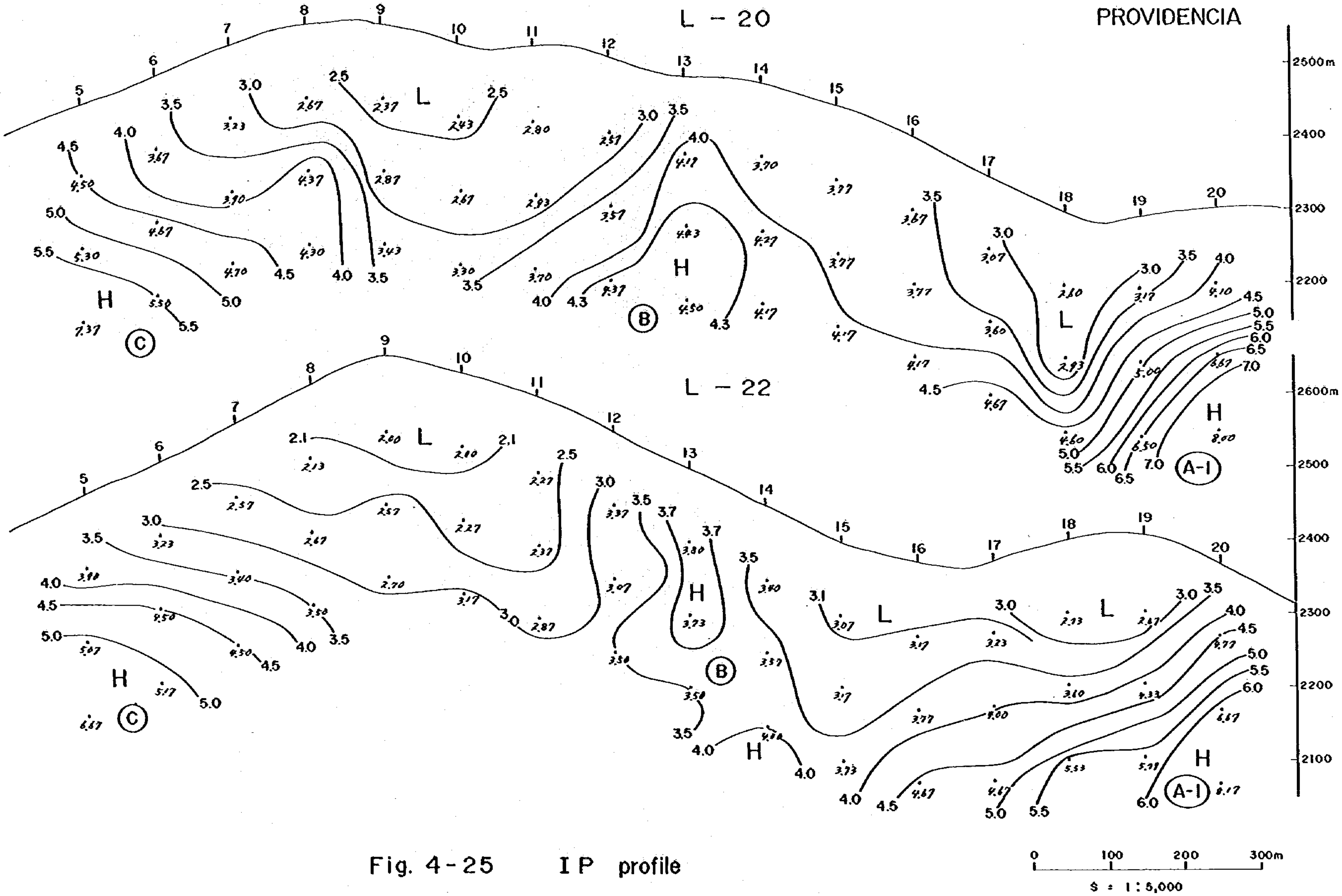

Fig. 4-25 IP profile

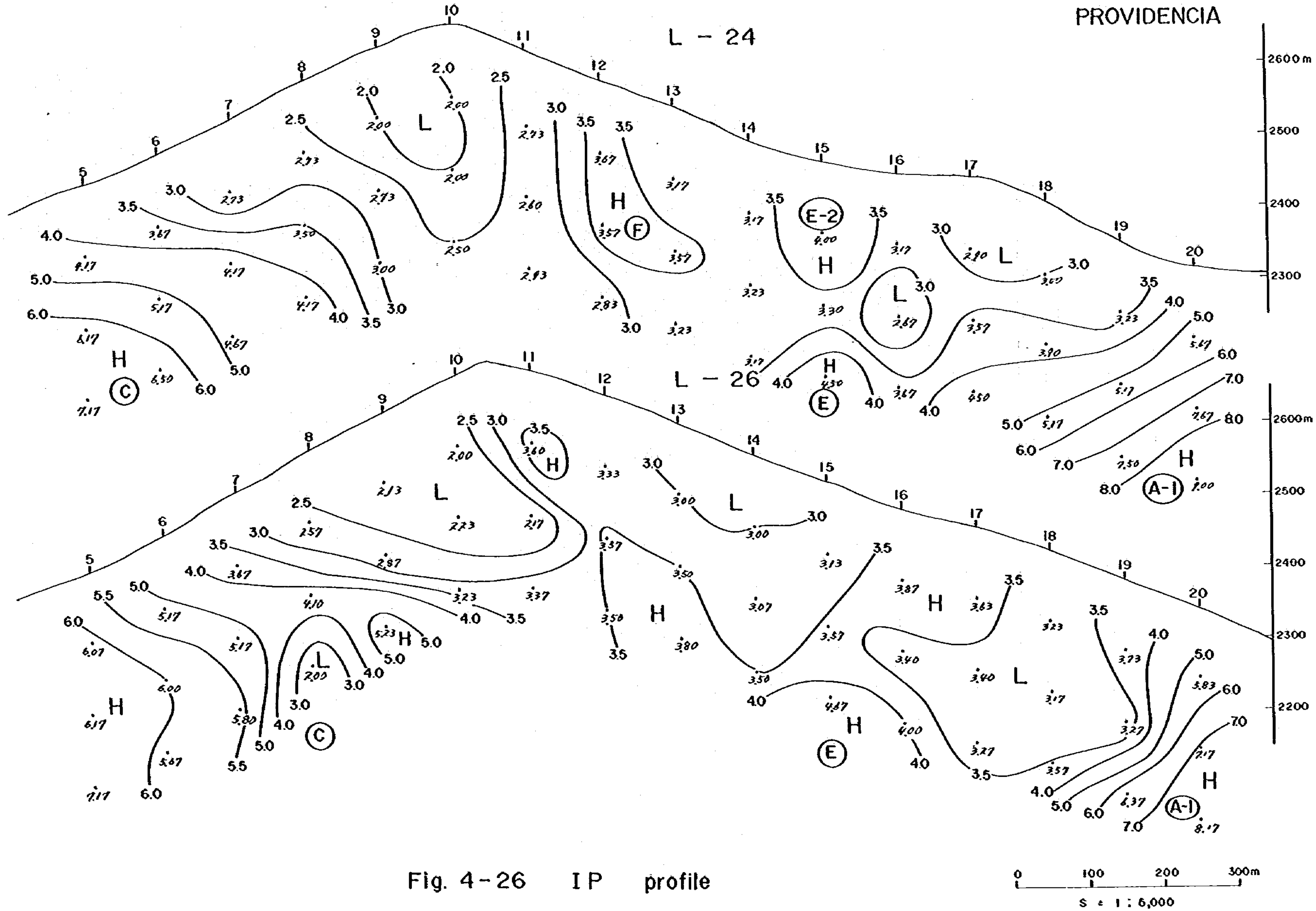

Fig. 4-26 IP profile

PROVIDENCIA

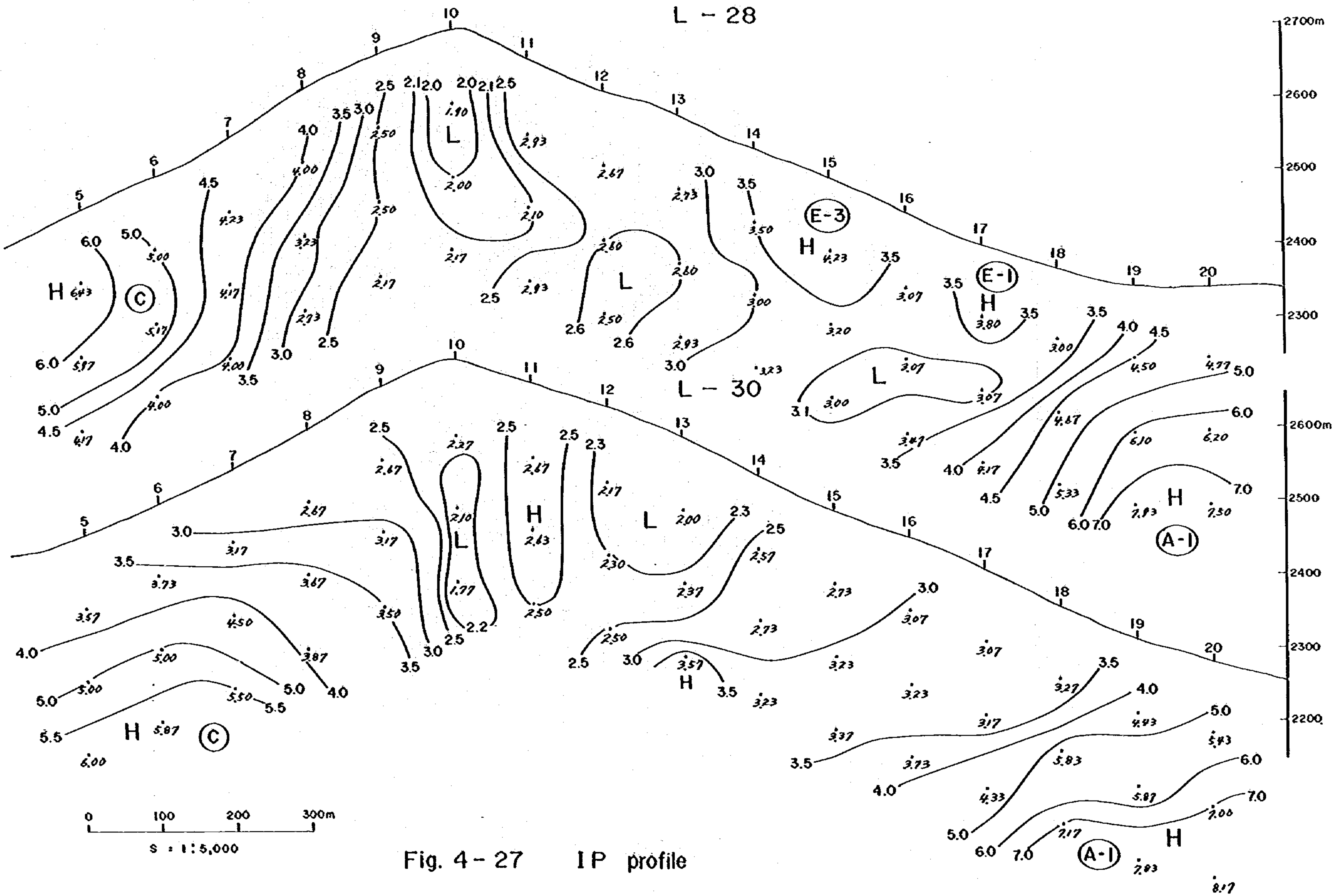

Fig. 4 - 27 IP profile

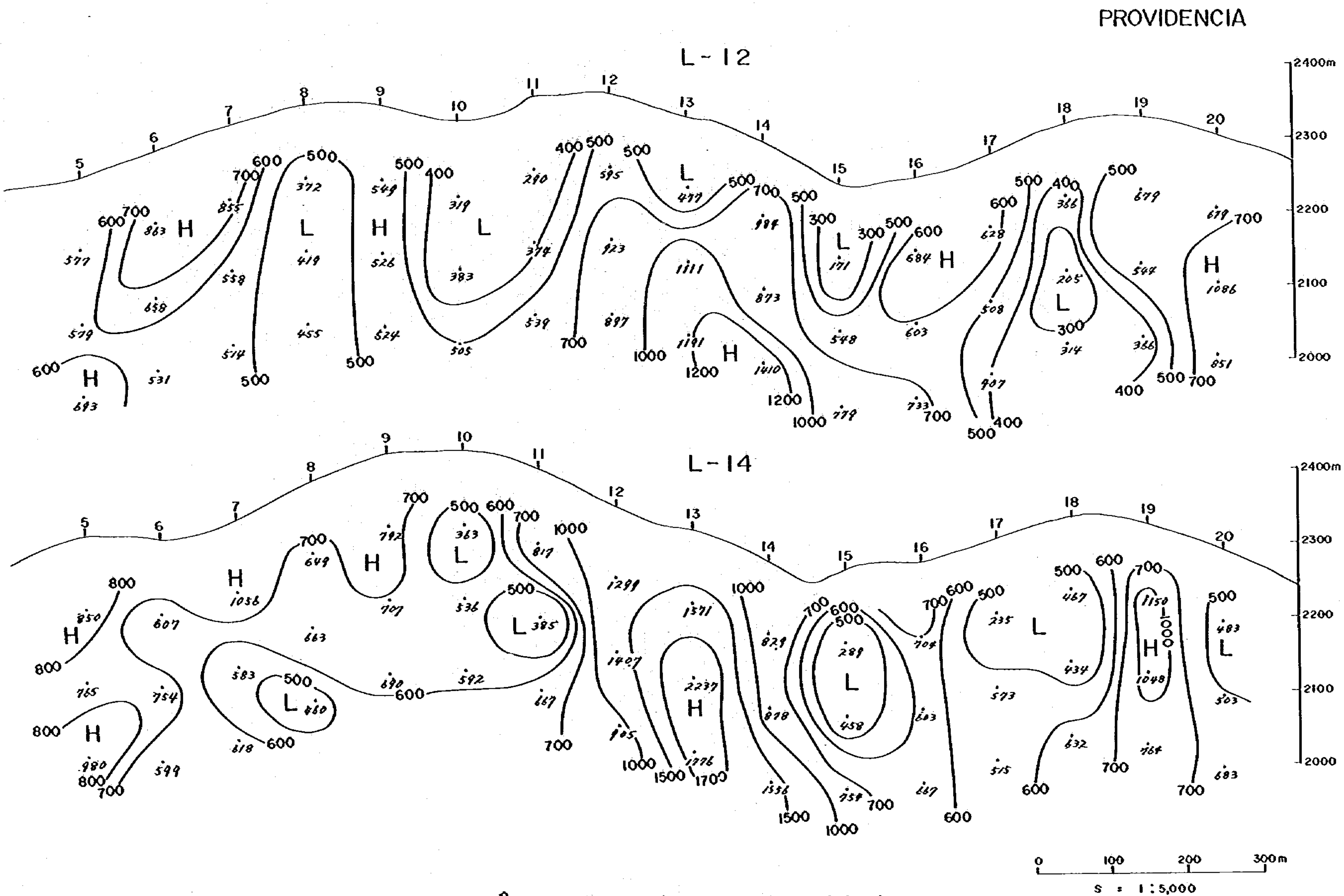

Fig. 4 - 28 ρ_a profile (Apparent Resistivity)

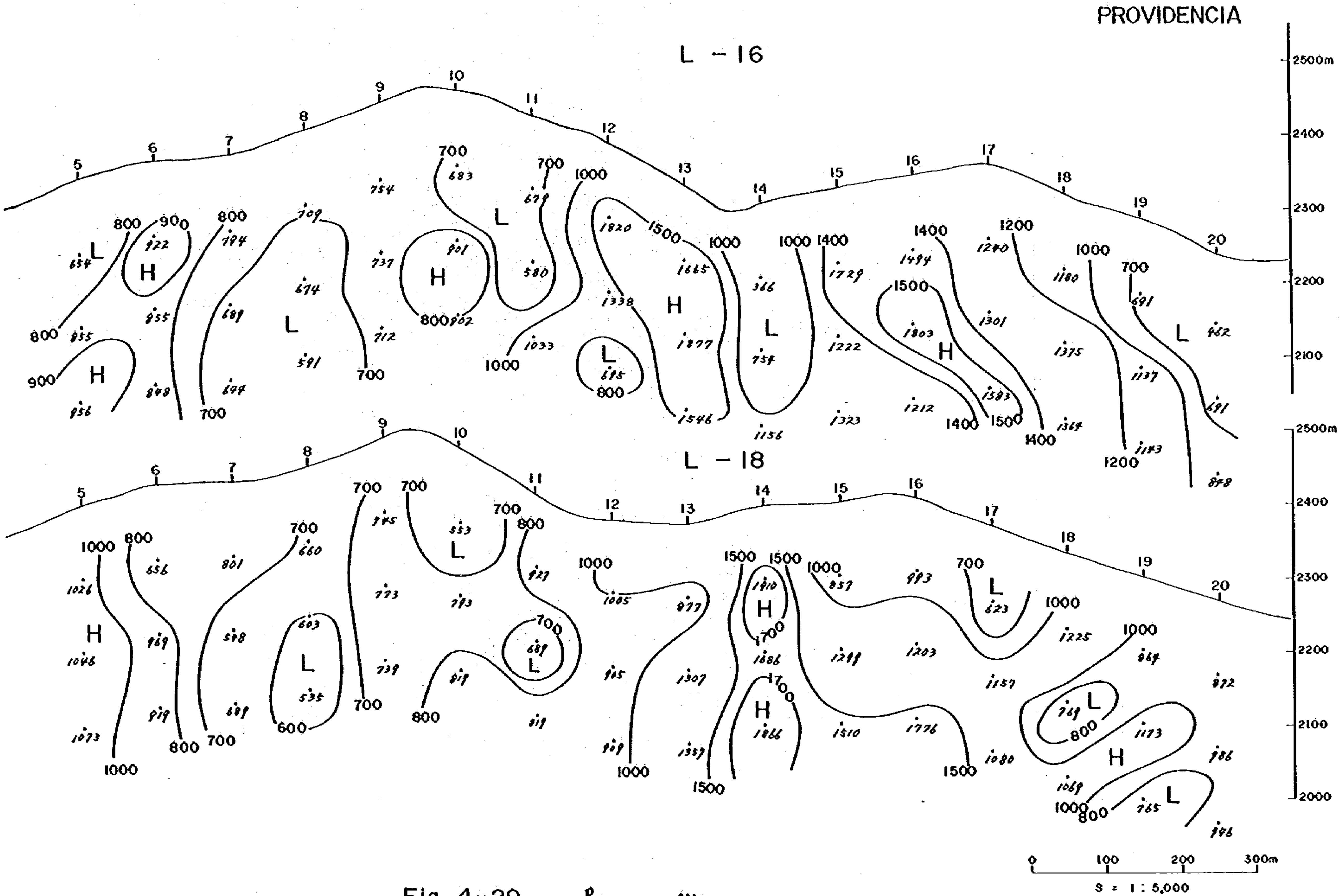

Fig. 4-29 ρ_a profile

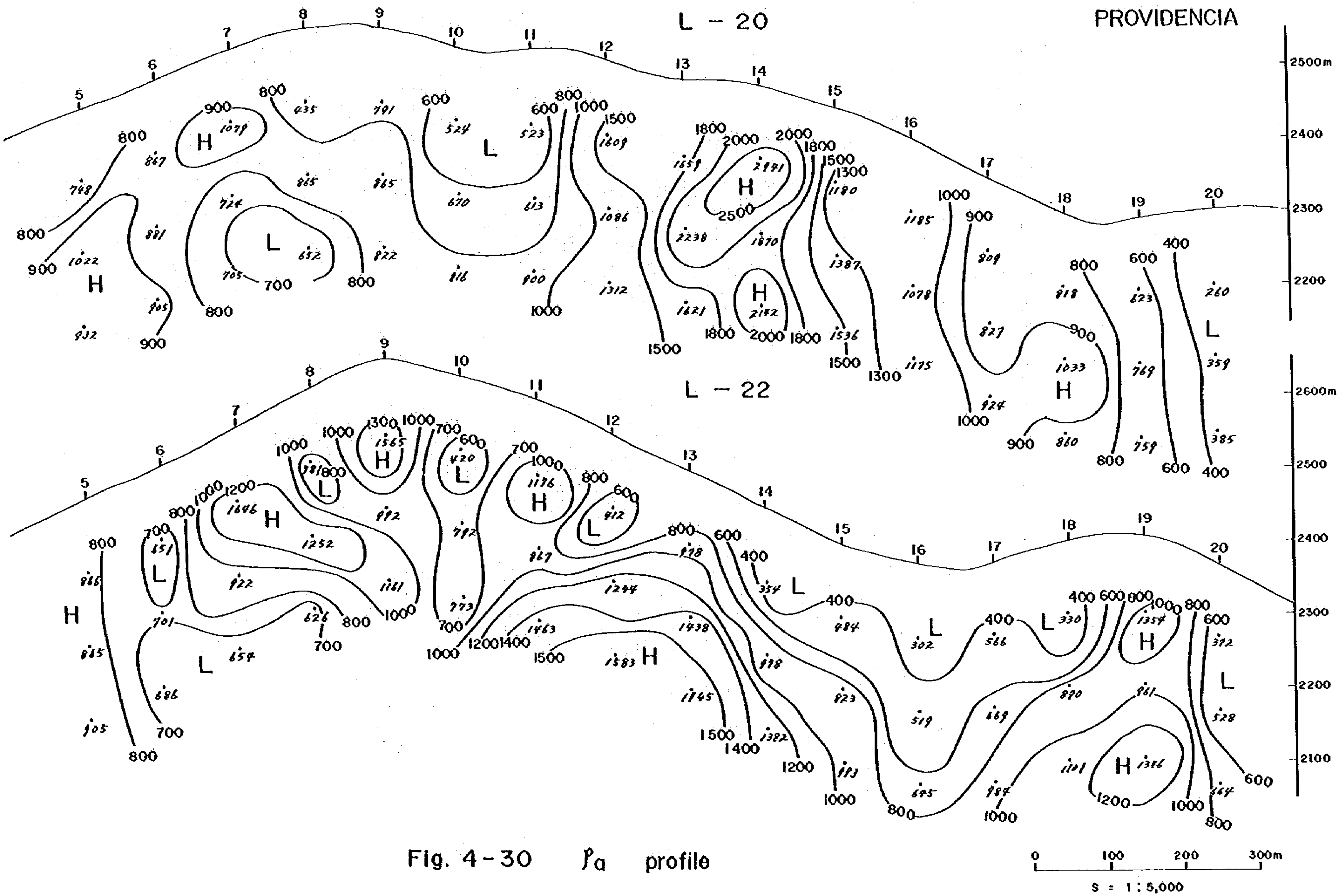

Fig. 4-30 ρ_a profile

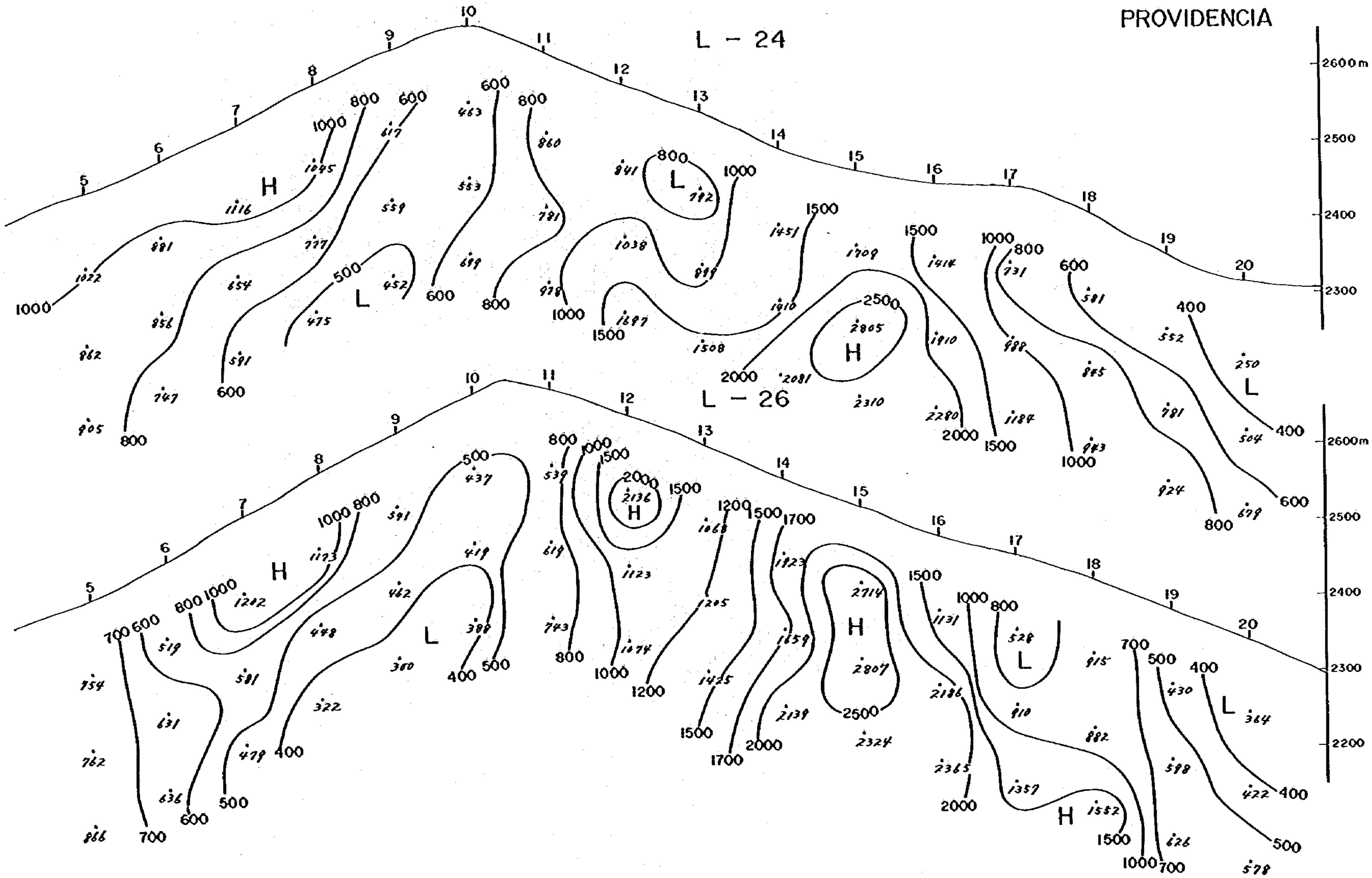

Fig. 4-31 ρ_a profile

0 100 200 300m
S = 1 : 6,000

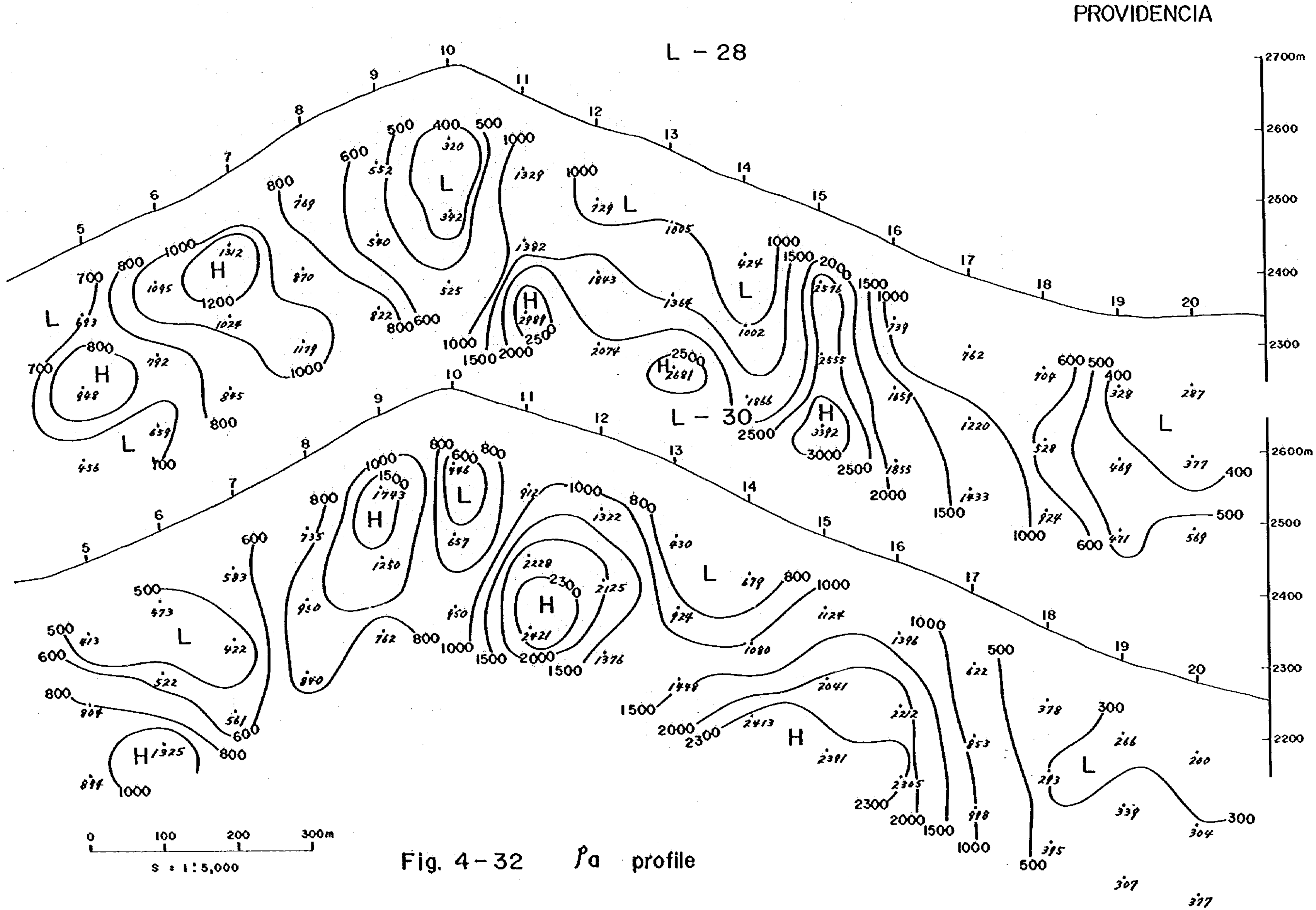

Fig. 4-32 ρa profile

PROVIDENCIA

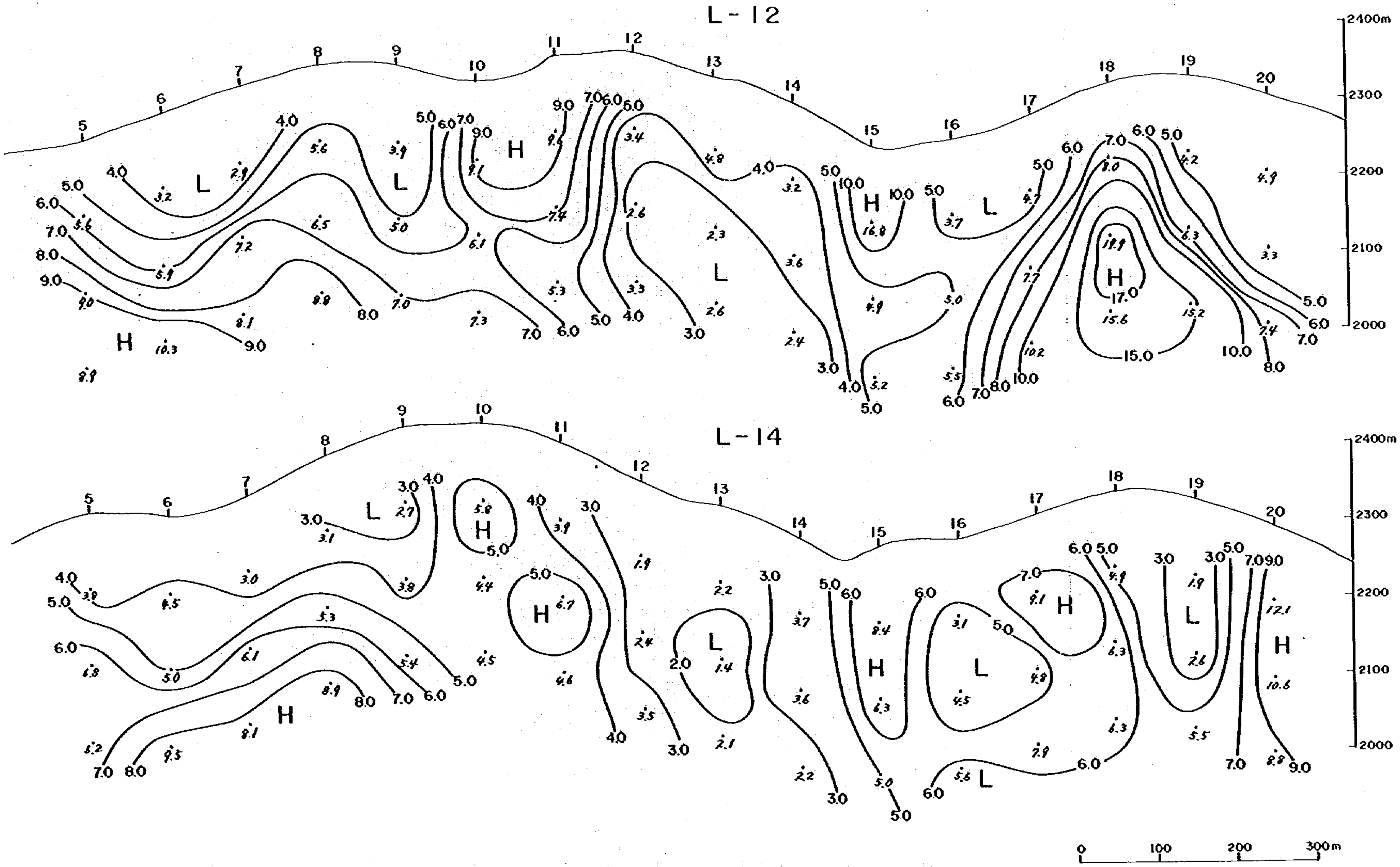

Fig. 4-33 AMF profile (Apparent Metal Factor)

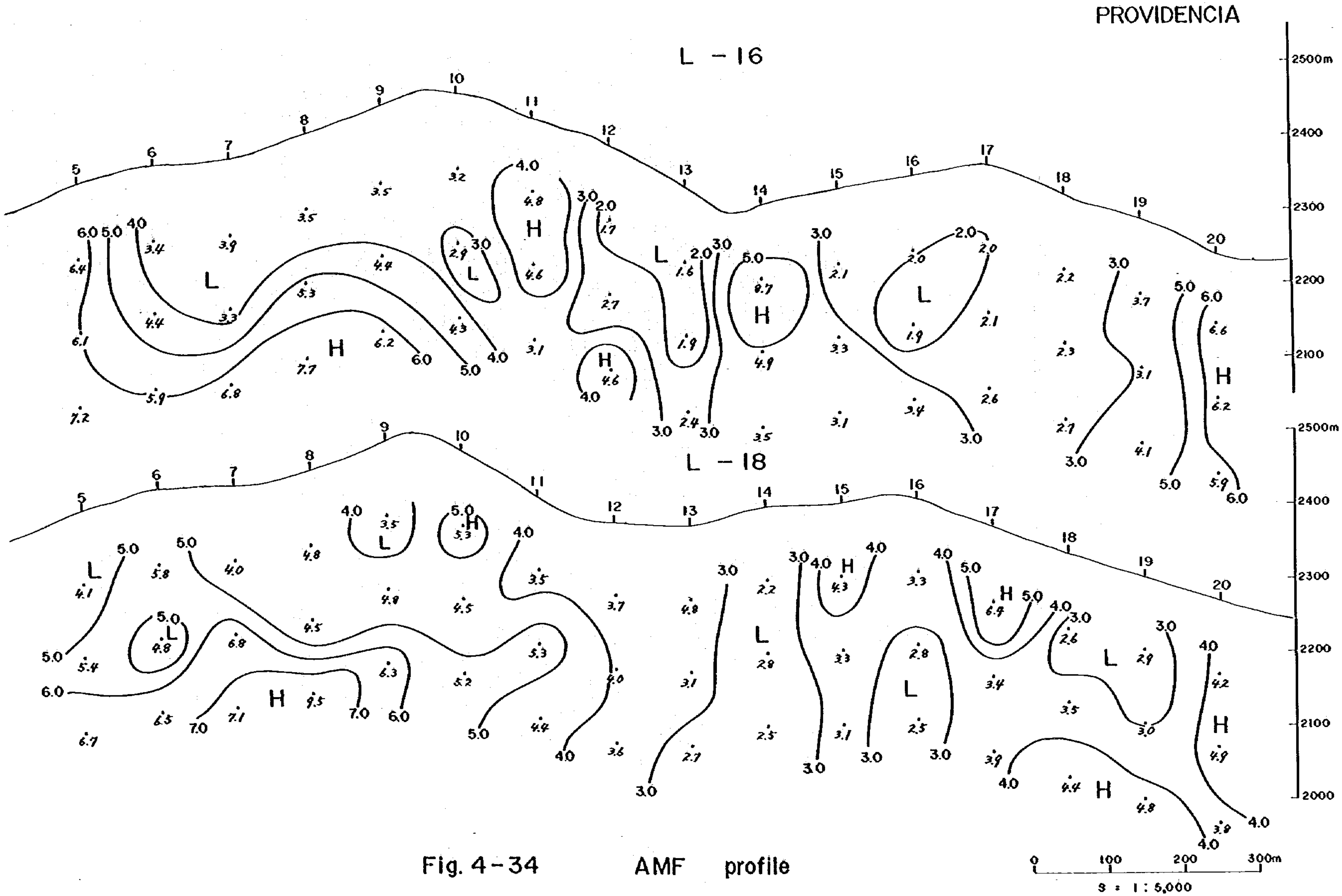

Fig. 4-34 AMF profile

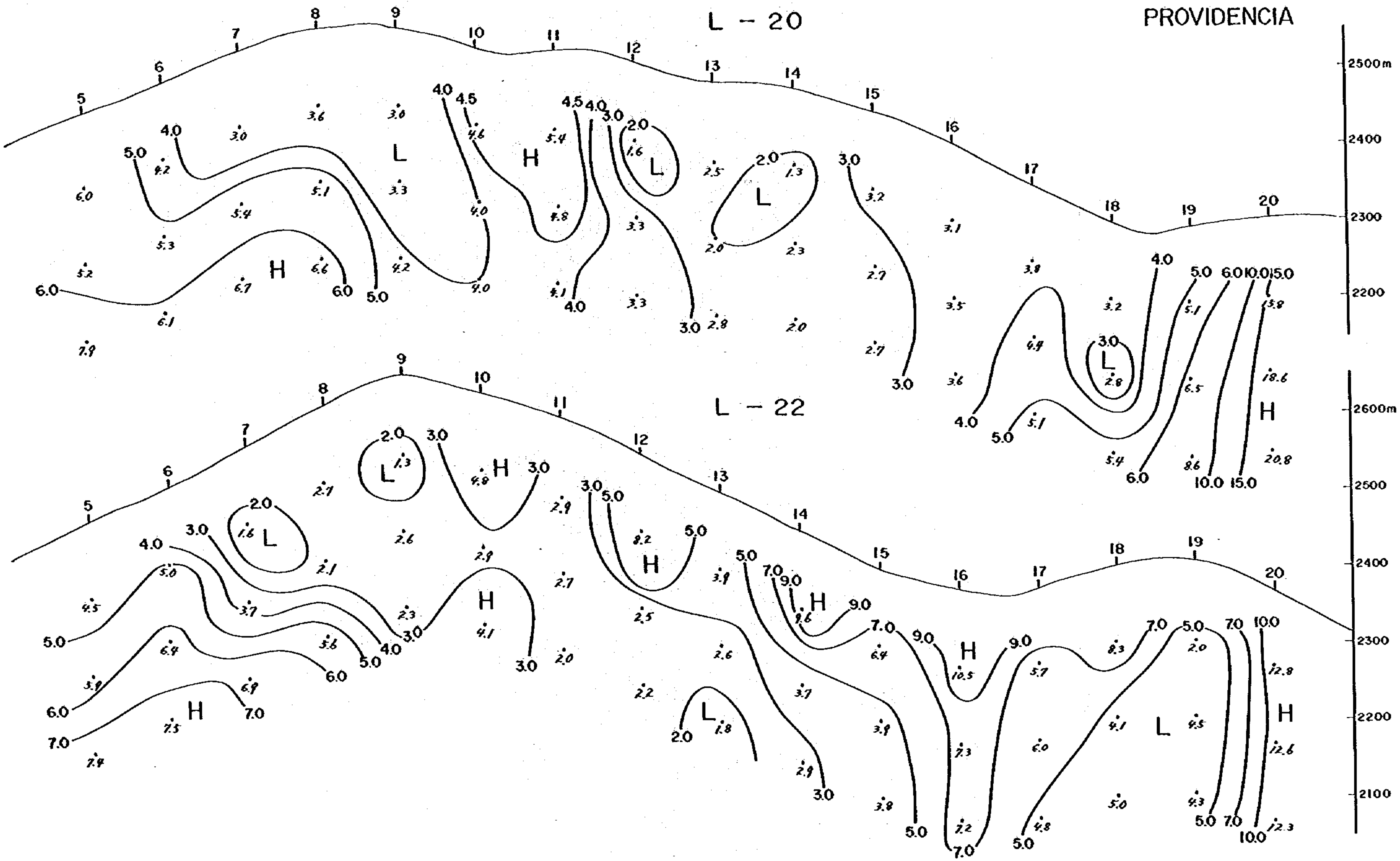

Fig. 4-35 AMF profile

0 100 200 300m

S = 1:5,000

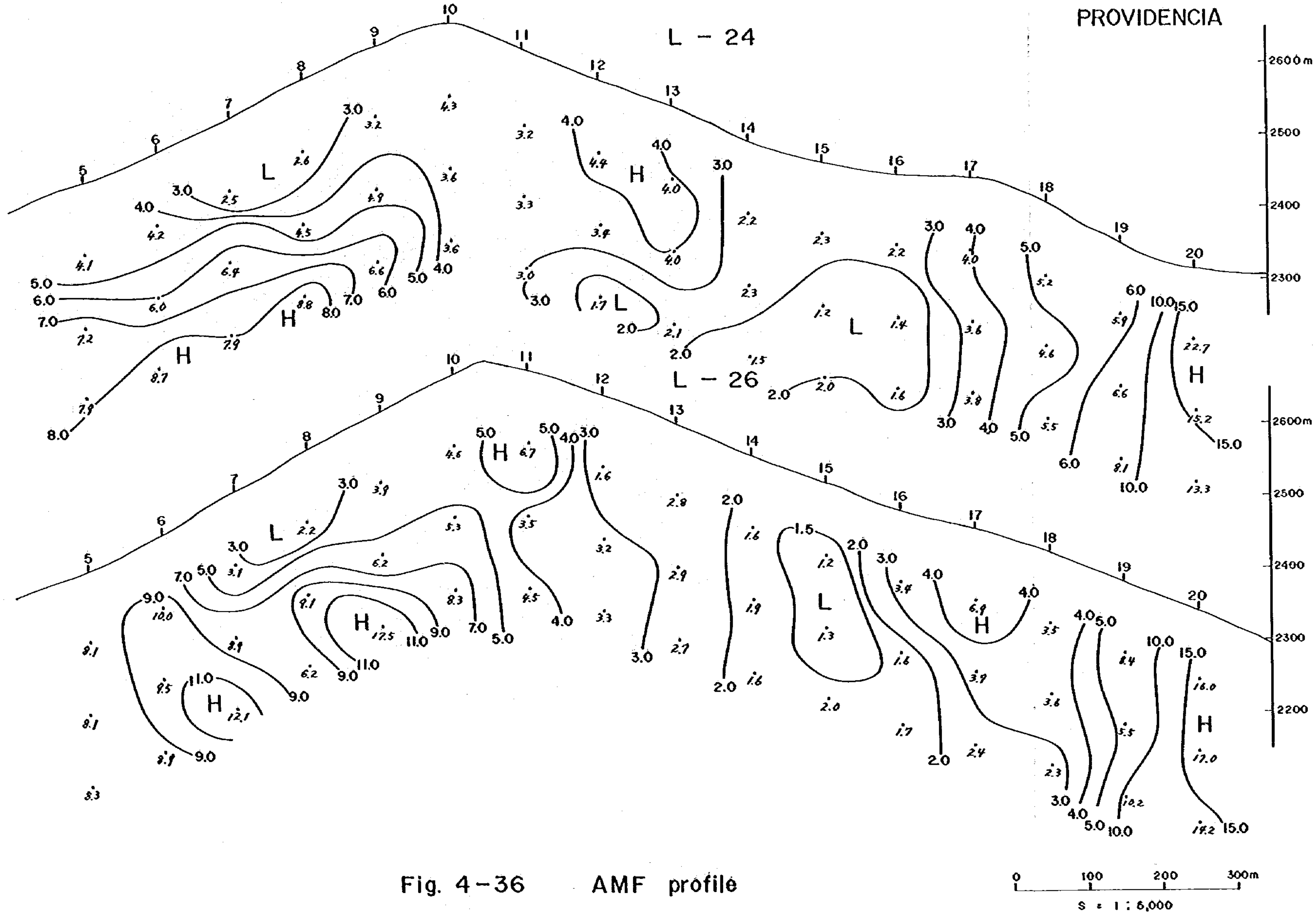

Fig. 4-36 AMF profile

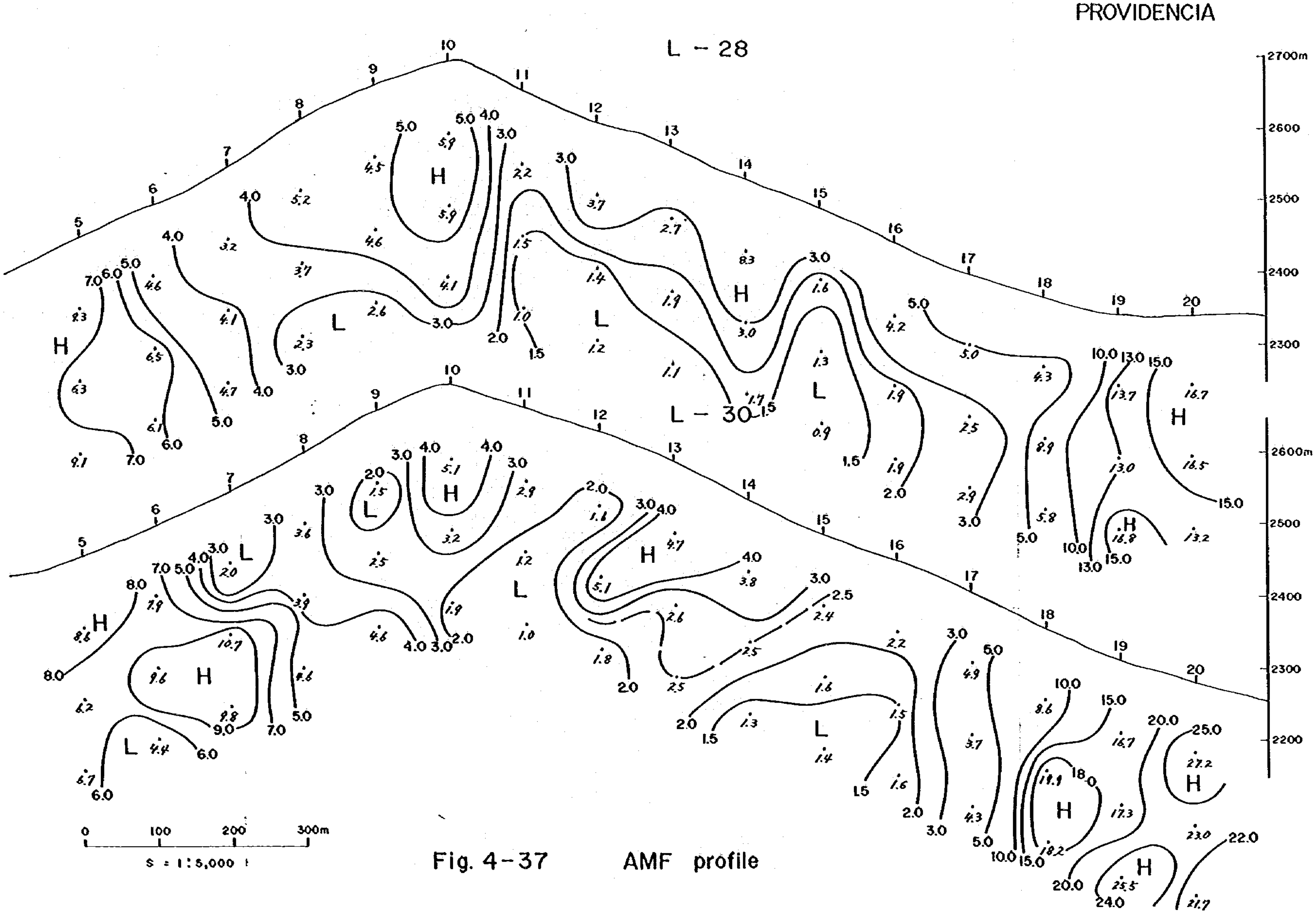

Fig. 4-37 AMF profile

4-5 IP Simulation

Since simulation of the time domain IP method used in this survey is theoretically impossible, simulation of a frequency domain IP method was carried out as a substitute and the results of the simulation were compared with the field data.

The frequency domain IP method is based on the principle that the resistivity of a medium with IP effect depends on the frequency of alternating current which is supplied to the medium. The IP effect at that time is called Frequency Effect (FE) and is expressed by the following formula:

$$FE = \frac{\rho L - \rho H}{\rho H} \times 100 \ (\%)$$

where, ρL : Resistivity in low frequency (Ω-m)

ρH : Resistivity in high frequency (Ω-m)

The simulation is performed by following procedure: At first, different resistivities (ρ_1, ρ_2) are given respectively to a medium of a certain shape with IP effect and to the surrounding medium without IP effect to find the apparent resistivity at each survey point. The varied resistivity (ρ'_1) corresponding to a certain FE value is provided to the medium which has IP effect without varying the resistivity of the surrounding medium to obtain apparent resistivity again at each survey point. By use of these two sets of apparent resistivity thus obtained and from the formula given above, FE values are calculated for each survey point to make a contour map of the FE values. Finally, model of underground structure and resistivity are so varied as to make the contour map agree with the field data as closely as possible.

The time domain IP method differs from a frequency domain IP method in the unit of measured value, and conversion of the value by time domain method to that by frequency domain method is theoretically impossible. But use of data measured by the both methods at the same location makes it empirically possible. In this simulation, FE value obtained at each survey point was multiplied by 2.6 to convert to simulated IP value on the basis of the empirical data.

Since the method has various problems as mentioned above, the underground structure was finally adopted in this simulation when the contour pattern made from measured data and that by simulation are most similar to each other, even if a considerable difference was noted between the IP values of the measured data and of simulation data.

In this simulation, such data as ground surface topography, shape of IP model, resistivity and FE values, and resistivity of the rock surrounding the IP model were given to a resistor network analog simulator.

4-5-1 EL TEJOCOTE Area

IP simulation was applied to line L-26 and L-28 chosen from 10 survey lines. The result of simulation are shown on Fig. 4-38 and Fig. 4-39 respectively.

L-26 : Contour pattern similar to that of field data was obtained by setting the structure with 10 and 20% FE below survey points 5∿11 and the structure with 10% FE below survey points 13∿18 shown as Fig. 4-38.

L-28 : Setting the structure with 10% FE shown as Fig. 4-39 below survey points 5∿7, 11∿13 and 15∿18 respectively, the most similar contour pattern to that of field data was obtained.

Values obtained by simulation cannot be treated as field data by the reason mentioned above. However, it is inferred that the real subsurface structure with a certain IP effect may be similar to the shape assumed here based on the similarity of contour pattern.

4-5-2 PROVIDENCIA Area

IP simulation was applied to L-18 and L-20 which cross the most remarkable anomaly of chargeability in this area. The result is shown on Fig. 4-40 and Fig. 4-41.

Assuming the structure with 20% FE shown as both figures, the most fitted contour pattern could be obtained.

It is inferred that there exist media with high IP effect at the both ends and the central part of each line.

One of them, below survey points 5∿9, is inferred to be coincides with shale, sandstone and marl, and it is supposed that the medium with high IP effect below points 18∿20 coincides with shale intercalated with siltstone, sandstone and mudstone.

And the other one which exists below points 12∿15 of these lines coincides well with the altered zone accompanied by copper, lead and silver. This altered zone can also be seen on the ground surface of the central part in this area.

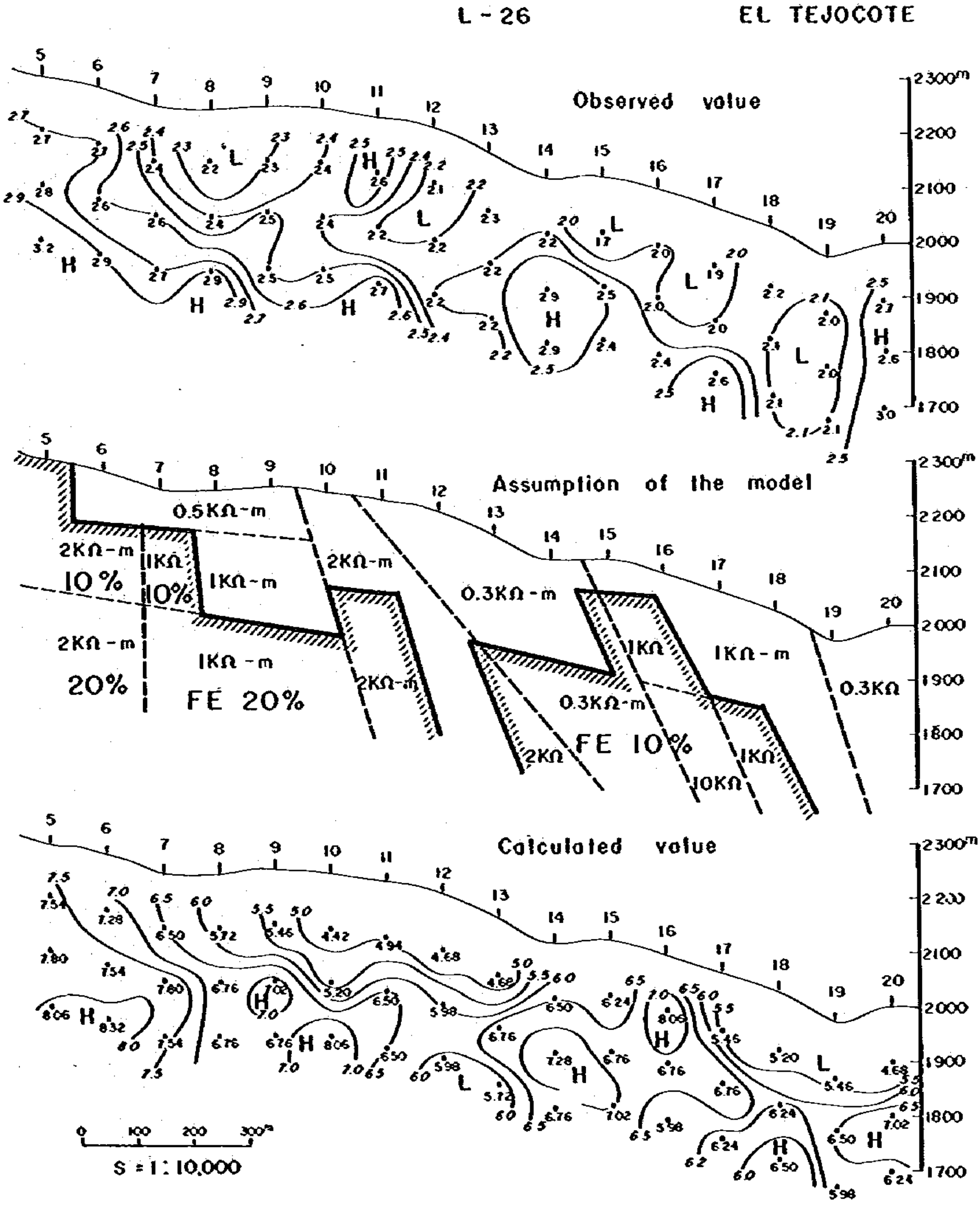

Fig. 4 - 38 Result of IP model calculation

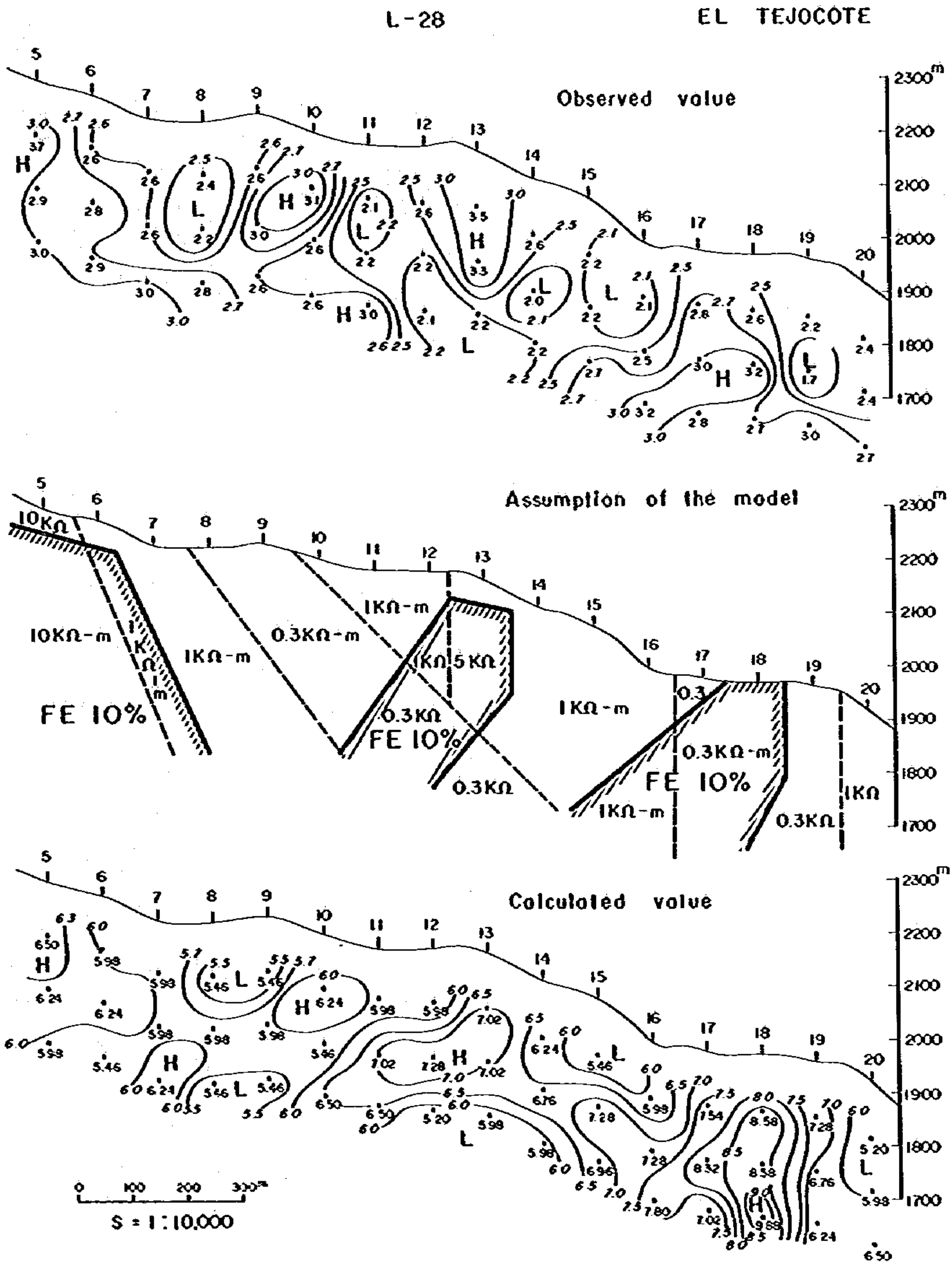

Fig. 4 - 39 Result of IP model calculation

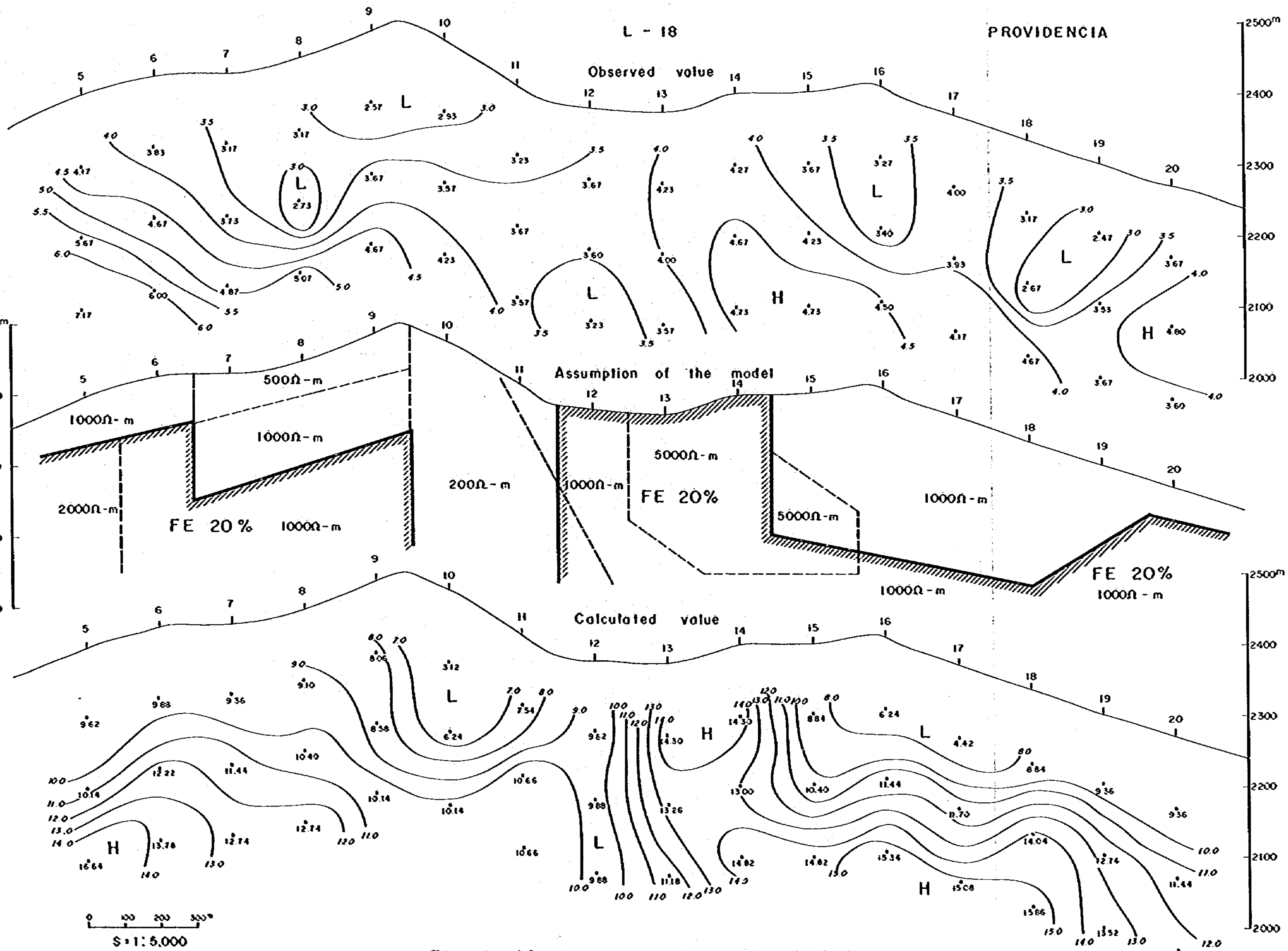

Fig. 4-40 Result of IP model calculation

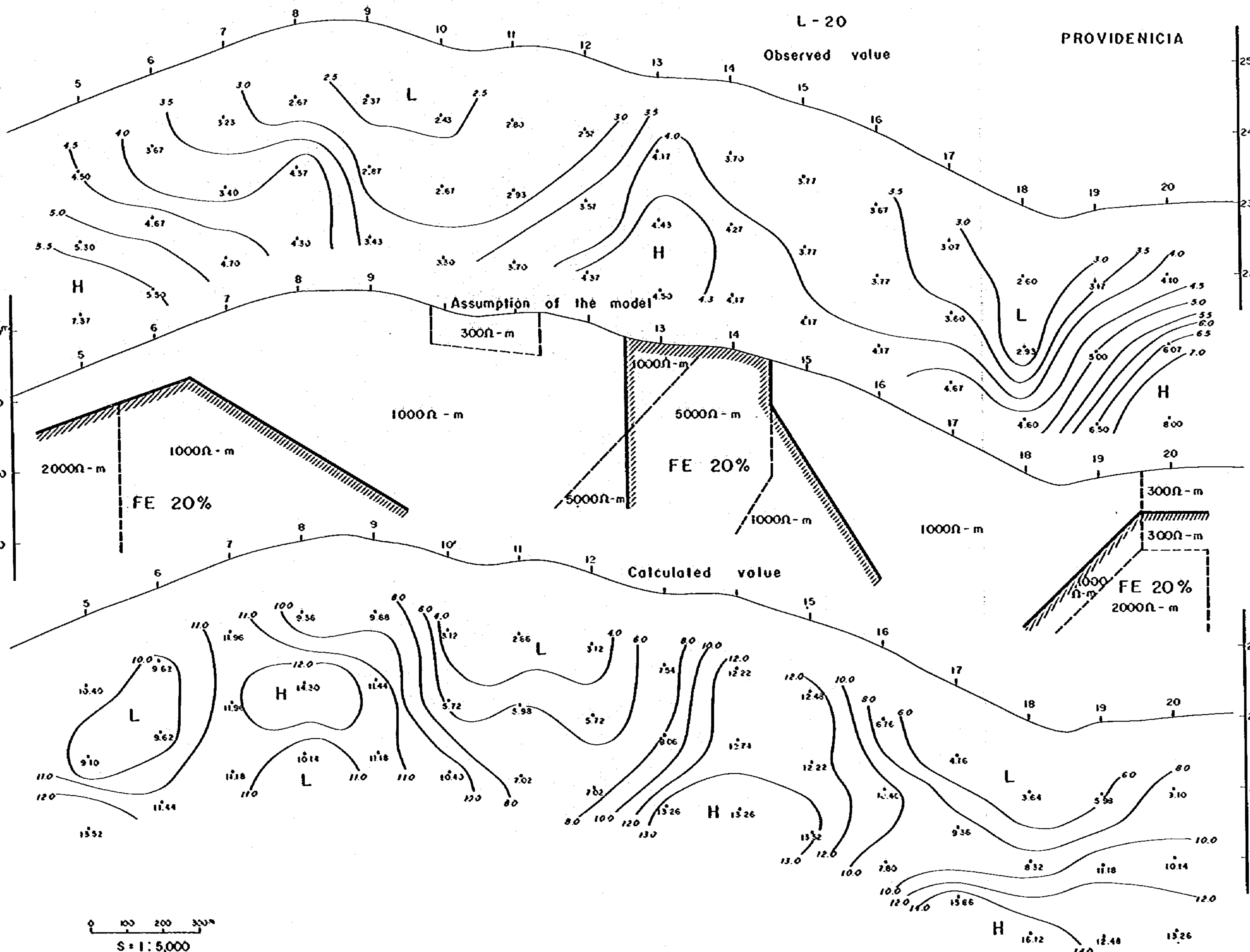

Fig. 4-41 Result of IP model calculation

4-6 Resistivity Measurement of Rock Samples

Resistivity of 34 rock samples collected in the both area (23 pcs in EL TEJOCOTE and 11 pcs in PROVIDENCIA) was measured in the laboratory. FE value in the frequency domain was also measured and was used for the interpretation multiplying this value by 2.6 in stead of time domain value.

The locality of samples is shown on PL. 4-3 (INTERPRETATION MAP OF IP SURVEY).

IP survey areas locate in the zone where limestone is distributed widely and most of sampled rocks are limestone, but the lithology of rocks differ from each other respectively.

The result of measurement is shown in Table 4-7 and it can be said as follows the result of measurement.

(1) Resistivity of limestone sample is greater than field data as whole, but it is inferred that these values are quite reasonable for limestone samples.

(2) It seems that FE values of muddy limestone and hematitized limestone samples are a little greater than other limestone samples.

(3) It is quite difficult to distinguish ore sample from other rocks by FE value measured here.

Table 4 − 7 List of Resistivity(ρ) and Frequency Effect(FE) of Rocks Sampled in the Survey Area.

№ of rock		Name of rock	ρ (Ω−m)	FE (%)	FE×2.6
1	EL TEJOCOTE	Limestone(light gray, muddy)	5,910	2.4	6.24
2		Limestone(fine grained)	22,688	0.9	2.34
3		Limestone(fine grained)	7,165	1.4	3.64
4		Limestone(light gray, muddy)	4,112	3.4	8.84
5		Limestone(dark gray)	2,937	1.5	3.90
6		Limestone(fine grained)	3,123	1.7	4.42
7		Limestone(light gray)	51,987	0.7	1.82
8		Limestone(dark gray)	67,585	1.3	3.38
9		Limestone(fine grained)	2,800	1.1	2.86
10		Limestone(fine grained)	9,968	1.2	3.12
11		Limestone(with hematite film)	970	1.8	4.68
12		Limestone(light gray)	13,724	1.2	3.12
13		Limestone(dark gray)	2,062	1.9	4.94
14		Diorite(hornblende-biotite)	706	2.0	5.20
15		Limestone(muddy)	61,268	0.3	0.78
16		Limestone(light gray)	16,991	0.8	2.08
17		Limestone(with calcite veinlets)	1,036	2.3	5.98
18		Limestone(muddy, recrystallized)	3,240	2.0	5.20
19		Limestone(muddy, light gray)	73,296	0.3	0.78
20		Limestone(dark gray, muddy)	1,963	1.6	4.16
21		Limestone(fine grained)	2,940	0.3	0.78
22		Limestone(fine grained)	4,193	1.0	2.60
23		Limestone(light gray)	5,187	1.5	3.90
24	PROVIDENCIA	Limestone(dolomitic)	3,983	1.3	3.38
25		Limestone(muddy)	805	3.5	9.10
26		Limestone(dark gray)	7,476	1.1	2.86
27		Limestone(hematite gossanized)	2,163	1.4	3.64
28		Oxidized ore	9,600	1.3	3.38
29		Limestone(strongly hematitized)	517	1.1	2.86
30		Limestone(hematitized)	11,322	1.7	4.42
31		Limestone(muddy or Marl)	25,405	1.8	4.68
32		Limestone(with iron gossan)	4,830	1.2	3.12
33		Marl(or muddy Limestone)	33,939	0.5	1.30
34		Limestone(thick bedded)	440	1.0	2.60

4-7 Conclusion

From the results of the present survey, following conclusions are derived.

EL TEJOCOTE Area

1) Chargeability measured in this area has the range of 0.67 ∿ 3.83 milli-sec. Those values are very small for anomalous values of chargeability, but the values between 0.67 and 2.50 milli-sec. were considered to be the background generally endowed with the rocks in the survey area, and the value higher than 2.50 milli-sec. were taken to be anomaly.

2) The values of apparent resistivity measured in the area were distributed in the wide range between 200 and 3700 Ω-m, and the average of resistivity is approximately 650 Ω-m. The area is widely underlain by limestones, and the range of measured values described above is considered to be a little small for apparent resistivity of the limestone.

3) Most of anomalous zones of chargeability in this area situate in high resistivity zone. Namely, they form high chargeability and high resistivity type anomaly, but the anomalous value of chargeability is only about two times as large as background value. From this fact, it cannot be inferred that those anomalies in this area are caused by existence of sulfide or mineralized zones.

4) But the anomaly C and F are in zones of high chargeability and low resistivity and coincide with anomalous zone of silver and lead in comparison with the result of geochemical analysis.

5) It cannot be concluded that those anomalous zones have possibility for ore deposit.

PROVIDENCIA Area

1) Chargeability in this area has the range between 1.90 and 9.00 milli-sec., this range is about two times as large as that of EL TEJOCOTE area. It was considered that lower values than 3.5 milli-sec. were background value and higher than 3.5 were taken to be anomalous value.

2) Apparent resistivity has the range of 170 ∿ 3400 Ω-m. In this area, shale, siltstone, sandstone and marl are distributed at the ends of all survey lines and the zones of those rocks coincide with low resistivity zone. Limestone is distributed in the central zone in this area between those rocks, and the resistivity of this zone is relatively high.

3) In this area, a tendency can be recognized that chargeability and resistivity become greater as the depth below ground surface increases and it is supposed by this fact that there may exist an original mineralized zone in the deep part, from which an influence of mineralization comes up to the near ground surface.

4) Anomalies A and C have high chargeability and low resistivity, and chargeability and resistivity of B and E anomalies are high.

5) A and C anomalies are distributed in the zone of shale ∿ marl mentioned above, and B and E anomalous zones coincide with the mineralized zone which is recognizable on the ground surface. In comparison with the result of geochemical

analysis, B anomaly has relation to the anomalous zone of silver and lead and E to the lead anomaly.

6) B anomaly has a large extent and is inferred to have strong possibility of being ore deposit, therefore it is strongly expected that the drilling will be done in the next stage of survey.

7) From the results of resistivity and IP measurement of rock samples, it can be said that resistivity of limestone sample is greater than field data as whole and FE values of muddy limestone and hematitized limestone samples are a little greater than other limestone samples. It is quite difficult to distinguish ore sample from other rocks by FE values of samples measured here.

By a complehensive study made on the maps and profiles of chargeability, and apparent resistivity and apparent metal factor, IP simulation, and surface geological maps, the result is compiled in PL. 4-3 (INTERPRETATION MAP OF IP SURVEY).

CHAPTER 5 CONCLUSION AND RECOMMENDATION

CHAPTER 5 CONCLUSION AND RECOMMENDATION

5-1 Conclusion

The third phase work was carried out in the three target areas with the purpose of obtaining the more detailed geological and geochemical data and of extracting substantial and promising mineralized zones to be of the target of future exploration.

On the basis of the survey results, necessity of further explorations for the three areas is concluded as follows:

EL TEJOCOTE Area

Geochemically anomalous zones of lead and silver, and IP high chargeability zones have been detected on a small scale, although no surface showing of mineralized zone has not been confirmed yet. It is, therefore, necessary to make a future plan after conducting a comparative study with other two areas about the priority of further exploration.

PROVIDENCIA Area

The comprehensive study on high-grade and large-scale geochemically anomalous zone, the arrangement of ore outcrops, the location and form of IP high-chargeability zone and its tendency to become stronger with the increase of depth, leads to the conclusion that the exploration work to the deeper part of the mineralized zone is recommended in the first place.

The area can be ranked the first class as the target of future exploration.

SAN CLEMENTE Area

The preliminary study conducted hitherto indicates that the scale and grade of the mineralized zone are in the same order to those of the gold-silver mines in the United States and Canada where low-grade ore is being mass-processed.

It is highly requested, therefore, that the exploration work are to be carried out to make clear the distribution of gold and silver grades on the surface by continuous channel sampling of the mineralized zone and to investigate the variation in grade and size of the zone up to the depth of several hundred meters.

The area can be ranked the first class as the target of future exploration.

5-2 Recommendation

It is recommended that the following exploration would be conducted in the two areas of the SAN CLEMENTE and the PROVIDENCIA.

SAN CLEMENTE Area

(1) Confirmation of the continuity of the mineralized zone by stripping, trenching and continuous channel sampling to grasp more precisely the distribution of gold and silver grades on the surface, is recommended putting emphasis on the western part of the A-mineralized zone.

(2) In order to investigate the presence or absence of economical ore at depth, diamond drillings are desired to penetrate the deeper extension of the mineralized zone horizontally from topographically lower place in the area.

PROVIDENCIA Area

(1) Prospecting of the deeper part by diamond drilling is to be carried out taking into account the relation between distribution and position of the anomalous zones of both geochemical and IP surveys.

(2) The detailed survey, sketch and sampling of the mineralized outcrops are recommended.

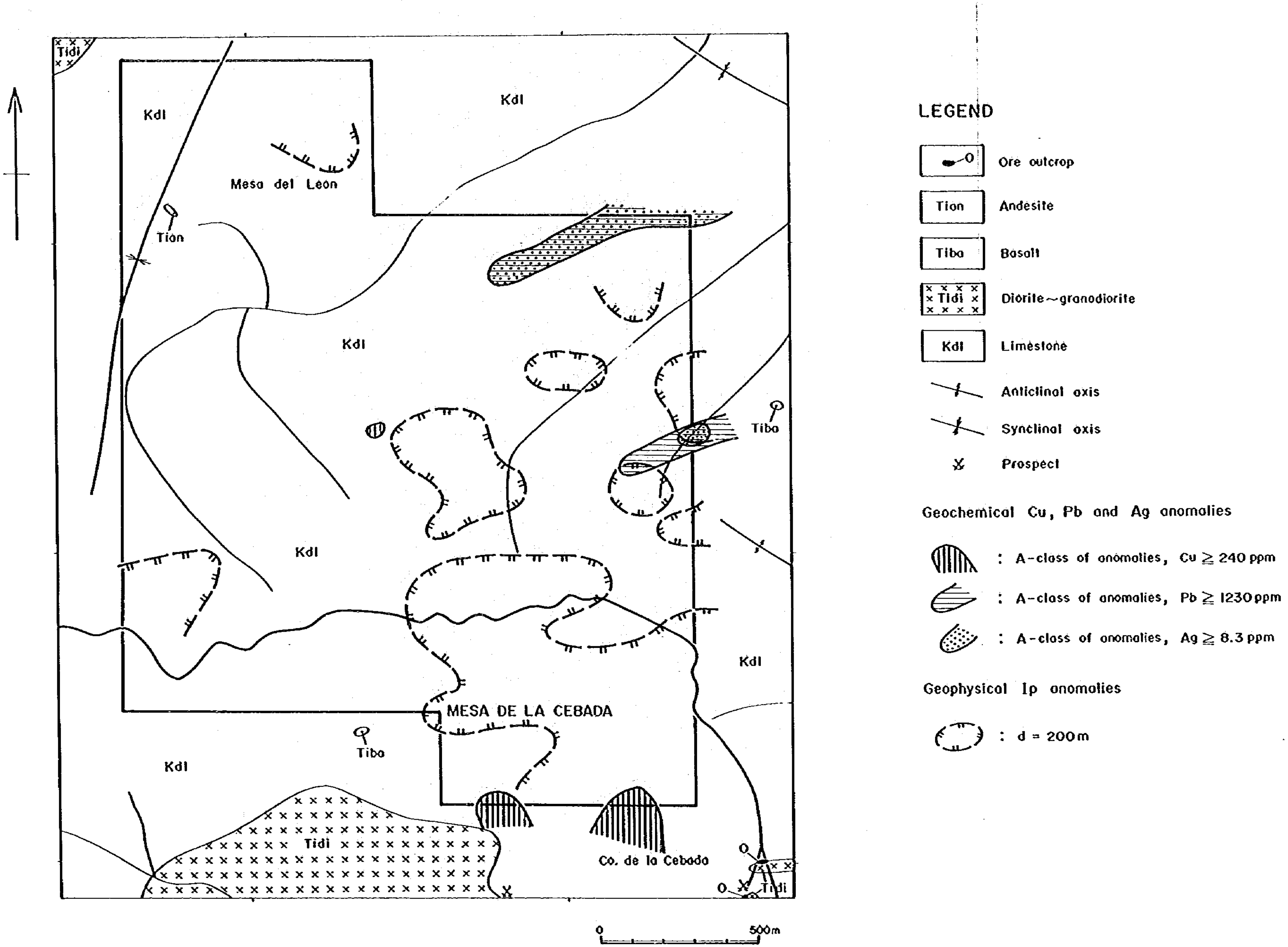

Fig. 5-1 Interpretation Map of the EL TEJOCOTE Area

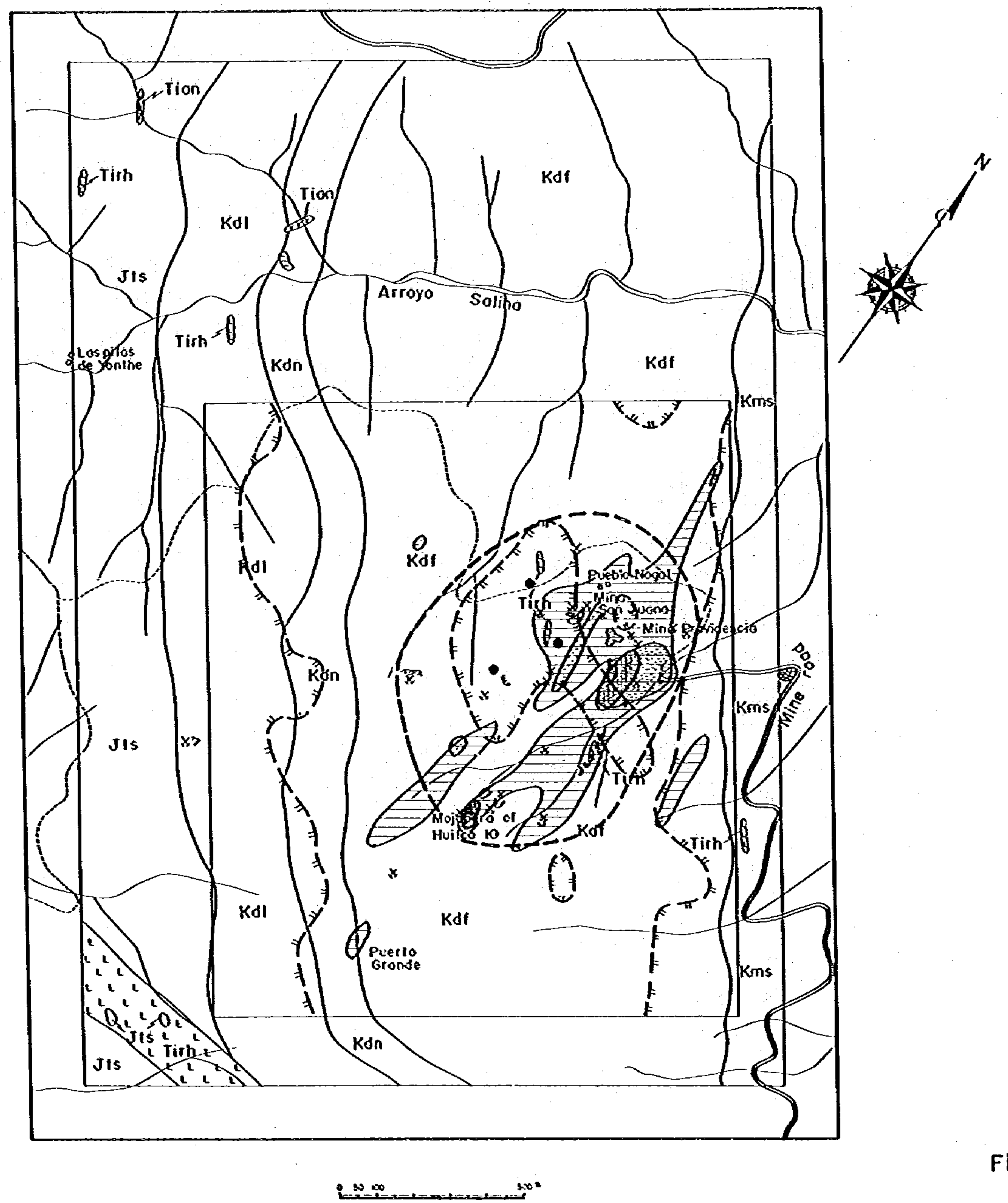

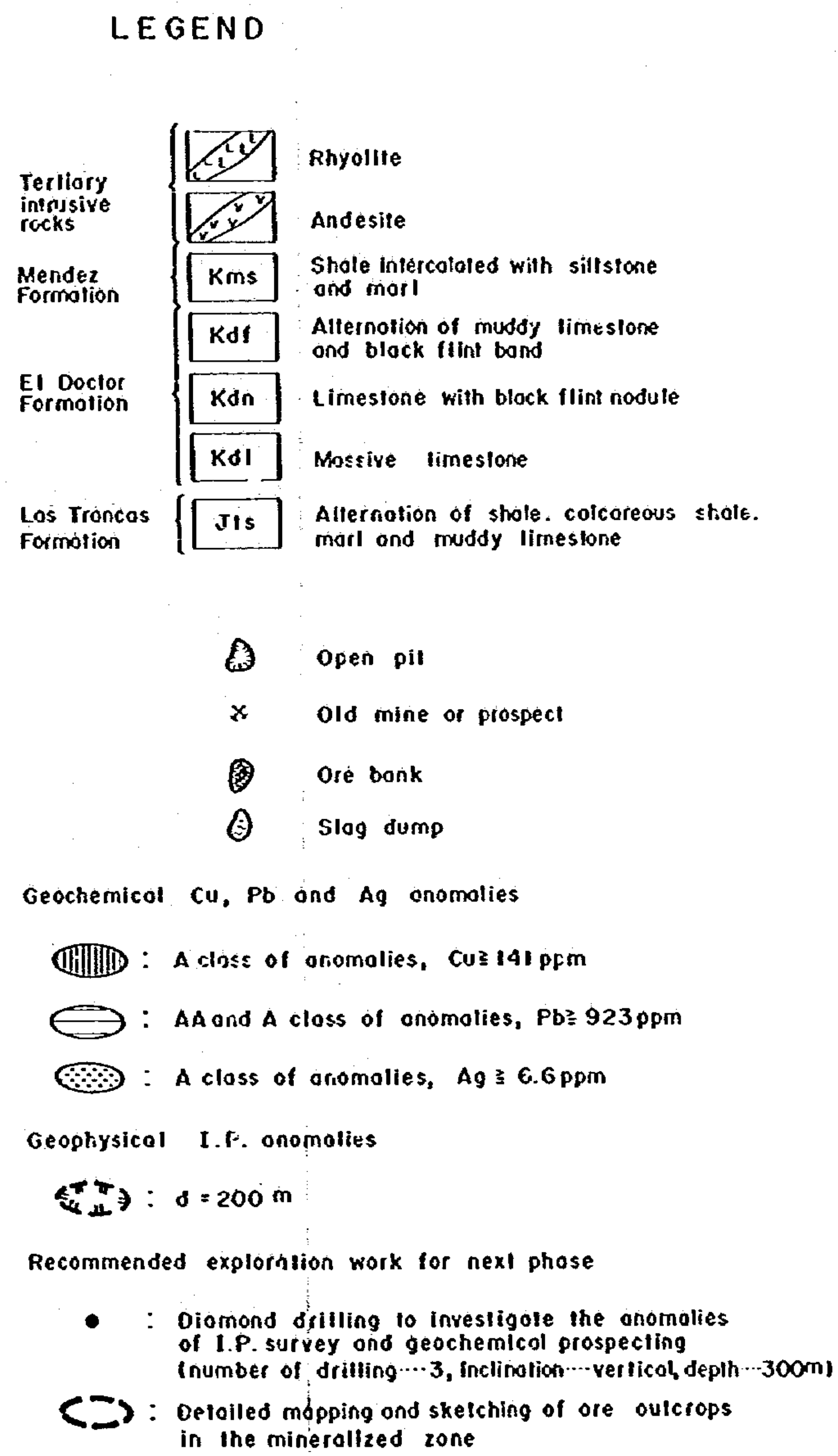

Fig.5-2 Interpretation Map of the PROVIDENCIA Area

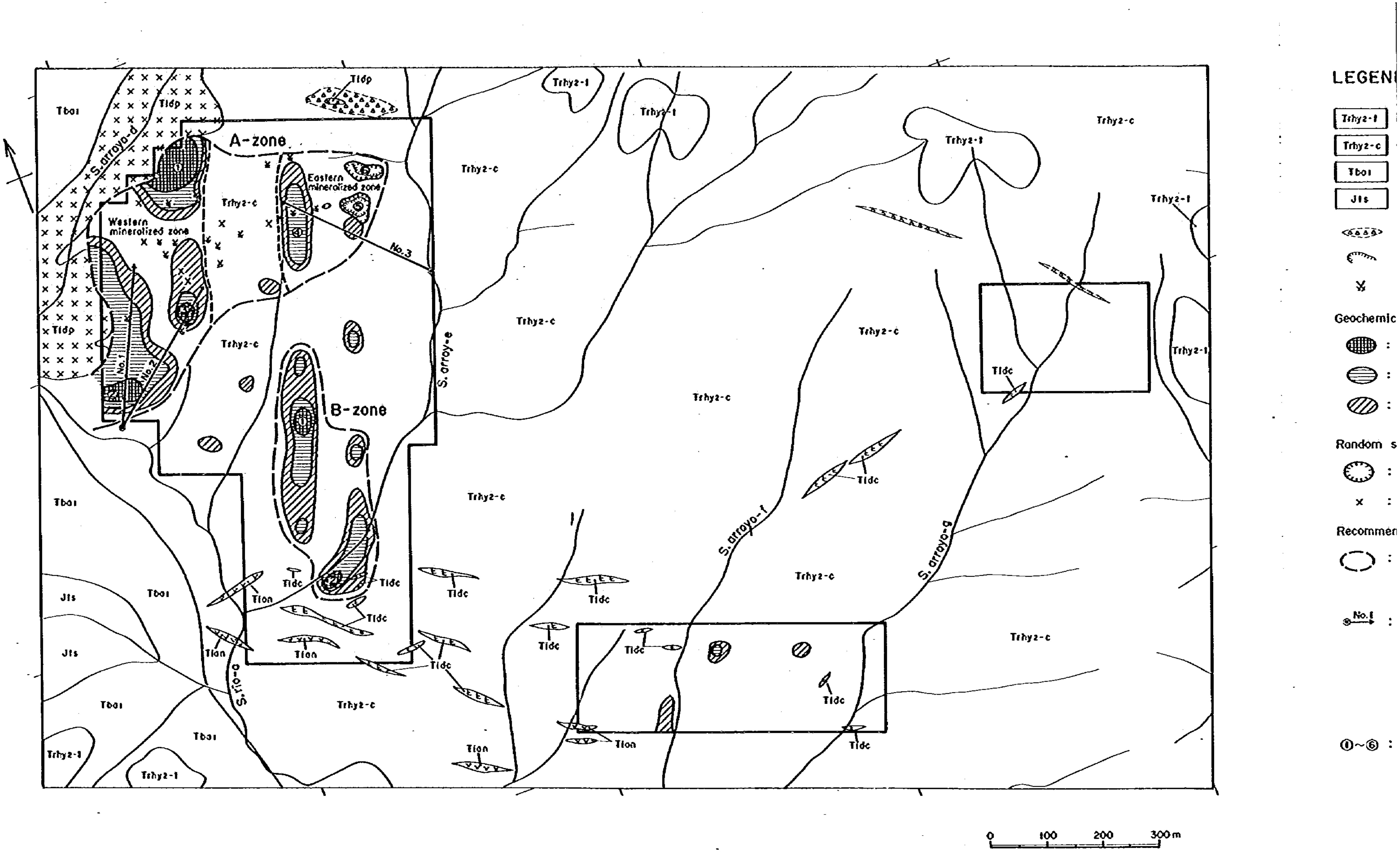

Fig. 5-3 Interpretation Map of the SAN CLEMENTE Area

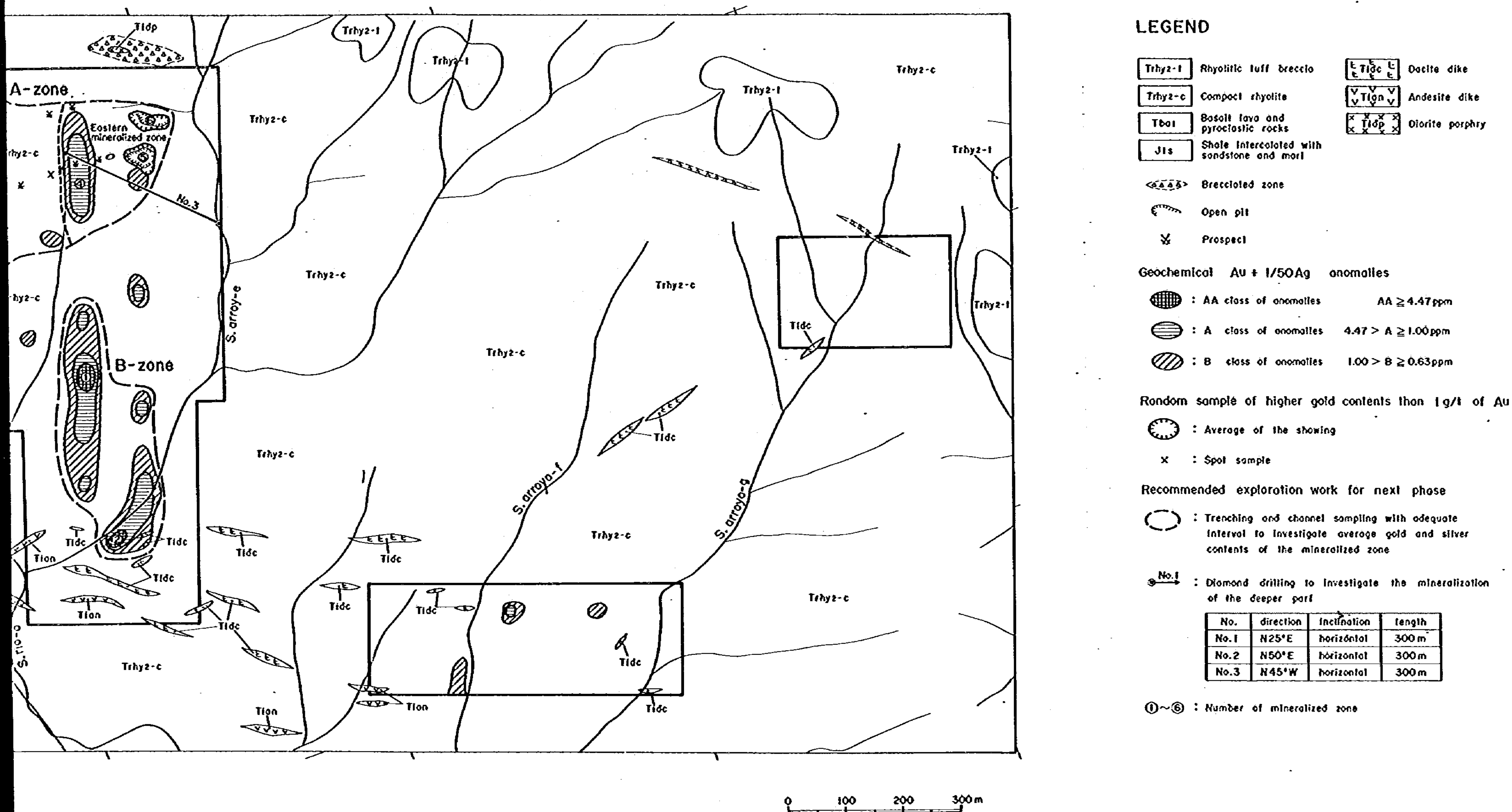

Fig. 5-3 Interpretation Map of the SAN CLEMENTE Area

REFERENCES

1) Aguilar Garcia, M., 1972 — Prospección geológico-minera de la región de Maconí, Zimapán, Pachuca, Edos. de Querétaro e Hidalgo : Tesis Profesional, I.P.N.

2) Bastin, E.S., 1948 — Mineral relationships in the ores of Pachuca and Real del Monte, Hidalgo, México : Econ. Geol., v. 43, p. 53-65.

3) Benites M., J.A., 1972 a — Informe mensual de la zona Cardonal, Hgo. : C.R.N.N.R. (inedito).

4) ________________ 1972 b — Informe preliminar de la zona Bonanaza, Hgo. : C.R.N.N.R. (inedito).

5) Boyle, R.W., 1976 — The geochemistry of gold and its deposits (together with a chapter on geochemical prospecting for the element) : Geological Survey of Canada, Bulletin 280.

6) Carrillo Bravo, J., 1965 — Estudio geológico de una parte del Anticlinorio de Huayacocotla : Asoc. Mex. Geol. Petrol., v. 13.

7) Casarrubias Jimenez, J.S., 1973 — Exploración geológico minera del área de el Cardonal, Estado de Hidalgo : Tesis Profesional, 52 p., I.P.N.

8) Chairez Blanco, J., 1978 — Estudio geológico-minero de la Mina San Miguel, la Pechuga, Mpio de Ixmiquilpan, Hidalgo : Tesis Profesional, I.P.N.

9) Cumming, G.L., et al., 1979 — Isotopic composition of lead in Mexican mineral deposits : Econ. Geol., v. 74. pp. 1395-1407

10) De la Crus, Trejo, M., 1975 — Guias útiles de la prospección de minerales en el distrito minero de Zimapán, Edo. de Hidalgo : Tesis Profesional, I.P.N.

11) De Pablo Galan, L., 1965 — Los minerales de manganeso de Molango, Hidalgo : Univ. Nac. Autón. Méx. Inst. Geol., Bol. 76, pte. 1, p. 1-38.

12) Fries, C., Jr., 1956 — Bosquejo geológico de la región entre México, D.F. y Taxco, Guerrero : Internat. Geol. Cong., 20th, Mexico, 1956, Guidebook Excursions A-4 and C-2, p. 11-35.

13) ________________ 1962 — Carta geologica de Mexico : Hoja Pachuca 14, Q.E. (11).

14) Galicia F., J., 1972 — Informes mensuales de la zona de Encarnación, Hgo : C.R.N.N.R.

15) Geyne, A.R., 1949 — Mineral relationships in the ores of Pachuca and Real del Monte, Hidalgo, México-a reply : Econ. Geol., v. 44, p. 233-234.

16) ____________ 1956 — Las rocas volvanicas y los yacimientos argentiferos del distrito minero de Pachuca-Real del Monte, Estado de Hidalgo : Internat. Geol. Cong., 20th: Mexico, 1956, Guidebook Excursions A-3 and C-1, p. 47-57.

17) Geyne, A.R., and Wilson, I.F., 1951 — Relación entre los cuerpos de mineral costable y los diques en el distrito de Pachuca-Real del Monte, Estado de Hidalgo, México (abstract) : Convención Interamericana de Recursos Minerales, 1a, México, 1951, Mem., p. 270.

18) Geyne, A.R., and Wilson, I.F., et al., 1963 — Geology and mineral deposits of the Pachuca-Real del Monte District, State of Hidalgo, México : C.R.N.N.R., Mem. 5 E.

19) Imlay, R.W., 1944 a — Cretaceous formations of Central America and Mexico : Bull. Amer. Assoc. Petrol. Geol., v. 28, p. 1077-1195.

20) ____________ 1944 b — Correlation of the Cretaceous formations of the Greater Antillers, Central America, and Mexico : Bull. Geol. Soci. Amer., v. 55, p. 1005-1046.

21 ____________ 1952 — Correlation of the Jurassic formations of North America, exclusive of Canada : Bull. Geol. Soci. Amer., v. 63, p. 953-992.

22) JICA and MMAJ, 1980 — Report on geological survey of the Pachuca-Zimapán area, central Mexico; phase I : 109 p., Japan International Cooperation Agency and Metal Mining Agency of Japan.

23) Krauskopf, K.B., 1979 — Introduction to Geochemistry : 721 p., MacGraw-Hill Book Co.

24) Kuno, H., 1976 — Volcanoes and Volcanic Rocks (in Japanese): 2nd ed., 283 p., Iwanami Press.

25) Lee Moreno, J.L., 1974 — Geochemical prospecting for epithermal precious metals veins in the vicinity of the Pachuca-Real del Monte mining district in Mexico : Soci. Min. Engn., AIME, p. 1-16.

26)	Miyashiro, A. and Kushiro, I., 1977	Petrology I, II and III (in Japanese) : Kyoritsu Press.
27)	Quintus Bosz, R.L., 1972	Estudio geológico de la zona fosforitica de San Francisco, Municipio de Pacula, Estado de Hidalgo : C.R.N.N.R., p. 28-45.
28)	Restovic Peres, I.V., 1973	Estudio geológico minero del área de Encarnacion, Mpio. de Zimapán, Edo. de Hidalgo : Tesis Profesional, U.N.A.M.
29)	Rösler, and Lange, 1972	Geochemical Tables : Elsevier
30)	Salas, G.P., 1975	Carta y provincias metarogeneticas de la Republica Mexicana : C.R.M. de México, Publicación 21E.
31)	Schulze, G., 1951	Mantos intrusivos en formaciones volcanicas en sus relaciones con vetas : Convención Interamericana de Recrusos Minerales, 1ª, México., 1951, Mem., p. 202-207.
32)	Segerstrom, K., 1956	Estratigrafía y tectónica del Cenozoico entre México, D.F. y Zimapán, Hgo. : Internat. Geol. Cong., 20th, Mexico, 1956, Guidebook Excursions A-3 and C-1, p. 11-22, also A-14 and C-6, p. 311-323.
33)	______________ 1961	Geología del suroeste del Estado de Hidalgo y del noreste del Estado de Mexico : Asoc. Mex. Geol. Petrol., Bol., v. 13, p. 147-168.
34)	______________ 1962	Geology of south-central Hidalgo and northeastern Mexico, Mexico : U.S. Geol. Survey, Bull., 1104-C, p. 87-162.
35)	Simons, F.S. and Mapes V.E., 1957	Geología y yacimientos minerales del distrito minero de Zimapán, Hidalgo : Instituto Nacional para Investigación de Recursos Minerales.
36)	Smith, R.L.et al.	Hidalgoite, a new mineral. : U.S. Geol. Survey, Washington, D.C., p. 1218-1224.
37)	Takeda, H., 1977	Las caracteristicas de la mineralización de los depositos de plomo, zinc, y plata en las calizas de la parte norte de la Sierra Madre Oriental, México : VI seminario interno sobre exploracion geológico-minera, de C.R.M.
38)	Tavera Amezcua, E., 1965	Yacimientos estanníferos del Fundo la Esperanza, Zimapán, Hgo. : Mineria y Metalurgía, v. 35, p. 67-75.

39) Tavera Amezcua, E. and Alexandri R., R., 1963 — Los yacimientos de manganeso del área de Molango, Hidalgo : V Convencion de la Asoc. de Ings. de Minas, Met. y Geologos de México, Torreon, Coahuila.

40) Thornburg, C.L., 1945 — Some applications of structural geology to mining in the Pachuca-Real del Monte area, Pachuca silver district, Mexico : Econ. Geol., v. 40, p. 283-297.

41) ____________ 1952 — The surface expression of veins in the Pachuca silver district, Mexico : Mining Eng., v. 4, p. 594-600.

42) Turban, E., 1947 — Estudio de la mineralización a la profundidad en los minerales de Pachuca y Real del Monte, Estado de Hidalgo : Minas y Petróleo, Bol., v. 16, p. 3-6.

43) White, D.E., 1947 — Diagenetic origin of chert lenses in limestone at Soyatal of Querétaro, México : Amer. Jour. Sci., v. 245, p. 49-55.

44) ____________ 1948 — Antimony deposits of the Soyatal district, State of Querétaro, Mexico : U.S. Geol. Survey, Bull. 960-B, p. 35-38.

45) Wilson, B.W., Hernandez, Pedro, and Meave T., Edgardo, 1955 — Un arrecife cretácico en la parte oriental del Estado de Querétaro : Soc. Geol. Mex., Bol., v. 18, p. 1-10.

46) Wisser, E., 1937 — Formation of the north-south fractures of the Real del Monte Area, Pachuca silver district, Mexico. : Amer. Inst. Mining Metall. Engineers, Trans., v. 126, p. 442-486.

47) Wisser, E., 1941 a — Discussion of paper by McKinstry on structural control of ore deposition in fissure veins : Amer. Inst. Mining Metall. Engineers, Trans., v. 144, p. 87-93.

48) ____________ 1941 b — The environment of ore bodies : Amer. Inst. Mining Metall. Engineers, Trans., v. 144, p. 96-110.

49) ____________ 1941 c — Discussion in Symposium on some observations in ore research : Amer. Inst. Mining Metall. Engineers, Trans., v. 144, p. 140-145.

50) ____________ 1942 — The Pachuca silver district, Mexico, in "Ore deposits as related to structural features" : ed. Newhouse, W.H., p. 229-235., Princeton Univ. Press.

51) Wisser, E., 1946 — Some applications of structural geology to mining in the Pachuca-Real del Monte area, Pachuca silver district, Mexico-a reply : Econ. Geol., v. 41, p. 77-86.

52) ____________ 1948 — Mineral relationships in the ores of Pachuca and Real del Monte, Hidalgo, Mexico-a reply : Econ. Geol., v. 43, p. 280-292.

53) ____________ 1951 — Tectonic analysis of a mining district-Pachuca, Hidalgo : Econ. Geol., v. 46, p. 459-477.

54) Wittich, E. and Vivar, G., 1913 — La celestita de Atotonilco el Grande, Hgo. : Soc. Geol. Mex. Bol., p. 5-8.

APPENDICES

APPENDICES

Abbreviations for Tables, Figures and Appendices

Stratigraphic unit

System	Unit	Symbol	Description
Quarternary System		QTcgs	gravel, sand, silt and ash
Tertiary System	Intrusive rocks	Tirh	rhyolite
		Tidc	dacite
		Tian	andesite
		Tiba	basalt
		Tidp	diorite porphyry
		Tidi	diorite, quartz diorite and granodiorite
	Volcanic rocks	Trhy$_2$	Trhy$_2$-l: banded rhyolite lava
			Trhy$_2$-t: rhyolitic tuff breccia
			Trhy$_2$-c: compact rhyolite
		Tba$_1$	basalt lava and pyroclastic rocks
	El Morro Fanglomerate	Tcg	conglomerate
Cretaceous System	Mendez Formation	Kms	shale, marl and sandstone
	El Doctor Formation	Kdf	flint banded limestone and marl
		Kds	shale and marl
		Kdc	calcirudite and calcarenite
		Kdn	limestone with black flint nodule
		Kdl	massive limestone
Upper Jurrasic to Lower Cretaceous System	Las Trancas Formation	Jts	shale, calcareous shale, sandstone and marl

Rock-forming minerals

qz; quartz
pl; plagioclase
ab; albite
or; orthoclase
an; anorthite
af; alkali-feldspar
fd; feldspar
ol; olivine
px; pyroxene
hy; hypersthene
ho; hornblende
ms; muscovite
bi; biotite
ap; apatite
ti; titanite
zr; zircon
gl; glass
op; opaque mineral
sr; sericite
ca; calcite
ch; chlorite
st; serpentine
sl; silica mineral
ga; garnet
ep; epidote
wo; wollastonite
ba; barite
mt; montmorillonite
kn; kaolin
hh; hydrated halloysite
cl; clay mineral
lf; lithic fragment
mfr; mineral fragment
mf; microfossil

Ore-minerals

gd; gold
cp; chalcopyrite
py; pyrite
sp; sphalerite
gn; galena
po; pyrrhotite
mg; magnetite
sd; siderite
ml; malachite
cv; covelline
hm; hematite
gt; goethite
lm; limonite
jr; jarosite
sm; smithonite
hem; hemimorphyite

Apx. 1 K−Ar Whole-rock Datings, Chemical Analyses and CIPW Normative Calculations of the Igneous Rocks.

K-Ar whole-rock datings

No.	Sample No.	Coordinates E	Coordinates N	Rock name	Strati-graphic unit	K (%)	SCC$^{40}Ar^R$ (10^{-5} g)	$^{40}Ar^R$ (%)	Age (Ma)
1	A57DTC	483500	2310810	Quartz diorite	Tidi	2.06 2.06 2.09	0.413 0.426	87.8 84.6	51.7±2.6
2	B44DTC	488385	2284625	Rhyolite	Tirh	2.74 2.75 2.77	0.272 0.279	82.7 80.9	25.5±1.3

$\lambda_e = 0.581 \times 10^{-10} yr^{-1}$; $\lambda_\beta = 4.962 \times 10^{-10} yr^{-1}$; $^{40}K/K = 1.167 \times 10^{-4}$; $^{40}Ar^R$, Ragiogenic argon 40 ;

analyses in duplicate

Chemical analyses

No.	Sample No.	SiO_2	TiO_2	Al_2O_3	Fe_2O_3	FeO	MnO	MgO	CaO	Na_2O	K_2O	P_2O_5	$H_2O(+)$	$H_2O(-)$	Total
1	A57DTC	62.4	0.76	16.4	2.75	2.50	0.09	1.76	4.80	3.50	2.46	0.39	0.72	0.51	99.04
2	B44DTC	73.8	0.25	13.1	1.38	0.49	0.07	0.30	1.52	3.47	4.08	0.13	0.49	0.60	99.68

weight %

CIPW normative calculations

No.	Sample No.	Q	C	or	ab	an	hy	mg	hm	il	ap	Sal. tot.	Fem. tot.	D.I.
1	A57DTC	20.45	0.18	14.68	29.90	21.50	5.67	4.03	0	1.46	0.91	86.71	12.07	65.03
2	B44DTC	34.78	0.52	24.19	29.40	6.72	0.75	1.08	0.64	0.48	0.30	95.61	3.25	88.37

weight %

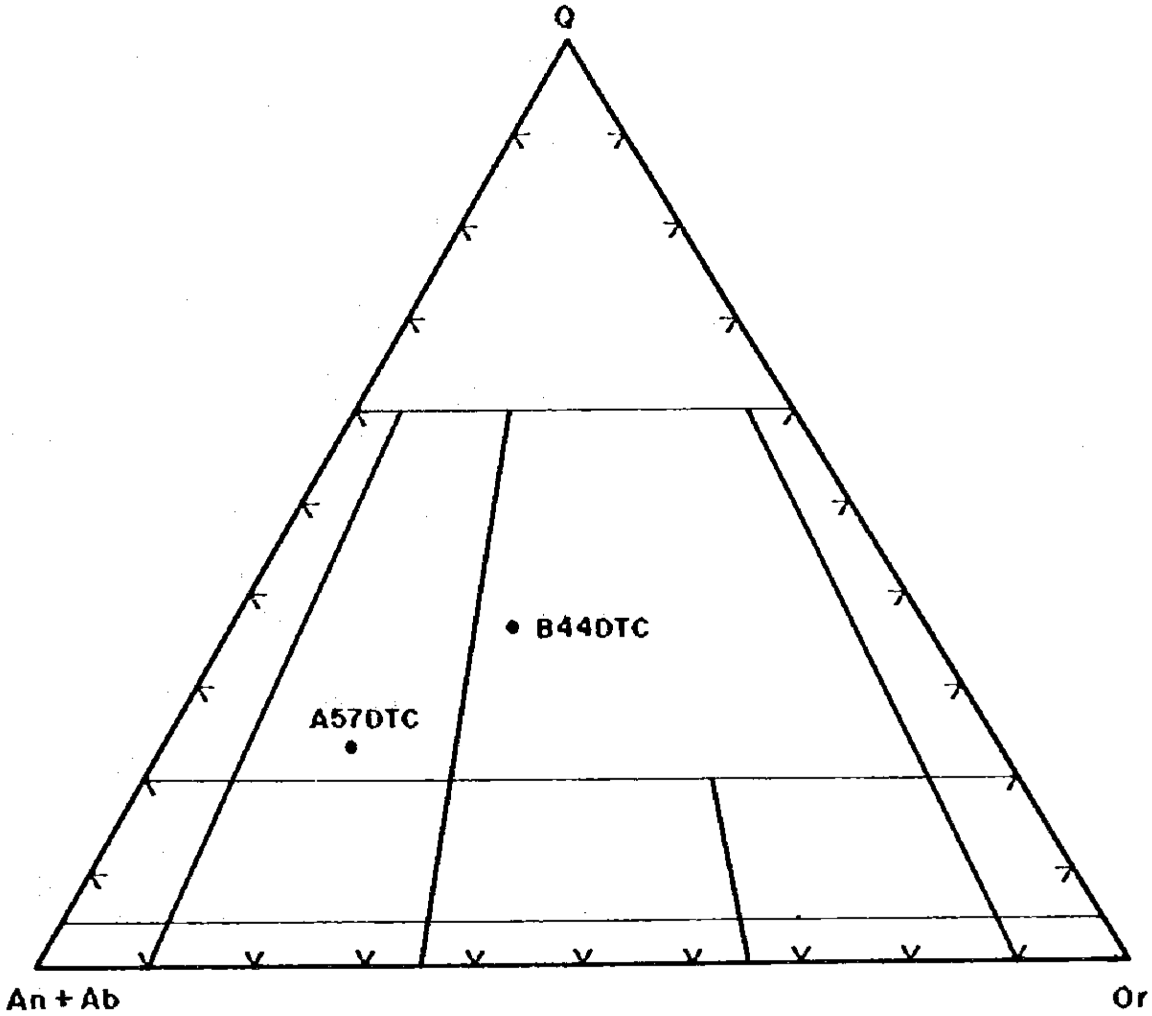

Apx.2 Normative Q-(An+Ab)-Or Diagram for the Igneous Rocks.

Apx. 3 Microscopic Observations of the Rock and ore Samples by thin Sections

Area	Ser. No.	Sample No.	Location Coordinates E	Location Coordinates N	Strati-graphic unit	Rock name	Texture	Primary mineral or material: ol	px	ho	bi	ms	ti	zr	ap	op	af	pl	qz	ca	lf	mf	gl	cl	mfr	Seco[ndary]: ga	wo	ep	af	sl	ca	ch
EL TEJOCOTE	1	A17T	481025	2309815	Tidi	Aplitic granite	Granular				•		•			•	◎	◎	◎													
	2	A23T	482980	2311700	Kdl	Limonitized limestone	Mosaic													◎										○		
	3	A24T	483175	2311720	Tidi	Skarnized granitoid	Porphyritic,porphyroblastic			•	•				•	•	○	◎	○							○		◎			○	
	4	A27T	482820	2309800	Tian	Ho andesite	Porphyritic, felty			○						•	•	◎	•												•	
	5	A30T	482750	2309910	Kdl	Limonitized limestone	Mosaic													◎												
	6	A32T	482750	2310050	Tcg	Breccia	Clastic												•	◎	◎			○								
	7	A34T	481360	2314160	Tidi	Ho-bi granodiorite	Mosaic			○	○					○	○	◎	○												•	
	8	A42T	481525	2308650	Sk	Wo skarn	Mosaic																				◎				•	
	9	A44T	477555	2308560	Kdl	Silicified limestone	Microcrystalline																						•	◎		
	10	A47PT	477110	2308185	Tidi	Skarnized granitoid	Porphyritic,porphyroblastic				•		•	•	•	•	○	◎	◎									○				○
	11	A50T	481500	2310385	Kdl	Crystalline limestone	Mosaic									•				◎												
	12	A57DTC	483500	2310810	Tidi	Ho-bi granodiorite	Porphyritic, poikilitic			•	○		•		•	•	○	◎	○													
	13	A67PT	480810	2317220	Sk	Mineralized ga skarn	Mosaic,porphyroblastic																			○			○	◎	○	
	14	bA18MTX	477700	2310365	Kdl	Limestone with ba vein	Mosaic													◎										•	•	
	15	bA19T	477675	2310120	Tiba	Ol-ho-px basalt	Porphyritic	◎	◎	◎						○		○													○	○
	16	bA20T	480400	2310100	Tidi	Ho-bi granodiorite	Mosaic,		•	○	○		•	•	•	•	○	◎	◎												•	
	17	bA22T	480780	2310090	Kdl	Crystalline limestone	Mosaic													◎												
	18	eA4T	478590	2308455	Tidi	Ho-bi quartz diorite	Mosaic, poikilitic		•				•		•	•	○	◎	○													
PROVIDENCIA	19	B 3T	487500	2284905	Tirh	Rhyolite	Porphyritic,spherulitic					•				•	◎	◎	◎													
	20	B 8T	486575	2285580	Tirh	Rhyolite	Porphyritic,spherulitic					•		•		•	◎	◎	◎													
	21	B 9T	486605	2285560	Tian	Altered andesite	Porphyritic									•	○	◎	○				•							○	◎	◎
	22	B11T	487470	2284680	Tirh	Rhyolite	Porphyritic,micrographic									•	◎	◎	◎													
	23	B22T	487410	2286635	Kdf	Limestone	Detritic												○	◎	○									•	•	
	24	B24T	486505	2285985	Kdl	Crystralline limestone	Fine-mosaic													◎		○										
	25	B29T	487745	2286355	Kdf	Limestone	Micritic													◎		○										
	26	B35T	488065	2086105	Tirh	Rhyolite	Porphyritic, micrographic									•	◎	○	◎											•		
	27	B39T	488615	2286030	Kdf	Limestone	Detritic													◎		?										

ock and ore Samples by thin Sections

ck name	Texture	Primary mineral or material																		Secondary mineral																Remarks
		ol	px	ho	bi	ms	ti	zr	ap	op	af	pl	qz	ca	lf	mf	gl	cl	mfr	ga	wo	ep	af	sl	ca	ch	st	sr	mt	lm	op	sm	ml	sd	ba	
anite	Granular				•		•			•	◎	◎	◎																							
ed limestone	Mosaic													◎										○						◎	•	•				ep → sm,lm
granitoid	Porphyritic,porphyroblastic			•	•				•	•	○	◎	○							○		◎			○											
e	Porphyritic, felty			○						•	•	◎	•												•											ca veinlet,pl → ca
ed limestone	Mosaic													◎																○						
	Clastic												•	◎	◎			○												○						lf,limestone
nodiorite	Mosaic			○	○					○	○	◎	○												•											pl,ho → ca
	Mosaic																				◎				•						•					
d limestone	Microcrystalline																						•	◎						○						limonitized
granitoid	Porphyritic,porphyroblastic				•		•	•	•	•	○	◎	◎									○				○				•	•		○			Cu-mineralized
ne limestone	Mosaic									•				◎																						
nodiorite	Porphyritic, poikilitic			•	○		•		•	•	○	◎	○																							
ed ga skarn	Mosaic,porphyroblastic																			○			○	◎	○						○			•		py > gn > cp imp.
with ba vein	Mosaic													◎										•	•				•						◎	
basalt	Porphyritic	◎	◎	◎						○		○													○	○	○									ol → ca,ch,st
nodiorite	Mosaic,		•	○	○		•	•	•	•	○	◎	◎												•											px → ca
ne limestone	Mosaic													◎													•	•								
rtz diorite	Mosaic, poikilitic		•				•		•	•	○	◎	○																							
	Porphyritic,spherulitic					•				•	◎	◎	◎															•		•						af → sr
	Porphyritic,spherulitic					•		•		•	◎	◎	◎															•	•	•						af,pl,gl → sr+mt
ndesite	Porphyritic									•	○	◎	○				•							○	◎	◎										mafic mineral:pl, gl → ca,ch,qz
	Porphyritic,micrographic									•	◎	◎	◎															•		•						af → sr,op → lm
e	Detritic												○	◎	○									•	•											lf:chert,ca·qz veinlets
line limestone	Fine-mosaic													◎		○																				
e	Micritic													◎		○																				
	Porphyritic, micrographic									•	◎	○	◎											•					•	•						qz veinlets
e	Detritic													◎		?																				

(Apx. 3. Continued)

Area	Ser. No.	Sample No.	Location Coordinates E	Location Coordinates N	Strati-graphic unit	Rock name	Texture	Primary mineral or material: ol	px	ho	bi	ms	ti	zr	ap	op	af	pl	qz	ca	lf	mf	gl		mfr	Secondary: ga	wo	ep	af	sl	ca	ch
PRUV.	28	B44DTC	Out of the area		Tirh	Granodiorite porphyry	Porphyritic,microgranular				○			•		•	○	○	◎													
	29	B45T	487385	2284650	Tirh	Rhyolite	Fluidal,microcrystalline									•	◎		◎													
	30	B46T	485955	2286895	Tian	Altered andesite	Porphyritic,ophitic		○							○		◎	○											○	◎	○
SAN CLEMENTE	31	C 1T	482542	2283857	Trhy$_2$-c	Rhyolite	Porphyritic,microcrystalline					•				•	◎	○	◎													
	32	C 2T	482603	2283879	Tian	Andesite	Porphyritic,ophitic									○	•	◎	○									○				
	33	C 3T	482581	2283954	Tidc	Dacite	Porphyritic,devitrification									•	○	◎	○													
	34	C 4T	482671	2283925	Tidc	Dacite	Porphyritic,devitrification									•	○	◎	○													
	35	C 5T	482600	2284308	Trhy$_2$-c	Rhyolite	Porphyritic,microgranular					•				•	◎	○	◎													
	36	C 6T	482702	2284601	Trhy$_2$-c	Rhyolite	Porphyritic,microcrystalline									•	◎	○	◎													
	37	C 7T	482793	2284840	Trhy$_2$-c	Rhyolite	Porphyritic,microcrystalline					•				•	◎	○	◎													
	38	C 8T	482625	2284216	Trhy$_2$-c	Rhyolite	Porphyritic,microcrystalline										◎	○	◎													
	39	C 9T	482772	2284627	Trhy$_2$-c	Rhyolite	Porphyritic,microcrystalline					•				•	◎	○	◎													
	40	C10T	482614	2284048	Trhy$_2$-c	Rhyolite	Porphyritic,myrmekitic									•	◎	○	◎													
	41	C11T	482875	2284643	Trhy$_2$-c	Rhyolite	Porphyritic,microcrystalline									•	◎	○	◎													
	42	C12T	482904	2284553	Trhy$_2$-c	Rhyolite	Porphyritic,microcrystalline									•	◎	○	◎				○									
	43	C13T	483018	2284784	Tidp	Brecciated anorthosite	Cataclastic									•		◎													•	•
	44	C14T	483056	2284739	QTcgs	Calcareous conglomerate												○		◎	◎			○								
	45	C15T	482872	2284320	Trhy$_2$-c	Rhyolite	Porphyritic,microcrystalline									•	◎	○	◎				○									
	46	C16T	483010	2284558	Trhy$_2$-c	Rhyolite	Porphyritic,microcrystalline									•	◎	○	◎													
	47	C17T	483002	2284528	Trhy$_2$-c	Rhyolite	Porphyritic,microcrystalline							•		•	◎	○	◎													
	48	C18T	482739	2284845	Tidp	Weak-altered anorthosite	Coarse-ophitic									•	◎	◎													○	○
	49	C19T	482641	2284722	Trhy$_2$-c	Rhyolite	Porphyritic, microgranitic									•	◎	○	◎													
	50	C20T	482446	2284448	Trhy$_2$-c	Granite porphyry	Porphyritic, microgranitic									•	◎	○	◎													
	51	C21T	482453	2284688	Trhy$_2$-c	Granite porphyry	Porphyritic, microgranitic									•	◎	○	◎													
	52	C48T	483918	2284293	Trhy$_2$-t	Crystal tuff breccia													◎		◎				•							
	53	C54T	484638	2282640	Tidp	Ho-quartz diorite	Holocrystalline			◎					•	•		◎	◎													
	54	C56T	484540	2282880	Tiba	Basalt	doleritic		○									◎	•													
	55	C63T	484695	2284490	Trhy$_2$-t	Crystal tuff													◎		○				○							•

name	Texture	Primary mineral or material																		Secondary mineral																Remarks
		ol	px	ho	bi	ms	ti	zr	ap	op	af	pl	qz	ca	lf	mf	gl		mfr	ga	wo	ep	af	si	ca	ch	st	sr	ml		op	sm	ml	sd	ba	
orphyry	Porphyritic,microgranular				O			•		•	O	O	◎																	•						
	Fluidal,microcrystalline									•	◎		◎																	•						
te	Porphyritic,ophitic		O							O		◎	O											O	◎	O	O									mafic mineral → st pl,or,gl → ca,qz
	Porphyritic,microcrystalline					•				•	◎	O	◎															•								pl → sr
	Porphyritic,ophitic									O	•	◎	O									O						O								mafic mineral → ep,sr
	Porphyritic,devitrification									•	O	◎	O															•								af,pl → sr
	Porphyritic,devitrification									•	O	◎	O																							
	Porphyritic,microgranular					•				•	◎	O	◎															O								pl → sr
	Porphyritic,microcrystalline									•	◎	O	◎																							
	Porphyritic,microcrystalline					•				•	◎	O	◎																							
	Porphyritic,microcrystalline										◎	O	◎																							
	Porphyritic,microcrystalline					•				•	◎	O	◎																							
	Porphyritic,myrmekitic									•	◎	O	◎																							
	Porphyritic,microcrystalline									•	◎	O	◎																							
	Porphyritic,microcrystalline									•	◎	O	◎				O																			
rthosite	Cataclastic									•		◎													•	•										mafic mineral → ch,ca
glomerate												O		◎	◎			O																		lf;chert,felsic volcanic rocks
	Porphyritic,microcrystalline									•	◎	O	◎				O																			
	Porphyritic,microcrystalline									•	◎	O	◎																							
	Porphyritic,microcrystalline							•		•	◎	O	◎																							
northosite	Coarse-ophitic									•	◎	◎													O	O										mafic mineral → ca,ch
	Porphyritic, micrograniltic									•	◎	O	◎																							
ry	Porphyritic, micrograniltic									•	◎	O	◎																							
ry	Porphyritic, micrograniltic									•	◎	O	◎																	O						
breccia													◎		◎				•																	
rite	Holocrystalline			◎					•	•		◎	◎																							
	doleritic		O									◎	•																							
													◎		O				O							•	•									

Apx. 4 Photomicrographs of the Representative Rock Thin Sections

(1)

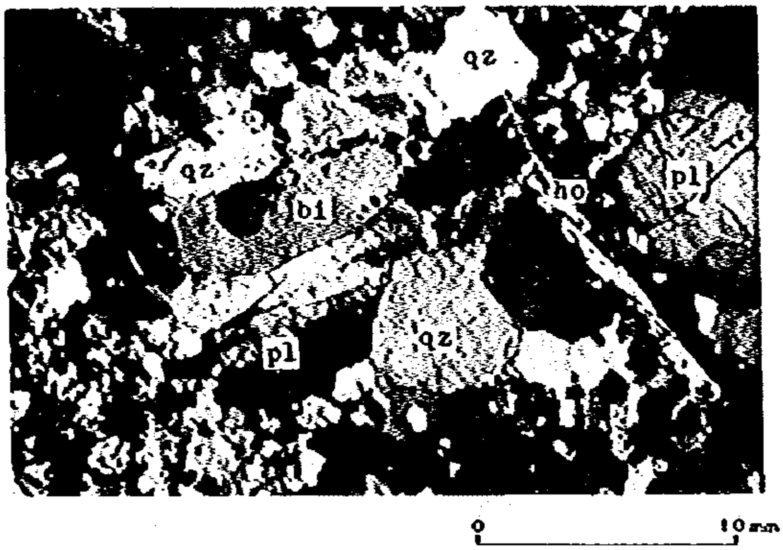

Crossed nicols

Sample: A57DTC(Tidi)

Rock name: Hornblende-biotite granodiorite

Location: EL TEJOCOTE Area

pl … plagioclase

qz … quartz

ho … hornblende

bi … biotite

(2)

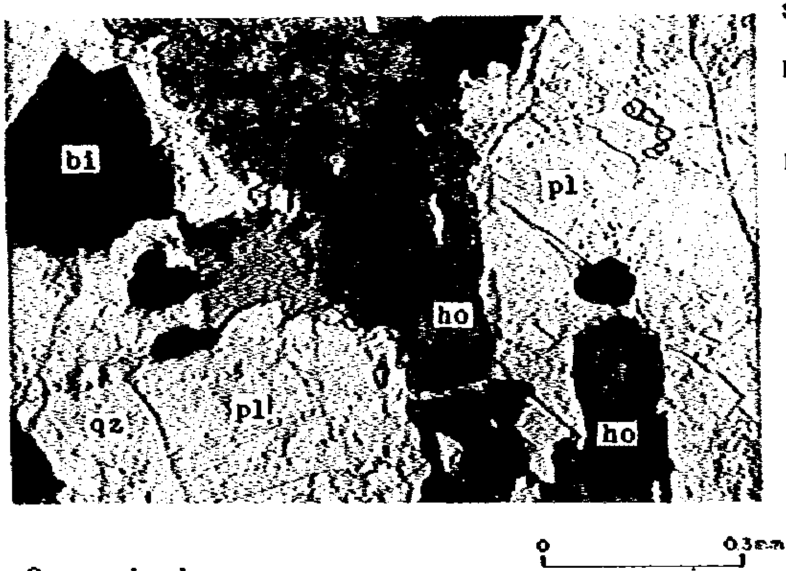

Open nicol

Sample: bA20T(Tidi)

Rock name: Hornblende-biotite gronodiorite

Location: EL TEJOCOTE Area

pl … plagioclase

qz … quartz

ho … hornblende

bi … biotite

Apx. 4 (Continued)

(3)

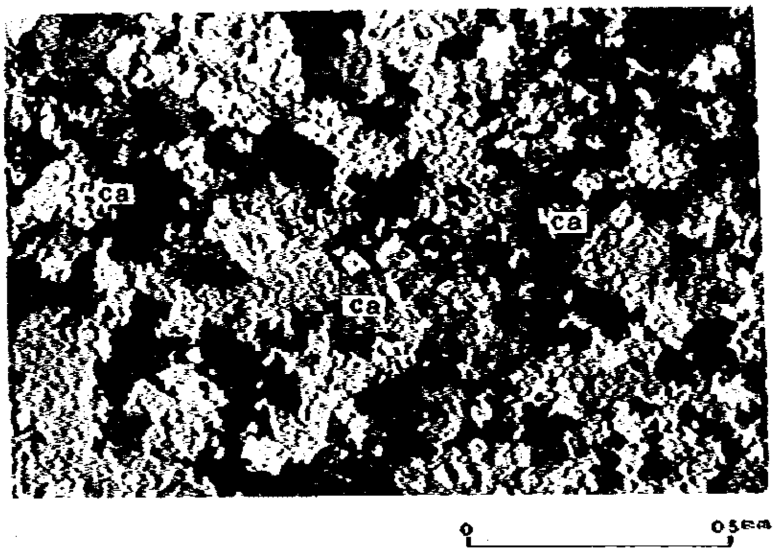

Sample: A50T(Kdl)

Rock name: Crystalline limestone

Location: EL TEJOCOTE Area

ca … calcite

Crossed nicols

(4)

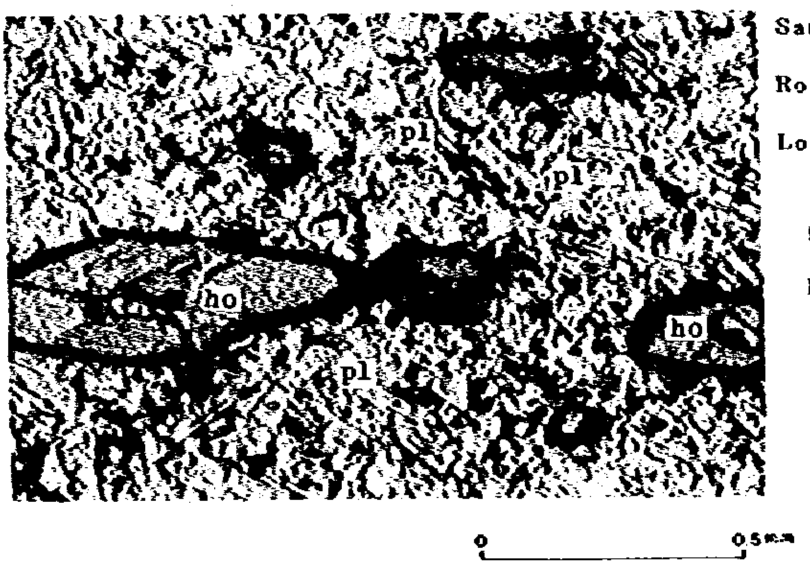

Sample: A27T(Tian)

Rock name: Hornblende andesite

Location: EL TEJOCOTE Area

pl … plagioclase

ho … hornblende

Open nicol

Apx. 4 (Continued)

(5)

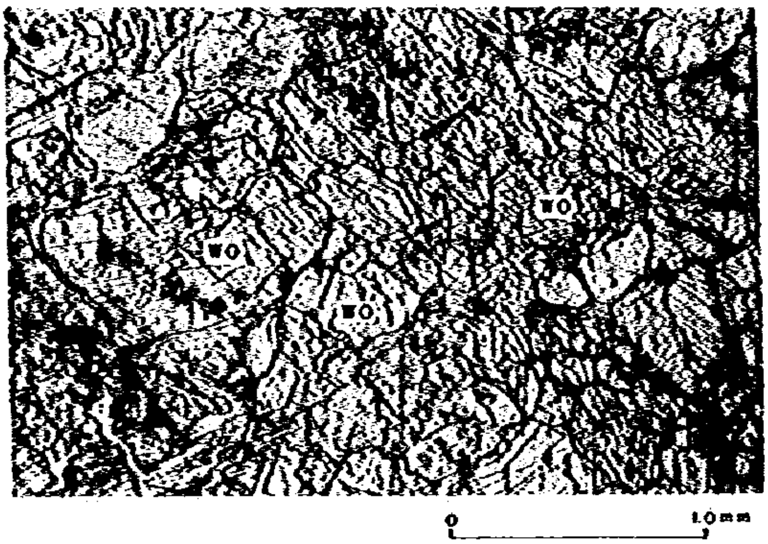

Sample: A42T

Rock name: Wollastonite skarn

Location: EL TEJOCOTE Area

wo ··· wollastonite

Open nicol

(6)

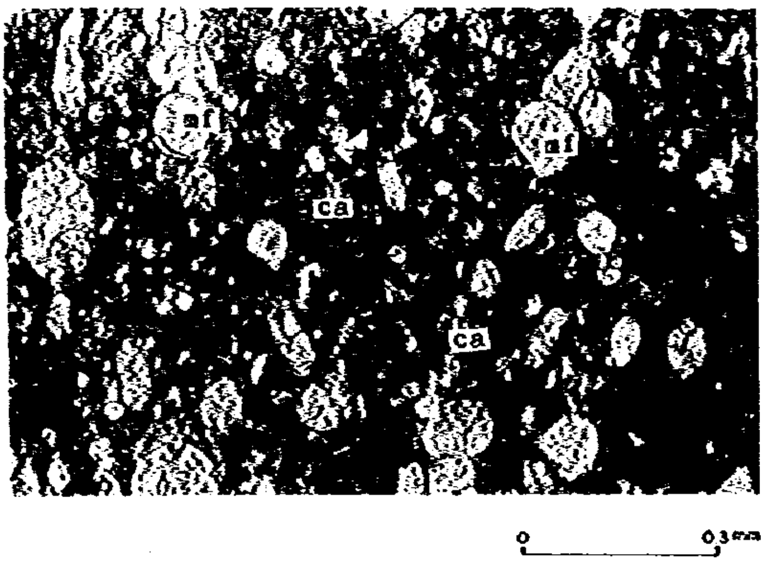

Sample: B39T(Kdf)

Rock name: Limestone

Location: PROVIDENCIA Area

ca ··· calcite

mf ··· microfossil ?

Open nicol

Apx. 4 (Continued)

(7)

Sample: B24T(Kdl)

Rock name: Crystalline limestone

Location: PROVIDENCIA Area

ca … calcite

Crossed nicols

(8)

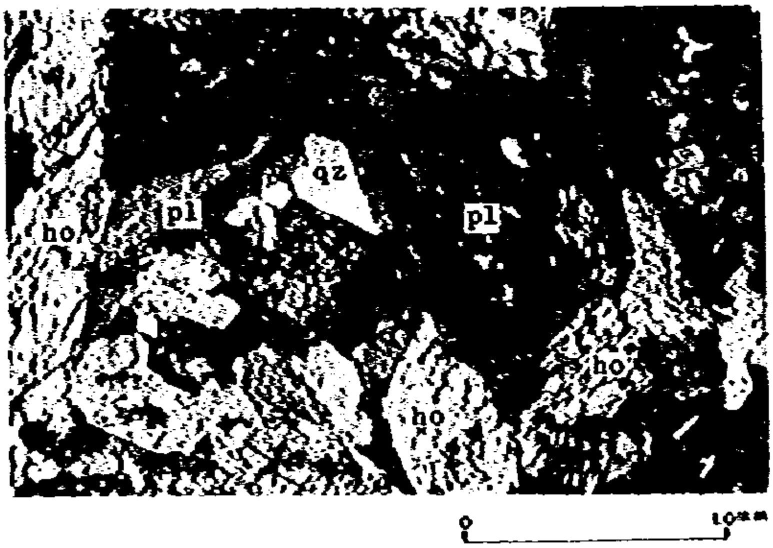

Sample: C54T(Tidp)

Rock name: Hornblende quartzdiorite

Location: SAN CLEMENTE Area

pl … plagiclase

qz … quartz

ho … hornblende

Crossed nicols

Apx. 4 (Continued)

(9)

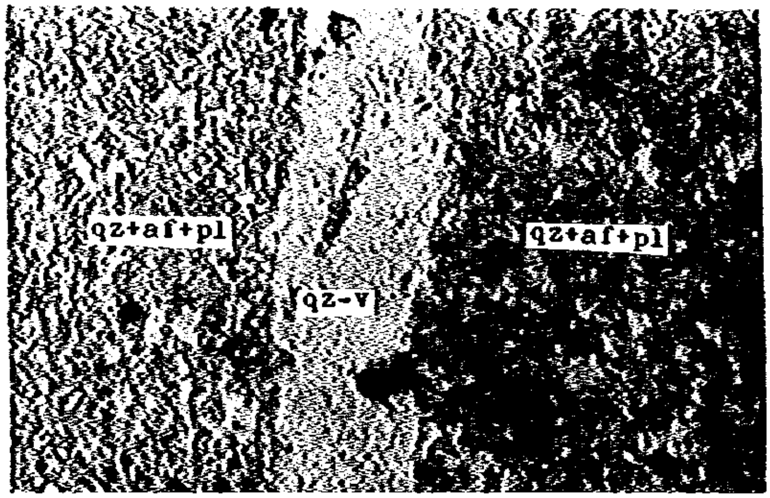

Open nicol

Sample: C9T(Trhy2-C)

Rock name: Rhyolite

Location: SAN CLEMENTE Area

qz … quartz

pl … plagioclase

af … alkali feldspar

qz-v … quartz vein

(9')

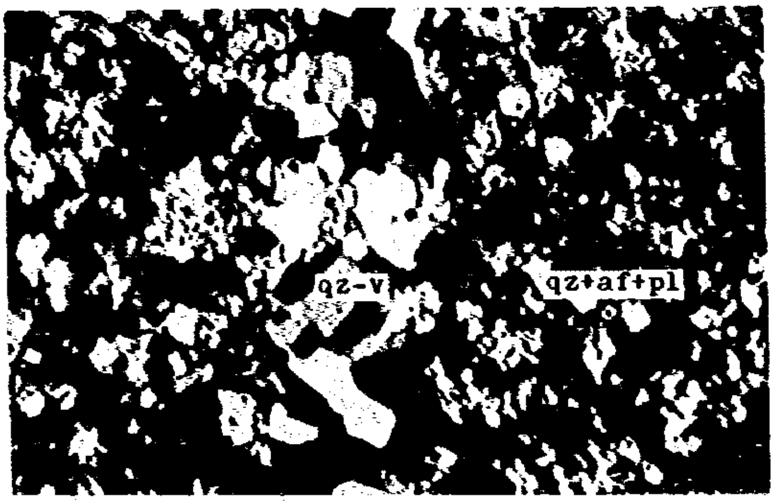

Crossed nicols

Sample: C9T(Trhy2-C)

Apx. 4 (Continued)

60

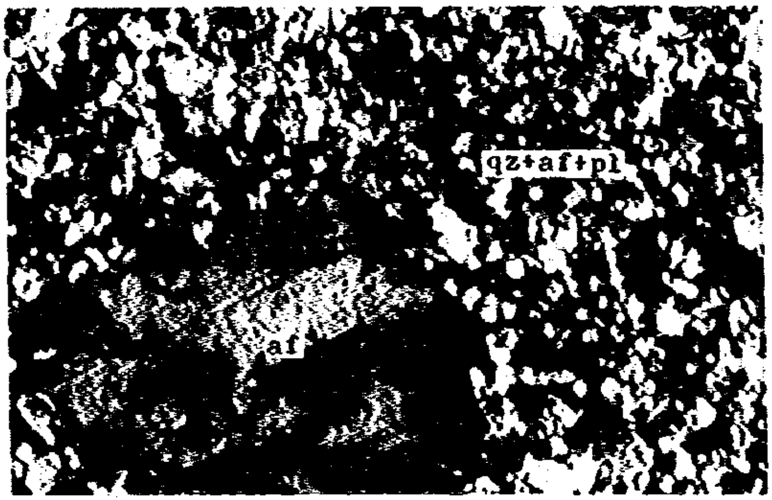

0 0.5mm

Crossed nicols

Sample: C17T(Trhy2-C)

Rock name: Rhyolite

Location: SAN CLEMENTE Area

pl … plagioclase

qz … quartz

af … alkali feldspar

61

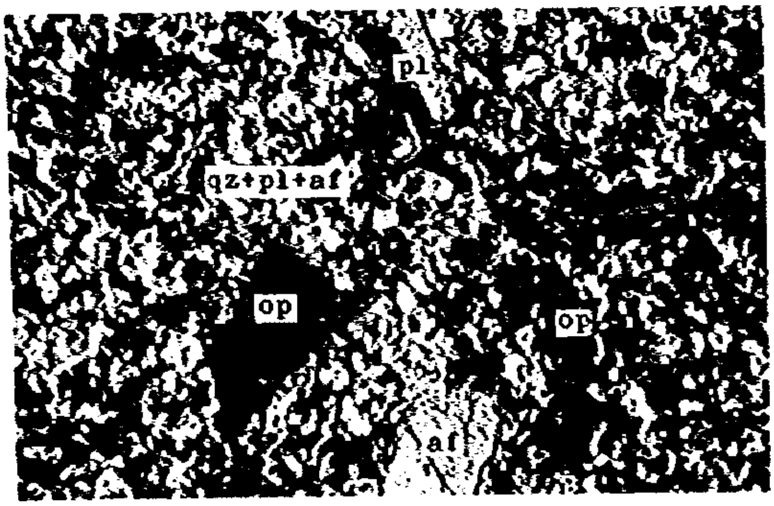

0 1.0mm

Crossed nicols

Sample: C20T(Trhy2-C)

Rock name: Granite porphyry

Location: SAN CLEMENTE Area

pl … plagioclase

qz … quartz

af … alkali feldspar

op … opaque mineral

Apx. 4 (Continued)

(12)

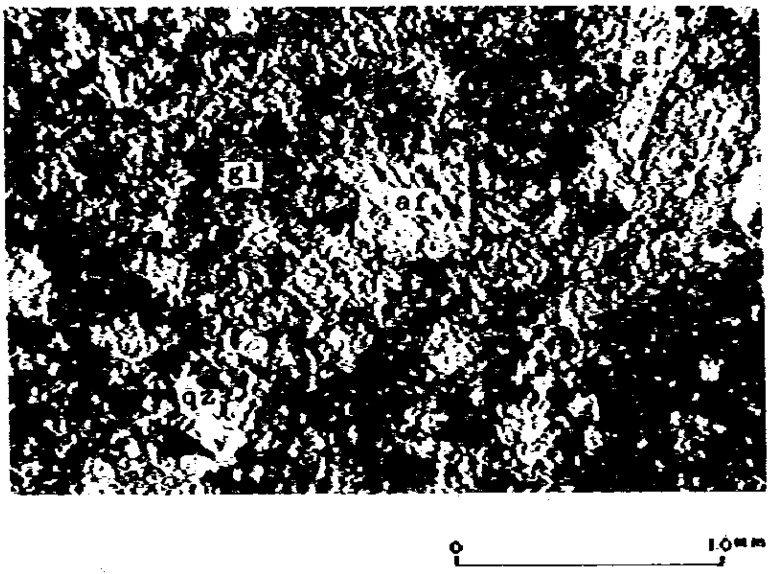

Sample: C4T(Tide)

Rock name: Dacite

Location: SAN CLEMENTE Area

qz … quartz

af … alkali feldspar

gl … glass

Crossed nicols

(13)

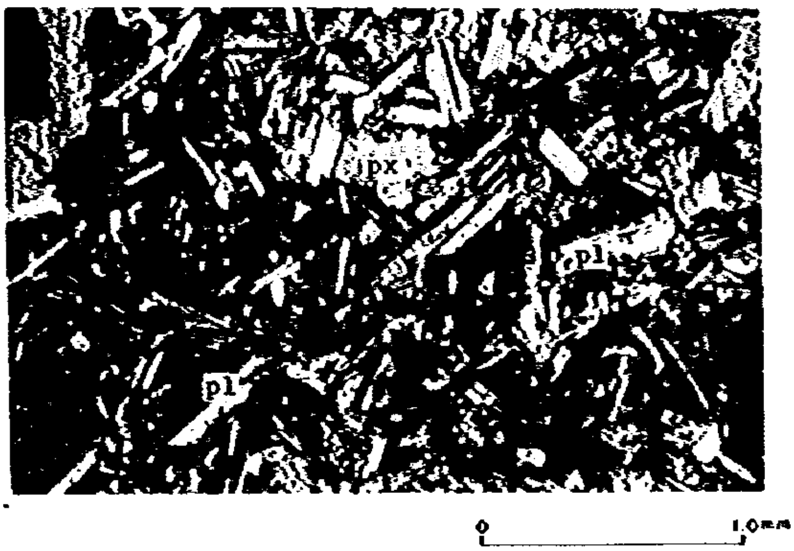

Sample: C56T(Tiba)

Rock name: Basalt

Location: SAN CLEMENTE Area

pl … plagioclase

px … pyroxine

Crossed nicols

Apx.5 Microscopic Observations of Ore Polished Sections

Area	Ser. No	Sample No	Location: Coordinates E	Location: Coordinates N	Name of mine	Occurrence	aimary mineral: el	cp	sp	gn	py	mg	ti	zr	bl		cv	cc	Secondary mineral: bn	mc	hm
EL TEJOCOTE	1	A11R	482590	2308610	Prospect	ml−spotted mg ore						◎									•
	2	A16R	480800	2309880	Prospect	cp−ml−spotted mg ore		•				◎					•				•
	3	A22R	487980	2311700	Outcrop	iron oxides															○
	4	A26R	483290	2311680	Floats	oxidized py-mg ore					○	○		•	•		•	•			○
	5	A29R	482750	2309910	Outcrop	mg ore						◎									
	6	A36R	479390	2308930	Prospect	oxides ore														•	◎
	7	A47RT	477110	2308185	Corral Viejo	ml-spotted skarn							•								•
	8	A54R	482000	2309645	Outcrop	mg ore					•	◎									•
	9	A56R	483350	2311000	Outcrop	mg ore					•	◎									
	10	A60R	481520	2309885	Nameless mine	mg ore					•	◎									
	11	A64R	478905	2308235	"Piedra Iman"	ml−spotted mg ore						◎									
	12	A65R	481285	2309400	Las Delicias	cp−py−spotted mg ore		○	•			◎					•	•	•		•
	13	A67RT	480810	2317220	Nuevo Encino Prieto	bl−gn−sp−spotted skarn			○	○	•				◎						
	14	A68R	480810	2317220	Nuevo Encino Prieto	black Mn ore					•					◎※					•
	15	A69R	480810	2317220	Nuevo Encino Prieto	py−gn−sp−spotted skarn			○	○	○	•			•	•	•				
	16	eA12MR	479955	2317900	Floats	oxidized mg ore						○									◎
PROVIDENCIA	17	B2MR	487225	2285195	Floats	iron oxides														•	◎
	18	B28MR	487750	2286325	San Juana	iron oxides															◎
	19	B47MR	487800	2286410	San Juana	iron oxides										○※					•
	20	B51MR	487945	2286400	Providencia	iron oxides															•
	21	B55MR	487985	2286305	Providencia	iron oxides															○
	22	B57MR	487985	2286305	Providencia	iron oxides															○
SAN CLEMENTE	23	SC1R	482950	2284600	San Severiano	hm vein										•※					○
	24	SC2R	482950	2284600	San Severiano	hm vein										○※					•
	25	SC3R	482950	2284600	San Severiano	hm vein								•							○
	26	SC4R	482950	2284600	San Severiano	rhyolite								•							•
	27	SC5R	482950	2284600	San Severiano	native gold	○														

Abbreviations : el ···electrum ; cp···chalcopyrite ; sp···sphalerite ; gn···galena ; py···pyrite ; mg···magnetite ; ti···titan
cv···covelline ; cc···chalcocite ; bn···bornite ; mc···marcasite ; hm···hematite ; gt···goethite ; ml···malac
◎··· abundant
○··· common
•··· rare

Polished Sections

ne	Occurrence	aimary mineral										Secondary mineral								Remarks
		el	cp	sp	gn	py	mg	ti	zr	bl		cv	cc	bn	mc	hm	gt	ml	lm	
	ml-spotted mg ore						◎									•	•	•		
	cp-ml-spotted mg ore		•				◎					•				•	O	•	•	
	iron oxides															O	◎			
	oxidized py-mg ore					O	O		•	•		•	•			O	◎			
	mg ore						◎													
	oxides ore														•	◎	O			
	ml-spotted skarn							•								•	•	O		
	mg ore					•	◎									•	O			
	mg ore					•	◎										O			
e	mg ore					•	◎										O			
	ml-spotted mg ore						◎										O	•		
	cp-py-spotted mg ore		O	•			◎					•	•	•		•				
Prieto	bl-gn-sp-spotted skarn			O	O	•				◎										
Prieto	black Mn ore					•					◎※					•	•			※ Mn-Fe oxides
Prieto	py-gn-sp-spotted skarn			O	O	O	•			•		•								
	oxidized mg ore						O									◎	O			
	iron oxides														•	◎	◎			
	iron oxides															◎	◎			
	iron oxides										O※					•	◎			※ Ti mineral ?
	iron oxides															•	◎			
	iron oxides															O	◎			
	iron oxides															O	◎			
o	hm vein										•※					O	•			※ Fe-Zn-Ca-(K)-Si mineral
o	hm vein										O※					•				※ Fe-Zn-(V)-(K)-Si-Ca mineral
o	hm vein								•							O				
o	rhyolite								•							•				
no	native gold	O																		

Abbreviations : el…electrum ; cp…chalcopyrite ; sp…sphalerite ; gn…galena ; py…pyrite ; mg…magnetite ; ti…titanite ; zr…zircon ; bl…boulangerite ;
cv…covelline ; cc…chalcocite ; bn…bornite ; mc…marcasite ; hm…hematite ; gt…goethite ; ml…malachite ; lm…limonite
◎…abundant
O…common
•…rare

Apx.6 Qualitative Analyses of Minerals by Electron Probe Microanalyzer

No.	Sample No.	Analyzed mineral	Au	Ag	Cu	Pb	Zn	Fe	Mn	Ti	Zr	V	Sb	S	Si	Ca	K
1	A11R	malachite ~ chrysocolla			◎		•	◎						•	◎	○	
2	A16R	covelline			◎		•	◎						◎	•	•	
3	A26R	chalcocite			◎			○						◎			
4	A26R	goethite						◎		•							
5	A26R	covelline		•	◎			○						◎			
6	A26R	goethite						◎							○	•	
7	A29R	silica mineral ?						○						•	◎	•	
8	A36R	marcasite						◎						◎			
9	A47R	titanite			•			○		◎		○			◎	◎	
10	A47R	titanite			○			○		◎		○			◎	◎	
11	A47R	malachite			◎		○									○	
12	A65R	sphalerite			○		◎	○						◎			
13	A65R	chalcocite ?			◎		◎	◎						◎			
14	A67RT	boulangerite				◎							◎	◎			
15	A68R	Mn oxides							◎								
16	A68R	Mn oxides							◎								
17	A68R	Mn — Fe oxides						◎	◎								
18	A68R	Mn — Fe oxides						◎	○								
19	A69R	galena				◎											
20	A69R	galena				◎											
21	A69R	boulangerite				◎							◎	◎			
22	A69R	boulangerite				◎	○						◎	◎			
23	SC1R	hematite						◎		•							•
24	SC1R	clay mineral ?					◎	◎							◎	◎	•
25	SC2R	clay mineral ?					◎	◎				•			◎	◎	•
26	SC3R	zircon									◎				◎		
27	SC5R	electrum	◎	◎													
28	SC5R	electrum	◎	◎													

◎ .... abundant, ○ .... Common • .... rare

Apx. 7 Quantitative Analyses of Minerals by Electron Probe Microanalyzer

	Sample No.	A26R		A65R			A69R					SC5R			
	Mineral	chalcocite		sphalerite			boulangerite			sphalerite		electrum		electrum	
		1	2	1	2	3	1	2	3	1	2	1	2	1	2
Weight %	Au	—	—	—	—	—	—	—	—	—	—	78.98	78.36	77.68	77.09
	Ag	0.16	0.16	—	—	—	—	—	—	—	—	21.43	22.07	22.78	22.55
	Cu	79.78	79.48	0.73	0.80	0.59	—	—	—	0.0	0.0	—	—	—	—
	Pb	—	—	—	—	—	57.20	57.09	56.86	—	—	—	—	—	—
	Zn	—	—	66.74	66.76	67.09	0.0	0.0	0.0	67.29	67.23	—	—	—	—
	Fe	1.65	1.67	0.69	0.73	0.70	—	—	—	0.69	0.17	—	—	—	—
	Sb	—	—	—	—	—	24.83	25.14	24.84	—	—	—	—	—	—
	S	18.50	18.51	32.10	32.08	31.93	18.59	18.65	18.51	32.07	32.16	—	—	—	—
	Total	100.09	99.82	100.26	100.37	100.31	100.62	100.88	100.21	100.05	99.56	100.41	100.43	100.46	99.64
Atomic %	Au	—	—	—	—	—	—	—	—	—	—	66.87	66.04	65.12	65.19
	Ag	0.08	0.08	—	—	—	—	—	—	—	—	33.13	33.96	34.88	34.81
	Cu	67.37	67.27	0.56	0.62	0.46	—	—	—	0.0	0.0	—	—	—	—
	Pb	—	—	—	—	—	26.05	25.91	26.00	—	—	—	—	—	—
	Zn	—	—	49.90	49.88	50.21	0.0	0.0	0.0	50.41	50.55	—	—	—	—
	Fe	1.58	1.61	0.60	0.64	0.61	—	—	—	0.60	0.15	—	—	—	—
	Sb	—	—	—	—	—	19.24	19.42	19.33	—	—	—	—	—	—
	S	30.96	31.05	48.94	48.87	48.72	54.71	54.68	54.68	48.98	49.31	—	—	—	—
	Total	99.99	100.01	100.00	100.01	100.00	100.00	100.01	100.01	99.99	100.01	100.00	100.00	100.00	100.00

Apx. 8 Photomicrographs of the Representative Ore Polished Sections

(1)

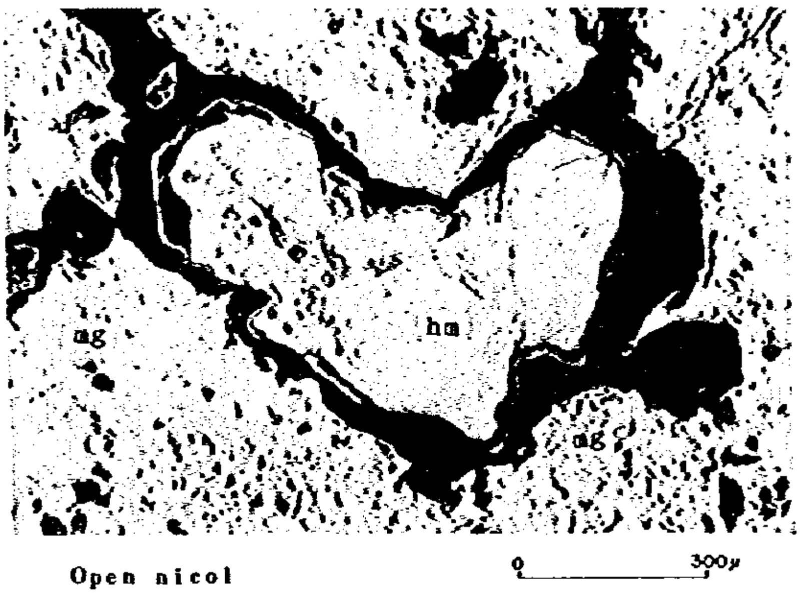

Open nicol

Sample: A11R

Granular magnetite, hematite in magnetite druse and goethite replacing hematite

Location: Prospect in the EL TEJOCOTE Area.

mg … magnetite

hm … hematite

gt … goethite

(2)

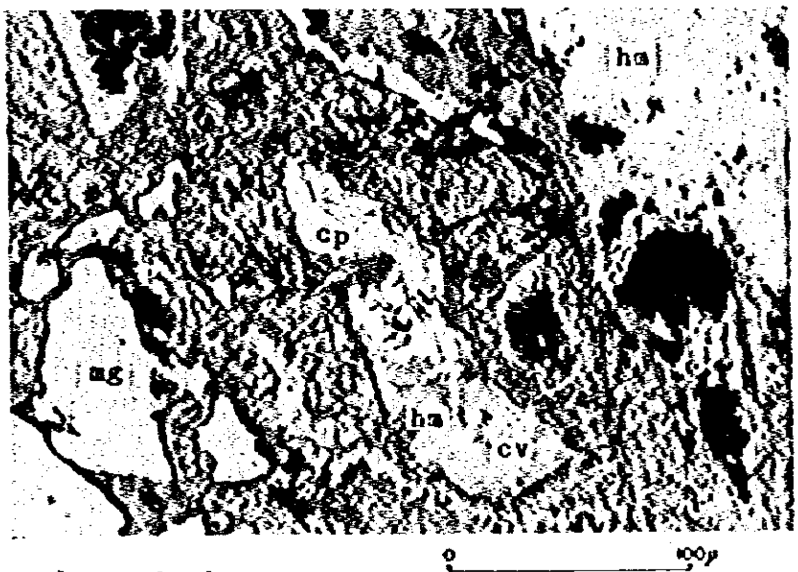

Open nicol

Sample: A16R

Granular magnetite and chalcopyrite replaced by covelline and hematite.

Location: Prospect in the EL TEJOCOTE Area.

mg … magnetite

cp … chalcopyrite

hm … hematite

cv … covelline

(3)

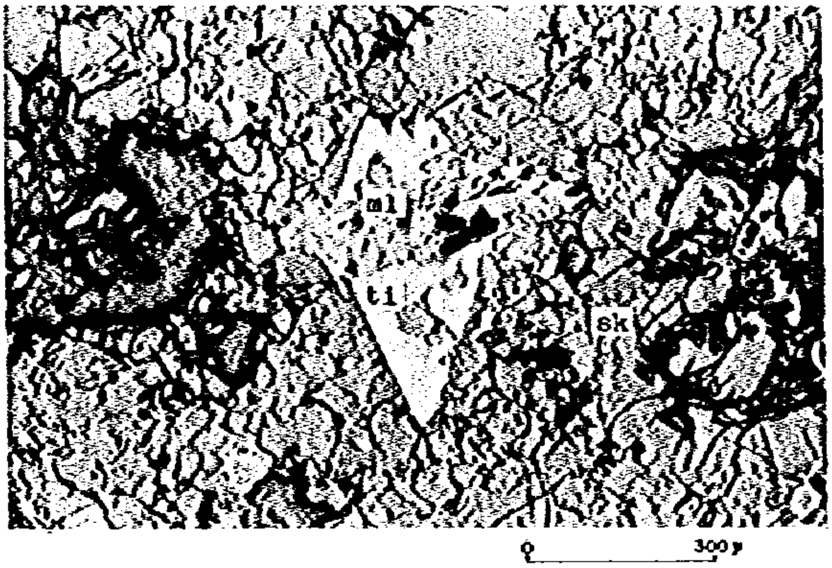

Open nicol

Sample: A47RT

Titanite and fibrous malachite in skarn.

Location: Corral Viejo mine in the EL TEJOCOTE Area.

ti … titanite

ml … malachite

sk … skarn

(4)

Open nicol

Sample: A64R

Coarse-grained magnetite and pyrite replaced by goethite.

Location: "Piedra Iman" mine in the EL TEJOCOTE Area.

mg … magnetite

py … pyrite

gt … goethite

(5)

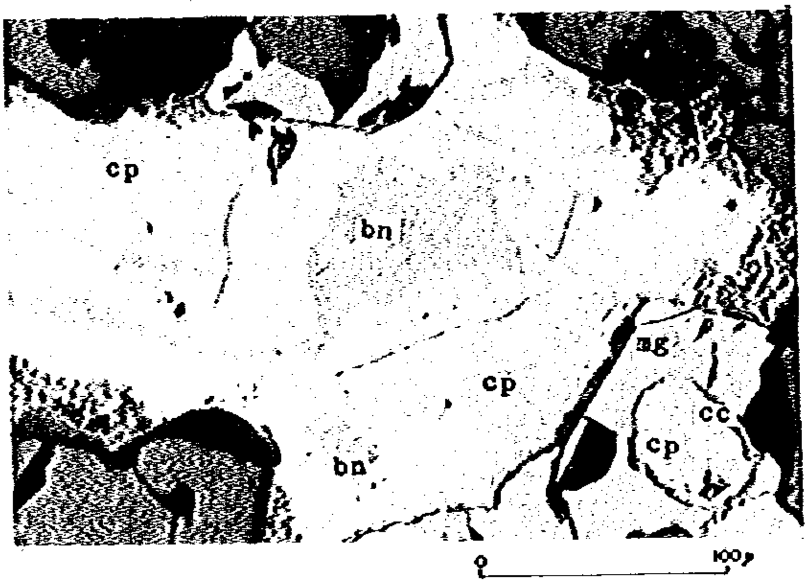

Open nicol

Sample: A65R

Granular magnetite, chalcopyrite, bornite with chalcopyrite lamella and chalcocite replacing bornite.

Location: Las Delicias mine in the EL TEJOCOTE Area.

mg … magnetite

cp … chalcopyrite

bn … bornite

cc … chalcocite

(6)

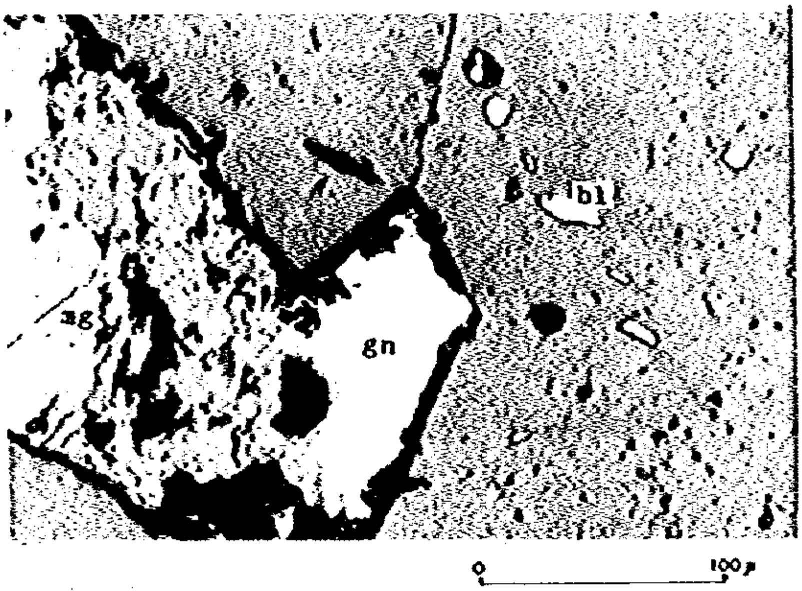

Open nicol

Sample: A69R

Magnetite, galena and boulangerite.

Location: Nuevo Encino Prieto in the EL TEJOCOTE Area.

mg … magnetite

gn … galena

bl … boulangerite

(7)

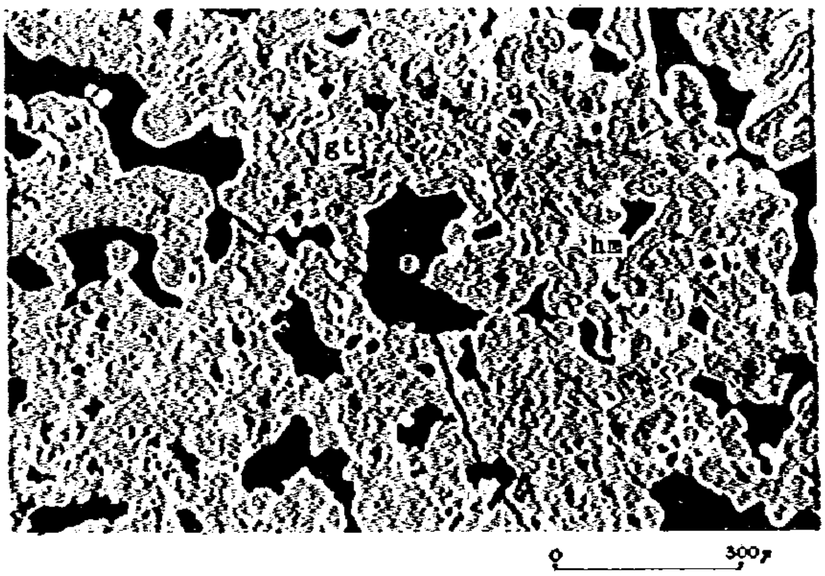

Sample: B28MR

Colloform structure of hematite and goethite.

Location: San Juana mine in the PROVIDENCIA Area.

hm … hematite

gt …goethite

Open nicol

(8)

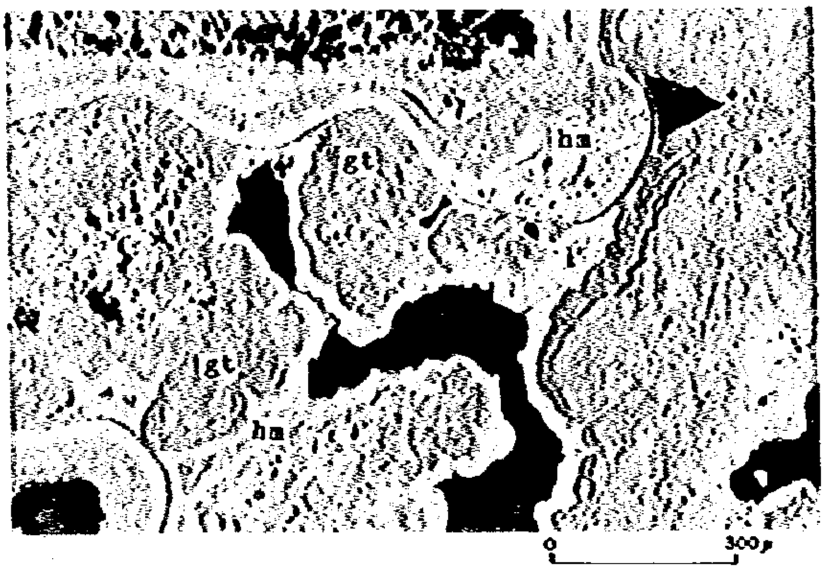

Sample: B55MR

Colloform structure of hematite and goethite.

Location: Providenia mine in the PROVIDENCIA Area.

hm … hematite

gt … goethite

Open nicol

Apx. 8 (Continued)

(9)

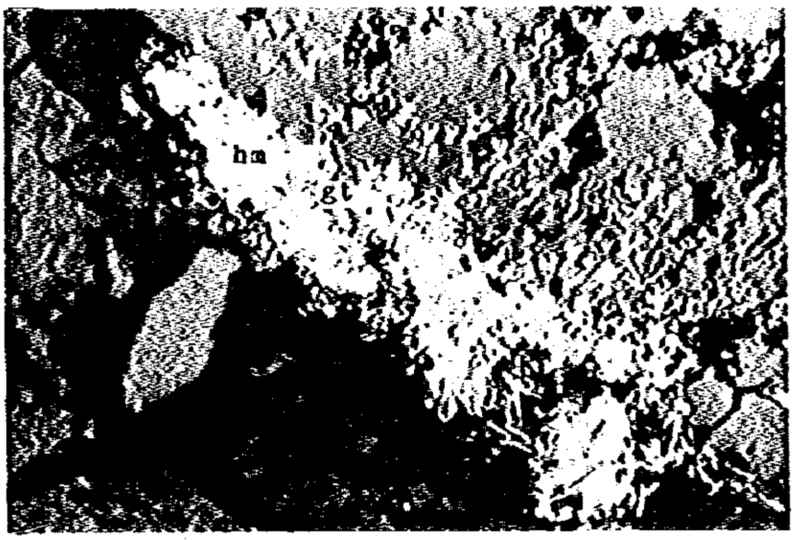

Sample: SC2R

Hematite and goethite

Location: San Severiano mine in the SAN CLEMENTE Area

hm … hematite

gt … goethite

Open nicol 0 ——— 100μ

(10)

Sample: SC5R

Electrum

Location: San Severiano mine in the SAN CLEMENTE Area

el … electrum

Open nicol 0 ——— 100μ